U.S. Department
of Transportation
**Federal Railroad
Administration**

Subsurface Evaluation of Railway Track Using Ground Penetrating Radar

Office of Research and
Development
Washington, DC 20590

DOT/FRA/ORD-09/08

April 2009

Notice

This document is disseminated under the sponsorship of the Department of Transportation in the interest of information exchange. The United States Government assumes no liability for its contents or use thereof.

Notice

The United States Government does not endorse products or manufacturers. Trade or manufacturers' names appear herein solely because they are considered essential to the objective of this report.

REPORT DOCUMENTATION PAGE	Form approved OMB No. 0704-0188

1. AGENCY USE ONLY *(Leave blank)*	2. REPORT DATE	3. REPORT TYPE AND DATES COVERED
	9/30/08	Final Report, 12/04 – 09/08

4. TITLE AND SUBTITLE

Subsurface Evaluation of Railway Track Using Ground Penetrating Radar

5. FUNDING NUMBERS

DTFR53-05-D-00200

6. AUTHOR(S)

Roger Roberts[(1)], Imad Al-Qadi[(2)], Erol Tutumluer[(2)], Jeff Boyle[(3)]

7. PERFORMING ORGANIZATION NAME(S) AND ADDRESS(ES)

[(1)] GSSI
12 Industrial Way
Salem, NH 03079

[(2)] Department of Civil Engineering
University of Illinois
Urbana, IL 61801

[(3)] Sperry Rail Service
46 Shelter Rock Rd.
Danbury, CT 06810

8. PERFORMING ORGANIZATION REPORT NUMBERS

DOT/FRA/ORD-09/08

9. SPONSORING/MONITORING AGENGY NAME(S) AND ADDRESS(ES)

U.S. Department of Transportation
Federal Railroad Administration
Office of Research and Development, MS 20
1200 New Jersey Avenue, S.E., MS-20
Washington, DC 20590

10. SPONSORING/MONITORING AGENCY REPORT NUMBER

11. SUPPLEMENTARY NOTES

12a. DISTRIBUTION/AVAILABILITY STATEMENT

This document is available through National Technical Information Service, Springfield, VA 22161.

12b. DISTRIBUTION CODE

13. ABSTRACT

This report details the implementation of 2 GHz horn antennas for measuring working ballast thickness using ground penetrating radar and the initial implementation of a 500 MHz horn antenna used for subballast and subgrade characterization. The work was performed as part of the first task order and modification task 1 in the fourth phase of a multi-phase ground penetrating radar research and development project. During the course of the project, it was found that the 2 GHz horn antennas produced data that contain reflections from the void space in clean ballast. The amplitude of the void space reflections was found to be indicative of the degree of fouling. A simple data processing scheme was implemented that converted the reflection amplitudes to color bands, which were assigned to relative degrees of ballast fouling. The 2 GHz antennas were tested on five different tracks covering more than 382 mi and produced color-coded data that correlated well with available ballast condition ground truth. Subballast and subgrade layering to depths extending beyond 6 ft and anomalous high amplitude reflection events were successfully identified with the 500 MHz antenna.

14. SUBJECT TERMS	15. NUMBER OF PAGES
	116
	16. PRICE CODE

17. SECURITY CLASSIFICATION	18. SECURITY CLASSIFICATION OF THIS PAGE	19. SECURITY CLASSIFICATION OF ABSTRACT	20. LIMITATION OF ABSTRACT
UNCLASSIFIED	UNCLASSIFIED	UNCLASSIFIED	

METRIC/ENGLISH CONVERSION FACTORS

ENGLISH TO METRIC	METRIC TO ENGLISH
LENGTH (APPROXIMATE)	**LENGTH (APPROXIMATE)**
1 inch (in) = 2.5 centimeters (cm)	1 millimeter (mm) = 0.04 inch (in)
1 foot (ft) = 30 centimeters (cm)	1 centimeter (cm) = 0.4 inch (in)
1 yard (yd) = 0.9 meter (m)	1 meter (m) = 3.3 feet (ft)
1 mile (mi) = 1.6 kilometers (km)	1 meter (m) = 1.1 yards (yd)
	1 kilometer (km) = 0.6 mile (mi)
AREA (APPROXIMATE)	**AREA (APPROXIMATE)**
1 square inch (sq in, in^2) = 6.5 square centimeters (cm^2)	1 square centimeter (cm^2) = 0.16 square inch (sq in, in^2)
1 square foot (sq ft, ft^2) = 0.09 square meter (m^2)	1 square meter (m^2) = 1.2 square yards (sq yd, yd^2)
1 square yard (sq yd, yd^2) = 0.8 square meter (m^2)	1 square kilometer (km^2) = 0.4 square mile (sq mi, mi^2)
1 square mile (sq mi, mi^2) = 2.6 square kilometers (km^2)	10,000 square meters (m^2) = 1 hectare (ha) = 2.5 acres
1 acre = 0.4 hectare (he) = 4,000 square meters (m^2)	
MASS - WEIGHT (APPROXIMATE)	**MASS - WEIGHT (APPROXIMATE)**
1 ounce (oz) = 28 grams (gm)	1 gram (gm) = 0.036 ounce (oz)
1 pound (lb) = 0.45 kilogram (kg)	1 kilogram (kg) = 2.2 pounds (lb)
1 short ton = 2,000 pounds (lb) = 0.9 tonne (t)	1 tonne (t) = 1,000 kilograms (kg) = 1.1 short tons
VOLUME (APPROXIMATE)	**VOLUME (APPROXIMATE)**
1 teaspoon (tsp) = 5 milliliters (ml)	1 milliliter (ml) = 0.03 fluid ounce (fl oz)
1 tablespoon (tbsp) = 15 milliliters (ml)	1 liter (l) = 2.1 pints (pt)
1 fluid ounce (fl oz) = 30 milliliters (ml)	1 liter (l) = 1.06 quarts (qt)
1 cup (c) = 0.24 liter (l)	1 liter (l) = 0.26 gallon (gal)
1 pint (pt) = 0.47 liter (l)	
1 quart (qt) = 0.96 liter (l)	
1 gallon (gal) = 3.8 liters (l)	
1 cubic foot (cu ft, ft^3) = 0.03 cubic meter (m^3)	1 cubic meter (m^3) = 36 cubic feet (cu ft, ft^3)
1 cubic yard (cu yd, yd^3) = 0.76 cubic meter (m^3)	1 cubic meter (m^3) = 1.3 cubic yards (cu yd, yd^3)
TEMPERATURE (EXACT)	**TEMPERATURE (EXACT)**
[(x-32)(5/9)] °F = y °C	[(9/5) y + 32] °C = x °F

QUICK INCH - CENTIMETER LENGTH CONVERSION

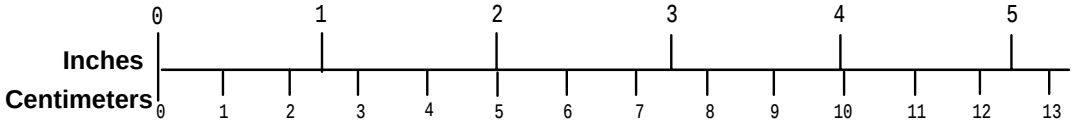

QUICK FAHRENHEIT - CELSIUS TEMPERATURE CONVERSION

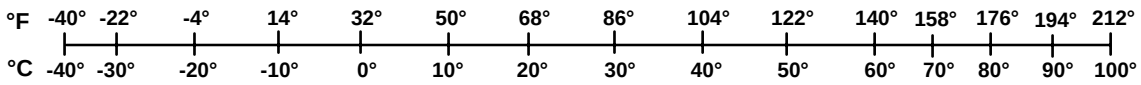

Table of Contents

Illustrations

Tables

Executive Summary

This report details the implementation of 2 GHz horn antennas for measuring working ballast thickness using ground penetrating radar and development and implementation of a 500 MHz horn antenna for characterizing the subballast and subgrade. The work was performed as part of the first task order and modification task one in the fourth phase of a multiphase ground penetrating radar research and development project. During the course of the project, it was found that the 2 GHz horn antennas produce data that contain reflections from the void space in clean ballast. The amplitude of the void space reflections was found to be indicative of the degree of fouling. An automatic data processing scheme was implemented that first converted the reflection amplitudes into reflection amplitude envelopes, then mapped the amplitude envelopes to color bands and calculated the thickness of clean ballast. The 2 GHz antennas were tested on six different track conditions. Data were obtained on the High-Tonnage Loop (HTL) track at the Transportation Technology Center (TTC) in Colorado, on Amtrak track south of Boston, MA, on tracks in Wyoming and Nebraska, and on the Alaska Railroad. Repeat data were obtained on the Wyoming and Alaska Railroad track before and after significant precipitation events. Sections of track indicating ballast distress via mud stains on the rails and ties correlated well with the evident distressed zones in the processed color-coded data. Other sections of track that were recently undercut are indicated as containing mostly clean ballast in the processed color-coded data. Samples were obtained for moisture content and sieve analyses from 40 locations in Wyoming and Alaska during Modification Task One performance period. Agreement was good between the clean ballast thickness calculated from the samples and from the GPR data. This developed methodology presents a feasible approach for routine inspection of working railroads and is especially suited to assess the ballast fouling condition near the bottom of railroad ties. In 2007, Burlington Northern Santa Fe (now known as BNSF) railroad, encouraged by the results, contracted out more than 1,000 mi of data to be obtained with the 2 GHz antennas. An air-launched 500 MHz horn antenna was developed as part of modification task one in 2007 for the purpose of mapping the subballast and subgrade. The performance of this antenna was assessed on the HTL loop at TTC. Layers extending over 4 ft in depth were identified in the GPR data and confirmed by cross trenches. The 500 MHz antenna was subsequently mounted between the rails for data collection in Wyoming and Alaska. Subballast and subgrade layer reflections observed in the GPR data compared well with ground truth in Wyoming. Automatic picking of the highest amplitude reflections between the depths of 30 inches (in) and 75 in was performed and the amplitude values were mapped in Google Earth. Some correlation was observed between the location of frost heaves and/or local bodies of water and anomalous high amplitude reflections. However, much more data and ground truth need to be obtained to better understand the relationship between these high amplitude reflection zones in the 500 MHz data and track structural problems.

1. Introduction

This report summarizes the work performed in the first task of Phase IV and Modification Task One of a multiphase track subsurface evaluation using ground penetrating radar (GPR) partially funded by the Federal Railroad Administration (FRA). The work presented here was focused on implementing GPR for automatically mapping the condition of ballast and characterizing the subballast and subgrade. With accurate and real-time information collected by GPR, severe hazards to railroad traffic can be prevented and remediation can be planned.

1.1. Statement of Problem and Task Goals

Railroad ballast is the uniformly graded coarse aggregate placed between and immediately underneath railroad ties. Subballast is sand or gravel used to provide drainage and, along with ballast, distributes the applied dynamic train loading into the subgrade. The ballast and subballast system are commonly referred to as the granular layer supporting track with a design thickness of typically 18–30 inches (in). In some instances, the ballast may be placed directly on stable subgrade. Figure 1 illustrates a typical active railroad cross-section. Often a transition area occurs at the ballast-subballast interface containing fines.

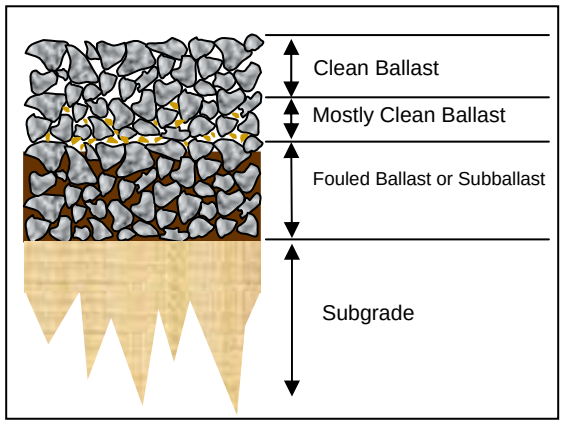

Figure 1. Typical active railroad ballast cross-section.

Over time, ballast is progressively contaminated by fine-grained aggregate and metal dust that fills the void space between ballast stones. This contamination is commonly referred to as fouling. The fouling index is used to describe the level of fouling in track and is calculated as the summation of the percentage of material passing the #4 sieve plus the percentage of material passing the #200 sieve (Selig and Waters, 1994). When the fouling reaches a specific threshold, the structural integrity of the contaminated ballast system can be compromised and the drainage ability of the ballast system is jeopardized. This leads to track instability and ultimately, without corrective maintenance, train derailments. Hence, early detection of ballast fouling is of utmost importance to maintain safe operation and cost-effective maintenance. Due to its critical location, evaluation of ballast condition near the bottom of the ties is highly desirable.

Figure 2 is an example of a typical ballast condition in the railroad. The top 10 in contain clean ballast. Beneath 10 in the ballast is fouled by fine-grained material. It is apparent that the condition of the ballast below the ties cannot be assessed visually without invasive methods such as cross-trenching. One major benefit of GPR is the ability to assess the condition of the ballast in a nondestructive manner.

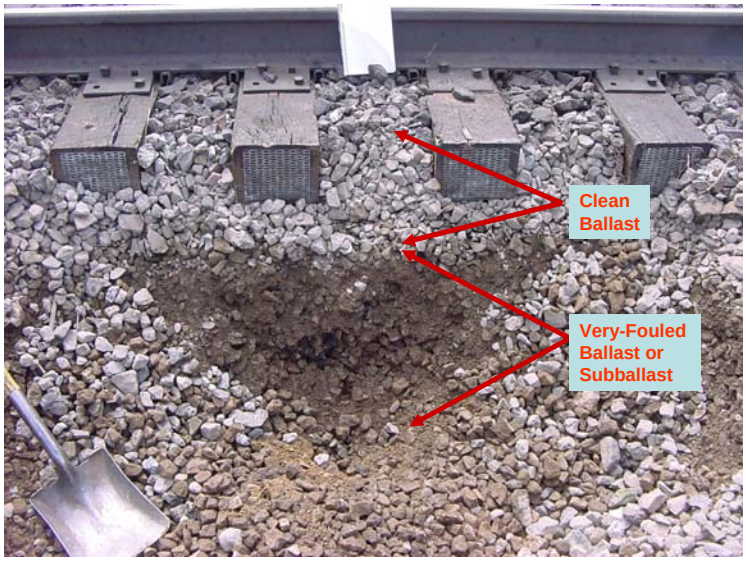

Figure 2. Typical ground truth cross-trench in railroad, showing ballast condition.

The range of track structural problems includes the portion of the roadbed below the ballast layer. These problems include, but are not limited to, subgrade failure, subgrade attrition, and trapped water (Hyslip et al, 2005). Antennas with center frequencies much lower than 2 GHz are necessary to penetrate to depths up to 7 ft or greater. The lower-frequency GPR antennas are useful for mapping the ballast-subballast and subballast-subgrade interfaces. The depths of the layer interfaces calculated from the GPR data provide useful information related to the stability of the structure. The relative amplitudes of the reflections from the interfaces mapped in the GPR data are typically indicative of the presence of excessive moisture. Consequently, the mapping of the roadbed structure below the ballast layer using GPR can potentially provide valuable information that will make track maintenance more efficient and hence save money.

The ultimate goal of this project is to advance GPR technology as a viable and efficient tool for rapid evaluation of track subsurface condition which is not amenable to visual inspection. The work presented in this report is part of the fourth phase of an ongoing FRA project. The immediate goals of the initial work done in Phase IV of this project were to: (1) develop automatic processing algorithms for evaluation of ballast condition from GPR data, (2) evaluate the performance of these algorithms on at least two separate ballast types. Subsequent to the initial task, the goals of modification task one were to: (1) further verify the performance of the ballast fouling assessment methodology on more track with different ballast conditions, and (2) enhance the ability to automatically detect and evaluate subballast and subgrade using 500 MHz GPR.

1.2 Previous Work

Ground penetrating radar is a nondestructive technique that has been evaluated over the past 2 decades to detect ballast contamination. The reported success of this evaluation is mixed. As part of this phase of the project, a review of previous work was performed. Technological advances continually provide new hardware and software that, in turn, permit the testing of new ideas and data collection and analysis methodologies. Often the case is that proper evaluation of ideas was not possible in the past due to equipment limitations that are no longer a factor. Consequently, periodically reviewing work that has already been done is important.

1.2.1 Summary of Literature Review

Much progress has been made using GPR for railroad investigations, especially in the past 5 years. The review presented below focuses on the recent work that has practical implications.

1.2.1.1 Ballast Fouling

Studies by Sussmann et al. (2002) and Clark et al. (2001) have established the relationship between the fouling and dielectric constant. The significant increase in dielectric constant associated with fouled ballast relative to clean ballast can be attributed to the fouling material filling the void space. In addition, the dielectric contrast between clean and fouled ballast is often magnified by the greater ability of the fouling material to retain moisture. The laboratory results of the dielectric constant for different ballast conditions from Sussmann (2002) are listed in Table 1.

Table 1. Laboratory measured value of Dielectric Constant for Different Ballasts modified from Sussmann (2002)

Material	ε_r Dry	ε_r Saturated	ε_r Drained
Granite ballast	3.2	26.4	16.0
Dolomite Ballast	3.7	25.5	16.5
Trap Rock Ballast (basalt)	4.3	31.4	4.8
Trap Rock Ballast (10% fouled)	5.0	22	17.0
Trap rock ballast (30% fouled)	3.5	28	20.6

Keogh et al. (2006) used the RAIL RADAR™ system to measure the signal travel time and material dielectric constant of each detected subsurface layer, as well as the tie condition. The RAIL RADAR™ is an integrated system for accurate tie and ballast condition assessment. Tie condition is determined based on the interpretation of a high-resolution down-looking digital camera. Ground penetrating radar is used to measure ballast condition, including

ballast layer thicknesses, ballast fouling and moisture-content variations. The GPR system used included a single transmit antenna and multiple 1.1 GHz receive antennae. It acquires samples at typically every 1–2 in and can resolve layers as thin as 1.5 in to a depth greater than 5 ft in normal railbed structure. The results showed that the RAIL RADAR^{TM} system has a layer thickness measurement accuracy of ±5 percent and is able to survey through wooden or reinforced concrete ties. The data collection speed is limited to 25 mph because ground-coupled antennae are used. Keogh et al. (2006) noted that the radar pulse propagation velocity significantly decreased (10-30 percent) from clean to fouled ballast as a result of increased fine particles. Accordingly, the RAIL RADAR^{TM} approach can be used to define an acceptable ballast threshold.

Kind et al. (2006) used an automated common midpoint measurement to obtain the wave propagation velocity. In the experimental setup, two 500 MHz antennae were set up on 13 ft by 13 ft test specimen. The transmitting antenna was placed in a fixed position with an elevation of 8 in above the ballast. The receiving antenna was mounted on the trolley in the same elevation. By changing the location of receiver, the wave propagation velocity can be obtained. According to related dielectric constant, the ballast fouling index can be estimated.

1.2.1.2 Subballast and Subgrade Mapping

Recent work using GPR for subballast and subgrade mapping has been focused on air-coupled antennas operated at 400 MHz to 1 GHz center-frequency.

Considering that the logistics requirement of ground-coupled antenna limit the GPR survey speed to about 25 mph, Kathage et al. (2005) used three 400 MHz and one 1 GHz horn antennae in the GPR survey on railway. Two Geophysical Survey Systems, Inc. (GSSI) SIR-20 control units were used for collecting the GPR data. The results showed that GPR can be a successful method for the investigation of railway embankments and structure at a surveying speed of 72 mph.

A GPR system mounted at the front of the train, using up to four air-launched antennae (IDS RIS-2K), was used by Al-Nuaimy et al. (2004). A number of digital video cameras collected optical and infrared video data from different angles, which was time-synchronized with GPS data. The data collection speed was up to 125 mph. Then, the following off-line processing stages were used: (1) gain normalization, (2) vertical and horizontal band-pass filtering, (3) clutter and air-wave removal, (4) distance normalization, (5) filtering and interpolating for GPS abnormalities, (6) topographic correction for water table, (7) extraction of sub-sleeper data, (8) data fusion, (9) ballast quality analysis and segmentation, (10) ballast depth reporting, and (11) suggestions for core sample positions. The results proved that GPR can effectively detect various degrees of ballast conditions including: ballast thickness, uneven settlement, perched water table, sinkholes, and subballast irregularities.

Eriksen et al. (2006) used 400 MHz IDS bow-tie antennae and a 1 GHz GSSI horn antenna for data collection. The control systems used were a RIS-2K unit for the IDS antennae and a SIR-20 unit for the 1 GHz horn antenna. The spatial resolution, which depends on the systems and number of channels used, ranges from 1 in at 62.5 mph to a maximum of 4 in at 125 mph. The raw data was post-processed using the following steps; (1) time-zero adjustment, (2) drift

removal, (3) sleeper-crib separation, (4) surface object detection, (5) background removal, (6) appropriate gain application, and (7) interactive layer tracking and depth assessment. These automatic processing methods were used to extract ballast layer thickness, reduce the effect of non-steel sleepers by separately analyzing the data from different positions. To obtain good data, Eriksen et al. (2006) listed the most important parameters for designing GPR antenna configuration; (1) operating frequency, (2) sampling interval, (3) station spacing, (4) antenna separation, (5) antenna orientation, (6) electrical properties of the host environment, (7) resolution frequency, (8) clutter frequency, and (9) external interference.

1.2.1.3 Other Developments

In the study of Silvast et al. (2006), the Fourier transform is used to obtain the frequency spectrum for each scan. This technique is suitable for a stationary signal whose properties, such as frequency, does not change with time. However, as the radar wave energy propagates through the ballast, the higher frequencies are attenuated more rapidly than the lower frequencies. Consequently, some propagation time dependency occurs in the frequency content of GPR data obtained on railroads. A full-scan Fourier transform is useful for assessing the total frequency content of a scan. Therefore, comparisons of the frequency content of GPR scans from clean ballast versus fouled ballast should be indicative of the relative fouling at the locations where the scans were obtained. However, all time-dependent information is lost when a Fourier transform is performed on an entire scan. This means the depth of clean ballast and the extent of fouling cannot be quantified using this methodology. An alternative approach using the Fourier transform on a moving portion of each scan provides the additional time (and hence depth) dependent frequency content information necessary to quantify the ballast fouling extent. This method is named the Short-Time Fourier Transform (STFT).

Al-Qadi et al. (2007) used the (STFT) to analyze the change in the frequency spectrum of the signal versus depth. Figure 3 shows the STFT of three scans representing different ballast conditions. The vertical axis of the images represents increasing depth and the horizontal axis represents the frequency spectrum. Near the ballast surface, the frequency spectra of the scans are very similar. However, with increasing depth there is a pronounced decrease in amplitude spectra amplitudes in the range from 0-3 GHz for the fouled ballast scan relative to the nonfouled ballast scan.

A second application of the STFT is isolating signal from coherent clutter in the data from external radio frequency interference (RFI). Figure 4 illustrates the STFT of a scan with significant RFI. The portion of the frequency spectrum associated with the scattering from the ballast aggregate is clearly isolated from the RFI band.

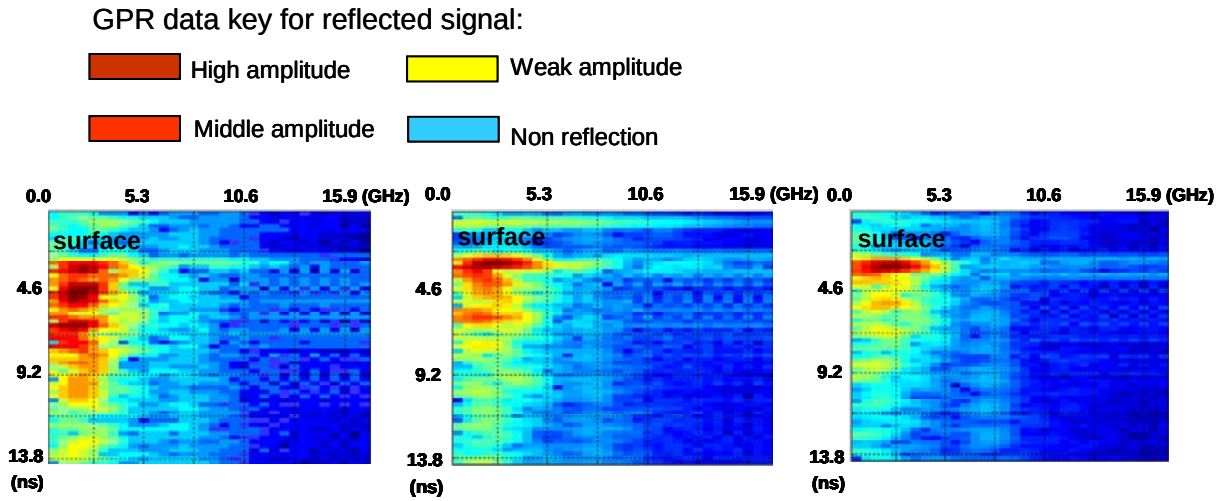

(a) Clean ballast. **(b) Moderately fouled ballast.** **(c) Fouled ballast.**

Figure 3. Results of ballast with various fouling conditions using short-time Fourier transform (Al-Qadi et al., 2007).

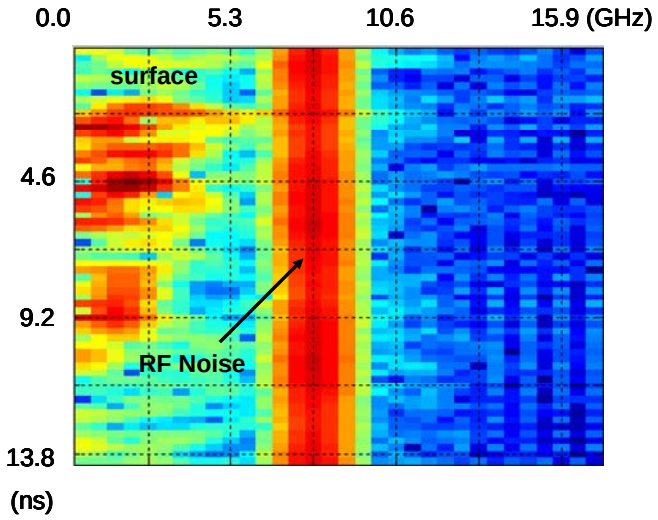

Figure 4. STFT result for the scan with coherent RF Interference (Al-Qadi et al., 2007).

Al-Qadi et al. (2007) used 2 GHz antenna to measure the effects of moisture on the clean and fouled ballast, as shown in Figure 5. A water truck was used to control the moisture content of a railroad section at the Transportation Technology Center (TTC). The data collected over the same section at various times showed that the clean ballast allows water to flow through easily. In slightly fouled ballast, fine particles partially block the air voids and influence drainage capability, resulting in greater saturation. Consequently, this results in a significant GPR reflection at this saturation contrast. Over time, the water drained from the slightly fouled section, resulting in much lower reflection amplitude. The results revealed that GPR may be an effective technique to measure moisture content in the ballast.

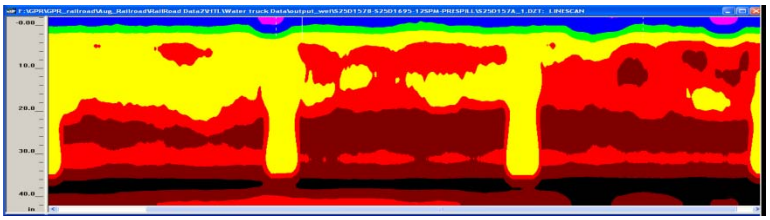

(a) Data collected before spray

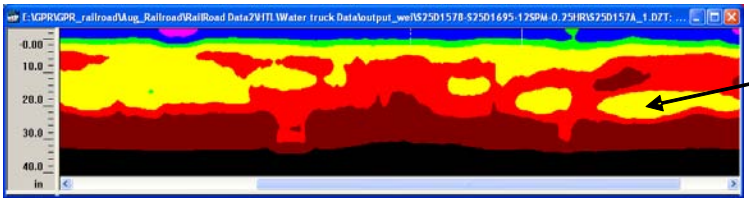

(b) Data collected 0.25 hr after spray.

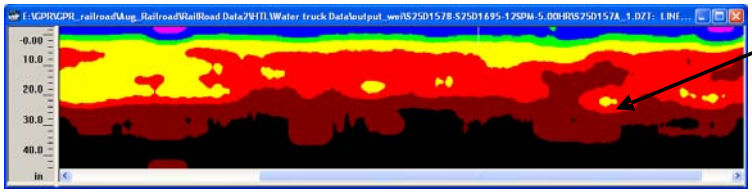

(c) Data collected 5 hr after spray.

Figure 5. Data collected from ballast after water sprayed on surface at various times (Al-Qadi et al., 2007).

Xu et al. (2004) used texture analysis methodology to process 400 and 900 MHz antenna data. The texture analysis was performed to track the interfaces between different layers. Xu derived a ratio edge detector in the wavelet domain. The results proved that the edge detector can successfully enhance the boundaries that separate different layers.

In general, a great deal of work using GPR for railroad structure assessment has been done in the past 3 years. Ground penetrating radar is clearly a useful tool that, if properly used, can benefit the railroad industry.

1.2.2 Phases I through III

The work performed in this task of the project builds on work performed in Phases I-III. Many important developments were made during the first three phases. These developments include: (1) determining the antenna type for data collection, (2) establishing the antenna configuration to use for data collection, (3) developing preliminary data processing methodologies, and (4) demonstrating the effectiveness of GPR for ballast condition assessment (Hyslip et al., 2005).

A significant quantity of data was obtained with 1 GHz horn antennas in the first three phases of this project. The strategy for processing data developed in the first three phases of the project involved mapping reflections associated with layer interfaces and quantifying textural

differences in the data to distinguish clean from fouled ballast. The textural differences in GPR data obtained from ballast using 1 GHZ horn antennas tend to be subtle and can be masked by clutter in the data. Figure 6 shows a section of data from the 1 GHz horn antennas presented in the Final Report from Phases I–III.

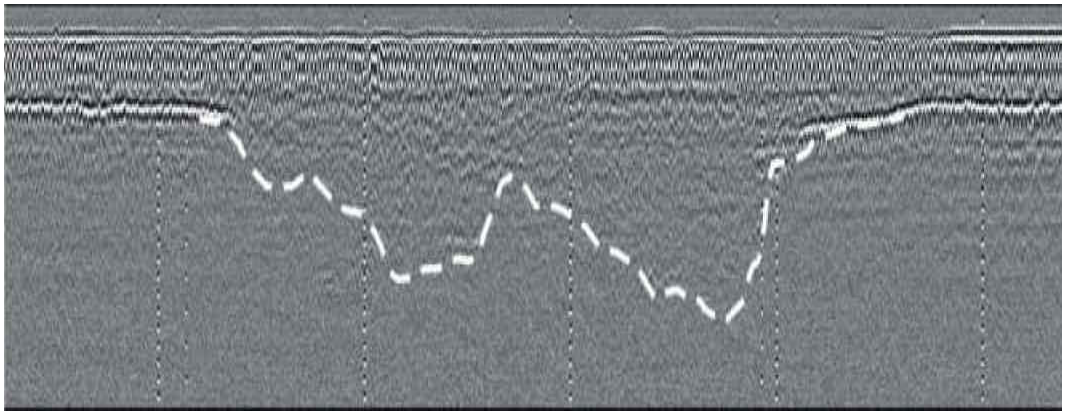

Figure 6. Section of GPR data obtained with 1 GHz horn antennas during first three phases of FRA project (modified from Hyslip et al., 2005).

Detailed inspection of Figure 6 reveals slight textural differences between the ballast and subballast layers in the central portion of the figure. A dotted line demarcates the interpreted boundary between the two layers. The inherent difficulty in accurately mapping the ballast condition and predicting ballast thickness in this region is readily apparent. This limitation in the technique has been eliminated using higher-frequency air-launched antennas. However, the trade-off of the enhanced resolution provided by the higher-frequency antennas is less penetration depth.

2. Utilization of 2 GHz Horn Antennas for Ballast Condition Assessment

Between phases III and IV of the project a 2 GHz horn antenna was developed at GSSI. This antenna was tested during initial data collection efforts at the High-Tonnage Loop (HTL) test track at TTC. The intent of the trip was to start collecting a database of 1 GHz data and ground truth for algorithm development. Fortunately, the 2 GHz horn antenna was brought along on the trip and a short section of data were collected to observe its performance compared to the 1 GHz horn antenna.

In Figure 7, a section of data collected in May 2005 from the 2 GHz horn antenna are compared to 1 GHz horn antenna data collected at the same time. As can be seen, much

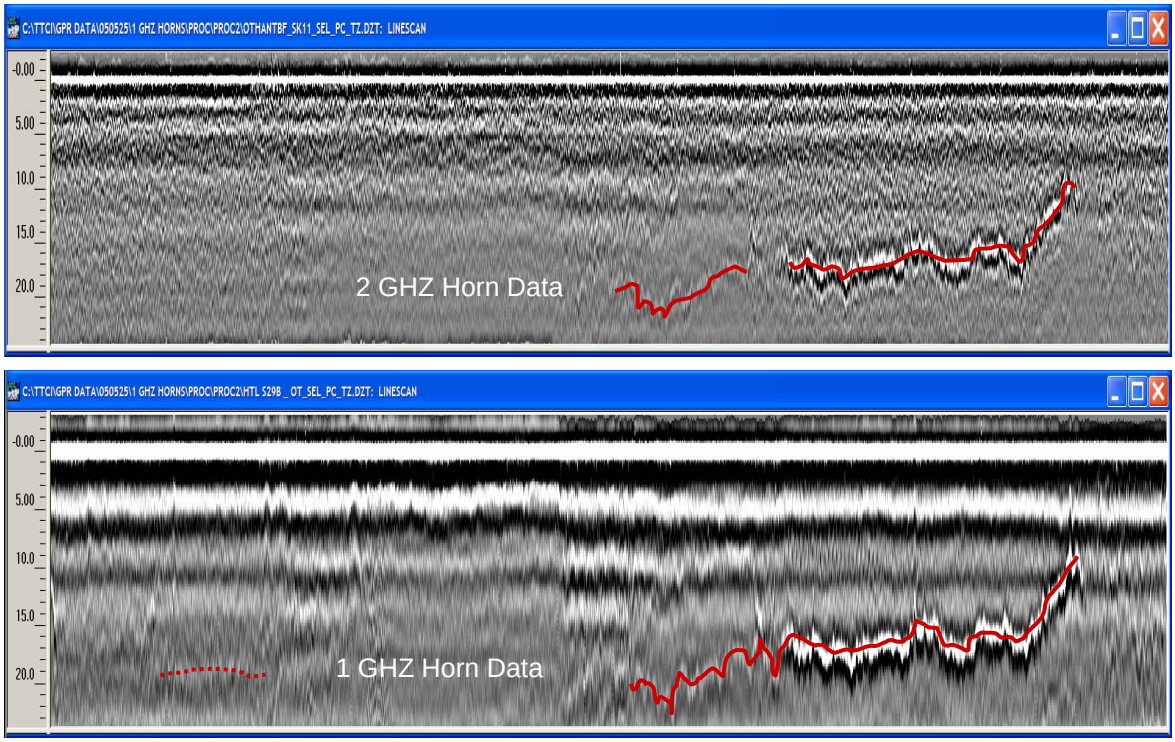

Figure 7. Comparison between 2 GHz (top) and 1 GHz (bottom) data obtained along same section of HTL loop track. Solid and dashed lines show interpreted ballast bottom. The only processing applied to this data was a time-zero correction. The depth units are inches in the vertical scales on the left side of the figure.

less horizontal banding is observed in the 2 GHz data. The clutter-free near-surface region between 0–10 in within the 2 GHz data is especially significant. The same depth range in the 1 GHz data contains a large consistent reflection associated with the reflection from the top of the rail. The reflection from the interpreted ballast bottom is easily tracked along approximately half of the section in data from both antennas in Figure 7. This leaves approximately half of the section that cannot be interpreted using layer-tracking algorithms.

Closer inspection of Figure 7 reveals significant textural differences in the 2 GHz data. These textural differences are manually tracked as shown by the yellow line and arrows in Figure 8 .

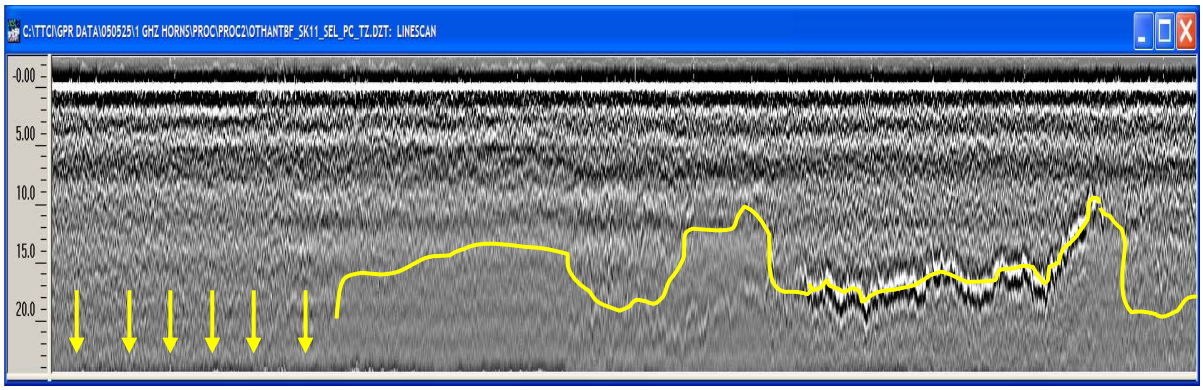

Figure 8. Interpreted 2 GHz horn antenna data from Figure 4 using textural differences in the data. The depth units are inches in the vertical scales on the left side of the figure.

The clear distinction in unprocessed 2 GHz data between areas that possess no reflections and areas that have a mottled appearance from numerous incoherent scattering from void space in the ballast aggregate was a very promising development that necessitated a change in data collection and processing strategy. This finding potentially meant that clean ballast could be distinguished clearly from fouled ballast without the requirement of a layer interface reflection. The next section describes the theory underlying this data interpretation approach.

2.1. Theory

The intensity of electromagnetic (EM) wave scattering from discrete scattering objects increases as the dimensions of the objects approach the wavelength of the radiated energy. In the case of clean ballast, the scattering objects are voids between the ballast aggregate. Ballast aggregate may vary depending on the railroad and track application. However, for the purposes of this report, in dimensions from 1.5 in to 4 in were assumed. The wavelength corresponding to the center frequency of the 2 GHz antenna is 5.9 in within air. The percentage void volume of clean ballast is on the order of 30 percent. The void size distribution in clean ballast necessarily depends on the ballast size and shape. To maintain a void volume percentage of 30 percent, a compacted, well-graded, equi-dimensional ballast must maintain void sizes ranging from less than 30 percent of the aggregate size to greater than 30 percent of the aggregate size. A roughly equi-dimensional void volume that is 30 percent of a uniformly dimensioned aggregate corresponds to sizes ranging from 0.5 to 1.2 in, which translates to a ratio of 0.08 to 0.2 of the dominant wavelength.

The reflection from a thin layer that is one-tenth of the radar wavelength can be discernable in GPR data. Randomly positioned voids totaling 30 percent of the volume of a material and sized one-tenth to two-tenths in relation to the dominant radar wavelength would predictably create a discernable scattering pattern that would vary laterally and vertically. Infilling of the void space with fines would effectively decrease the void space, resulting in diminished

scattering. This is, in fact, observed in GPR data collected with the 2 GHz horn antennas. Figure 9 schematically illustrates the concept.

Implementation of this model for assessing the depth of clean ballast simply entails detection of the depth corresponding to significant loss in scattering energy in the GPR data after corrections have been made to accommodate signal scattering, spreading, and absorption losses that attenuate the energy received from increasing depths. This is the approach that has been taken thus far in the project.

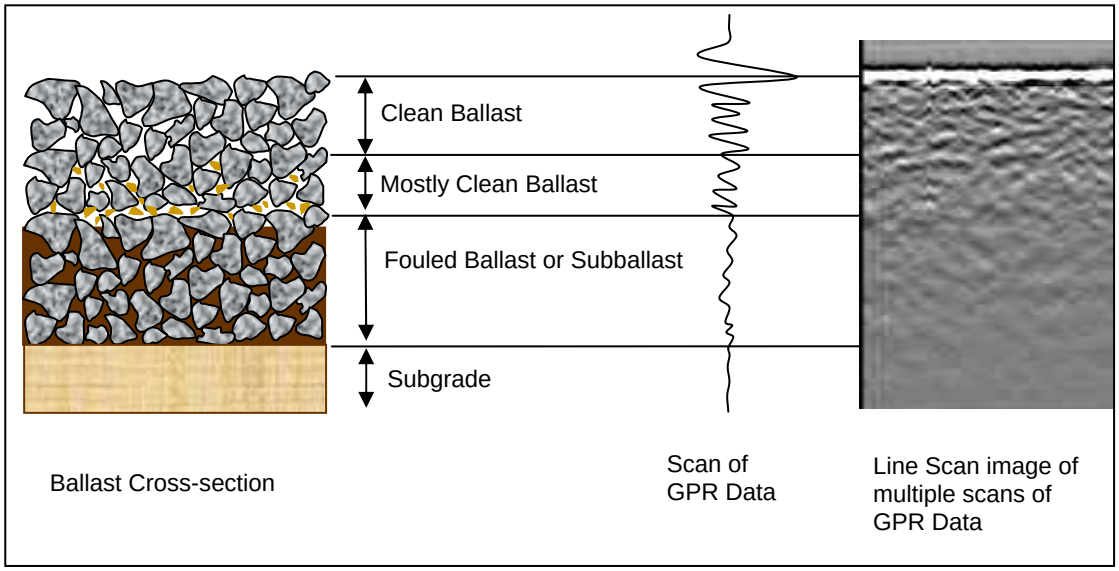

Figure 9. Interpretation of 2 GHz horn antenna data.

2.2. Implementation

Data were collected with three 2 GHz air-launched antennas mounted as shown in Figure 10. This is nearly the same as the configuration established in the first three phases of the project. The notable difference between the two setups is the data obtained from the center antenna. In the first three phases, two antennas were positioned between the rails with one antenna transmitting to a second antenna positioned parallel to the first antenna in a manner so that both antennas were alternately positioned over a tie or between two ties (Olhoeft and Selig, 2002). The 2 GHz horn antennas radiation pattern is much more focused than the 1 GHz horn antennas. Data collection using a single 2 GHz horn antenna mounted between the rails and orientated with the same polarization as the outer two antennas provided reasonable data. The outer antennas are mounted 6 in outside the end of the ties and at a height of 14–16 in. It should be noted that this configuration, while optimum for obtaining air-launched antenna data for the 2 GHz antennas, does not meet Plate C specifications, which specify that the minimum clearance above the ties at that location is greater than 32 in. The height limitation was not a factor in data obtained in Wyoming and Alaska. However, the antennas had to be moved at passenger platforms during data collection on Amtrak.

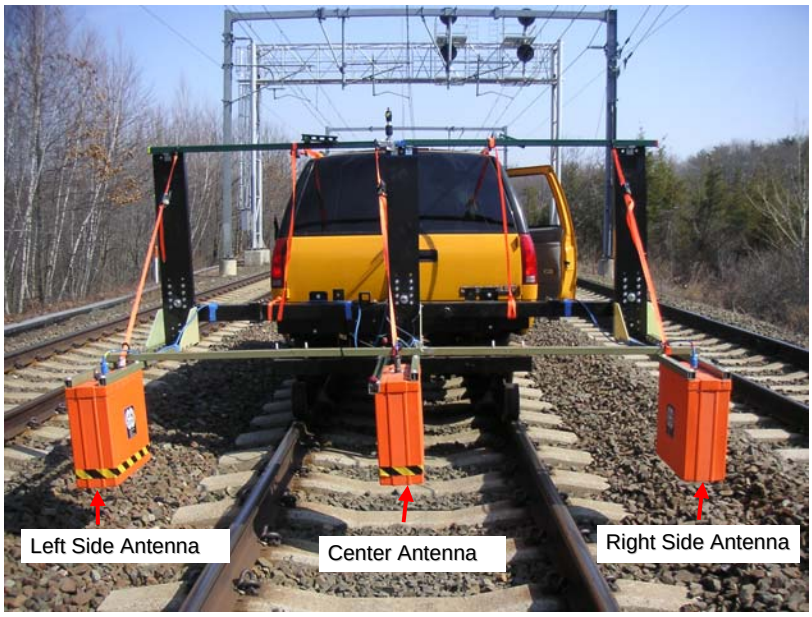

Figure 10. Data collection setup for the 2 GHz horn antennas.

The antennas were mounted at as low a height as practical to clear obstacles during data collection. Most data were obtained with the antennas at a height of 14–15 in above the ties. Table 22 lists the data collection settings on the GSSI SIR-20 units used for all the data.

Table 2. Two GHz Data Collection Settings on SIR-20s

Setting	**Value**
Time Range	15 ns
Scans/ft	4-12
Transmit Rate	Center antenna 200 KHz, Outer antennas 300 KHz
Gain	Single Point, varied depending on antenna
Vertical Low-Pass Hamming Filter	5000 MHz
Vertical High-Pass Hamming Filter	250 MHz

Two of the 2 GHz antennas used to collect data were FCC certified. The other antenna was built prior to the introduction of FCC radiation limitations. The output power of this antenna is approximately 6 dB higher than the other antennas. Consequently, this antenna is much less sensitive to external noise, which in some locations, significantly interfered with the reflections from the ballast.

Initial data obtained at TTC were collected at a density of 12 scans per foot. These data were subsequently decimated to different degrees and processed. Some loss in horizontal resolution was necessarily observed in processed data at lower scan densities, but this was the only notable difference in processed data quality. The upside of collecting data at lower scan densities is that it increases the maximum speed at which the data can be collected. Data obtained with a density of 4 scans/ft permitted data collection at a speed of 25 mph.

A 15 nanosecond time range yields data to a depth of approximately 30 in. It is possible to collect data at longer time ranges and thereby increase the depth range. However, the intent of this study was mapping the clean ballast thickness, which is of particular concern near the bottom of the ties.

The GPR data were collected using two GSSI SIR-20 control units. A distance-measuring instrument (DMI) was attached to the lug nuts of one of the back wheels of the hi-rail vehicle. The DMI provided pulses at regular distance intervals that were used to trigger the GPR control units. GPS and video data were obtained in addition to the GPR data at each data collection location.

3. 500 MHz Horn Antenna Development

An antenna with a center frequency much lower than 2 GHz is necessary to image the ballast and subballast layering to depths of 5–7 ft. This depth range is typically imaged by 400–500 MHz GPR antennas. However, these commonly used GPR antennas are designed to be in contact with the ground. This restriction is unacceptable for data collection on railroads at a reasonable data collection speed. Air-launched antennas are designed differently than ground coupled antennas. The air-launched design, commonly referred to as a horn antenna, focuses the radiated energy into the ground. GSSI developed a 500 MHz horn antenna in the spring of 2007 for use in modification task one.

3.1. Theory

The theoretical underpinning behind the use of GPR for mapping the subballast and subgrade is the fact that the ballast, subballast, and subgrade are typically comprised of materials with dissimilar EM properties. Hence, a radar wave will typically be reflected at the ballast-subballast and subballast-subgrade layer interfaces. The magnitude of the reflection is related to the contrast in EM properties. Equation 1 is a commonly used equation that approximates the reflection amplitude at the layer interface to the layer properties on either side of the interface assuming that the layers contain no magnetic minerals:

$$\rho = \frac{\sqrt{\epsilon_1} - \sqrt{\epsilon_2}}{\sqrt{\epsilon_1} + \sqrt{\epsilon_2}} \qquad (1)$$

where:

ρ = reflection coefficient;
ϵ_1 = relative permittivity of upper layer; and
ϵ_2 = relative permittivity of lower layer.

Given that clean ballast typically possesses a relative permittivity of 3–4 and dry subballast and subgrade possess relative permittivities on the order of 5–9, it is reasonable to expect a substantial reflection from the ballast–subballast interface. Water has a relative permittivity of 81. The huge difference between the relative permittivity of water and typical track substructure materials means that the presence of water is typically inferred from anomalous high amplitude reflections in GPR data from track substructure.

It is not certain that there will always be a reflection at the interfaces between the different substructure layers. The relative permittivity of fouled ballast increases as the fouling material invades the void space between the aggregate. Additionally, the fouling material has a higher moisture adsorption capacity, which means that all other things being considered, a fouled ballast will have more moisture than an adjacent clean ballast. As a result, a weak or non-existent reflection is not uncommon from the ballast–subballast interface in areas where the ballast is substantially fouled. Likewise, there are scenarios where there is no reflection from

the subballast–subgrade interface due to the fact that the relative permittivity of the subballast can be nearly the same as common coarse-grained subgrade.

The absence of layer reflections and the relative amplitudes of the reflections at the layer interfaces can be an important indicator of the condition of the track substructure. This is the rationale behind the use of GPR for mapping the subballast and subgrade layers. Numerous examples of the application of GPR exist for detecting track structural problems associated with these deeper layers in the report from Phases 1–3 of this project (Hyslip et al, 2005).

3.2. Implementation

The newly developed 500 MHz air-launched antennas were tested on the HTL at TTC in June, 2007. The data obtained at TTC were obtained with two antennas, one mounted between the rails and the other mounted 6 in off the end of the ties. Several antenna orientations were tested. By mounting the antennas at an orientation of 45 degrees relative to the rails, the reflections from the rails and reinforcement in the concrete ties were optimally reduced. Figure 11 shows the data collection setup. This configuration was subsequently used for data collected in Wyoming and Alaska in 2007.

Figure 11. Data collection setup for initial TTC data collection.

A series of 12 cross trenches were dug to verify the outer and inner antennas could map the subballast and subgrade layer interfaces. Good correlation was observed between the layers tracked in the 500 MHz antenna data and the observed layering in the cross trenches. Figure 12 shows the 500 MHz data versus ground truth at one of the ground truth locations.

Several findings from examination of Figure 12 included: (a) good correlation occur between the locations of reflections in the GPR data and the ground truth; (b) the reflections from the layers are observed in data obtained from the center antenna and the antenna on the shoulder, though the data from the shoulder is less cluttered because there are no tie reflections; and (c) the deepest reflection in the GPR data corresponding to a layer interface in the cross-trench is at 42–48 in. Though no ground truth was obtained from layers below 48-inches deep at TTC, it was anticipated that the antenna would be able to resolve deeper layers because the amplitude of deeper reflections at TTC were well above the noise floor of the data. This assumption was validated by analysis of data obtained in Wyoming and Alaska, which is presented later in this report.

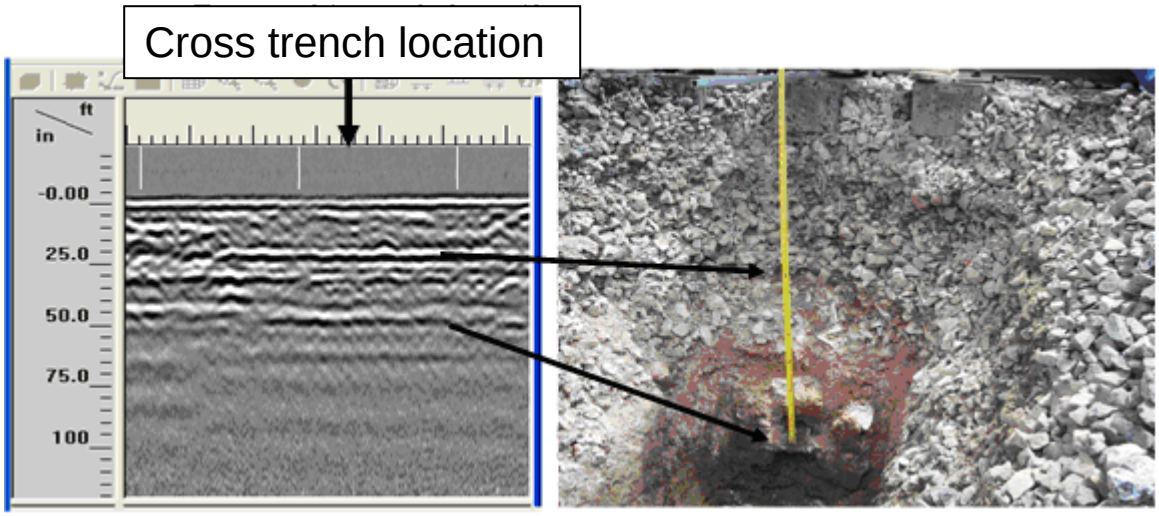

(a) 500 MHz data on shoulder **(b) picture of cross trench**

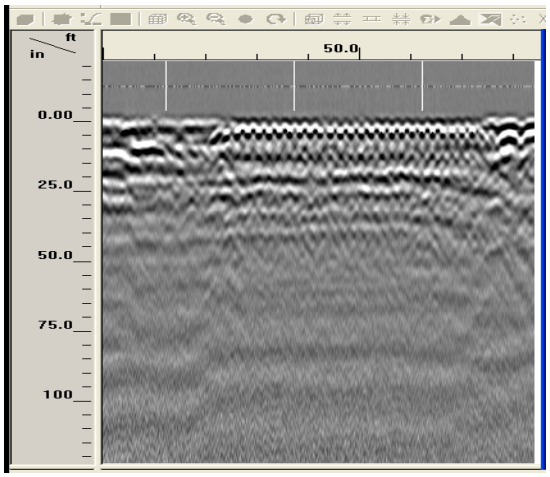

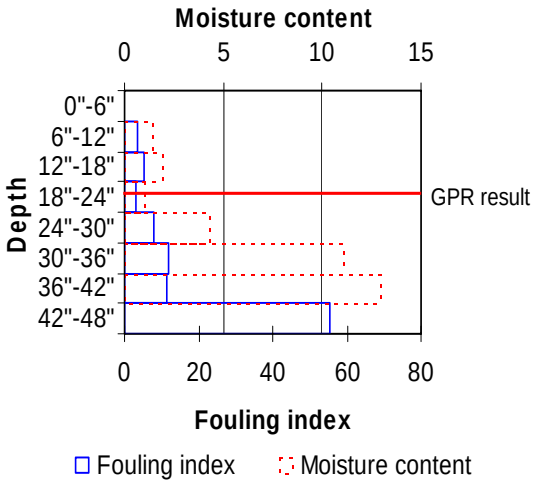

(c) 500 MHz data from between rails **(d) fouling index and moisture content vs. depth**

Figure 12. Comparison of 500 GPR data and ground truth at one of cross trenches dug at TTC: (a) 500 MHz data on shoulder; (b) picture of cross-trench; (c) 500 MHz data from between rails; and (d) fouling index versus moisture content obtained from analysis of samples extracted from cross-trench.

The optimal data collection configuration with the 500 MHz antenna was found to be at a 45-degree angle relative to the ties and rails. A configuration was successfully tested at TTC with the 500 MHz antenna mounted between the rails and the 2 GHz horn antennas mounted on the shoulders. This configuration was subsequently used for data collected in Wyoming and Alaska in 2007.

Table 3. 500 MHz data collection Settings on SIR-20s

Setting	**Value**
Time Range	50 ns
Scans/ft	4-12
Transmit Rate	200 KHz
Gain	Single Point, varied depending on antenna
Vertical Low-Pass Hamming Filter	1645 MHz
Vertical High-Pass Hamming Filter	50 MHz

4. Data Processing

The first task of the project was focused exclusively on data collection and analysis of the 2 GHz horn antenna data. The follow-on task, Modification Task One, involved the development and testing of a 500 MHz antenna. The data processing approach associated with the 500 MHz antenna was necessarily much different than the 2 GHz data. The different data processing methodologies are described below.

4.1. 2 GHz Horn Antenna Data

Initial inspection of the 2 GHz horn antenna data revealed the broad amplitude decay characteristics of scattering from the void space in clean ballast. An amplitude envelope could be constructed by connecting the peaks of the reflections down a scan as shown in Figure 13. A very low amplitude envelope could then be associated with fouled ballast or subballast. Likewise, a sudden change in the slope of the amplitude envelope would indicate a change in ballast condition. This is the principle behind the scattering amplitude envelope approach. To achieve the effective amplitude envelope a number of standard data processing steps have been implemented. These steps have been developed based on data collected with extensive ground truth at one location and applied to data collected on commercial railroads elsewhere in the country. A brief description of each data processing step follows.

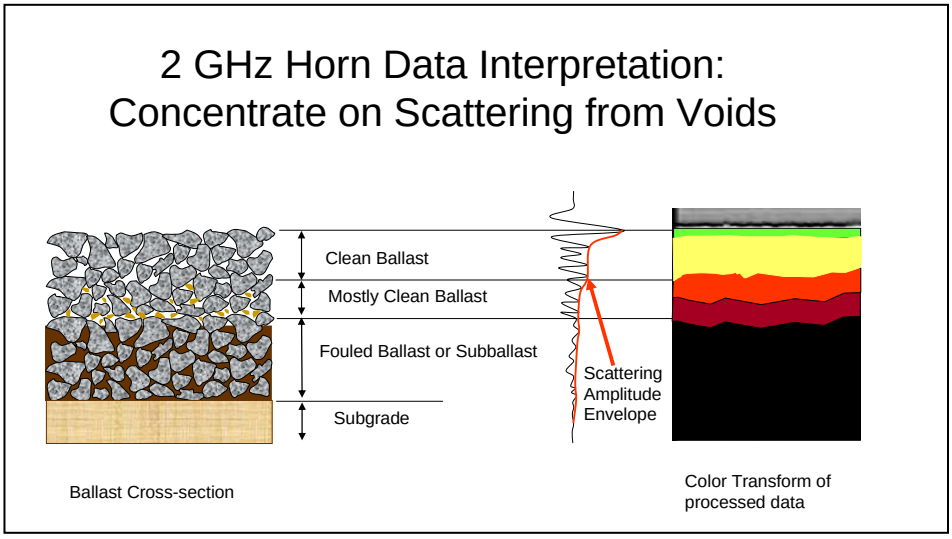

Figure 13. Construction of scattering amplitude envelope from GPR data.

- *Time-Zero Correction*. The first significant reflection following the direct-coupling between the transmit and receive horn antennas is the reflection from the ballast surface. This reflection is the "time-zero" to which all subsequent reflections are referenced. Figure 14(a) and Figure 14(b) show a section of data before and after application of a time-zero correction, respectively. This processing step is typically performed on GPR data.
- *Background Removal.* Close examination of the time-zero corrected data shown in Figure 14(b) reveals a dark horizontal band in the data corresponding to an arrival

time of 2.5 ns. Low amplitude horizontal banding in horn antenna data collected over rails can be due to reflections from the rails or antenna clutter. The banding is readily removed using a background removal filter as shown in Figure 14(c). The background removal filter chosen for the data was a moving average subtraction with a window of 1,023 scans. Because the scattering from voids associated with clean ballast are not correlated in time over distances greater than a fraction of a foot, the background removal filter is a very effective clutter reduction tool. This is readily apparent from comparison of the pre- and post-background removal filtered data in Figure 14(b) and Figure 14(c), respectively. This type of filtering is safe when preservation of layer boundary reflections is not a concern. Layer boundary reflections will vary in time to some degree and therefore will not be eliminated by the background removal filter. Some amplitude and phase distortion will typically occur, however. This distortion does not hinder the detection of significant layer reflections in the fully processed data.

- *Gain Restoration*. All of the GPR data were collected using a single point gain. This means that no amplitude adjustment was applied to the signal arriving from greater depths. The later arriving signal will naturally possess lower amplitude in clean ballast due to spreading, scattering, and absorption losses. This natural loss of signal strength was corrected empirically by assessing the log-linear gain curve that would negate the amplitude decay in an exceptionally thick, clean ballast section. This correction was found to be a 0–18 decibel (dB) correction, where 0 dB was applied at the top of the scan, 18 dB applied on the bottom of the scan, and the linearly interpolated gain values applied to samples in between. This correction appears to be robust in that it has been successfully applied to data from two substantially different ballast compositions and conditions. Figure 14(d) shows a section of data after the gain restoration step. Equation 2 presents the relationship used to compute the decibel level from reflection amplitudes:

$$L_{dB} = 20 \log_{10}\left(\frac{A_1}{A_0}\right) \quad (2)$$

where:

L_{dB} = change in amplitude in terms of dB between A_1 and A_0
A_1 = Amplitude value;
A_0 = reference amplitude value.

- *Hilbert Transform*. The reflections in GPR data contain waveforms with positive and negative polarity peaks. Construction of an amplitude envelope requires only one polarity. This leaves a number of options, including, but not limited to, selecting only the positive peak, selecting the peaks after calculating the absolute amplitude of the signal, and selecting the peaks following application of the Hilbert Transform. The Hilbert Transform magnitude yields an amplitude envelope of each reflection waveform. This envelope encompasses both the positive and negative polarity portions of the waveform and is thus the most intuitive peak-amplitude representation of waveforms. Figure 14(e) shows the data appearance following the Hilbert Transform.

- Horizontal Smoothing
  Scan-to-scan variations in the locations and amplitudes of the reflections from voids in ballast are evident in Figure 14(e). These random fluctuations are effectively minimized by performing a horizontal boxcar moving average. The length of the moving average window necessarily determines the maximum horizontal resolution of ballast thickness variations. All data were processed using an 8-ft horizontal moving average. This filter length is subject to change depending on the type of survey. For network-level surveys, a larger moving average may be desirable. For detailed project-level surveys where ballast thickness variations on the order of several ties in length are preferable, a smaller moving average window is necessary. Figure 14(f) shows data following application of the horizontal moving average.

- Vertical Smoothing
  Subsequent to horizontal smoothing, the data are smoothed in the vertical (i.e. time) direction by applying a 200 MHz Hamming window filter. Post-filtered data are shown in Figure 14(g). Application of the vertical low-pass filter diminishes the vertical resolution of the data.

The final step transforms the data from amplitude values to color ranges, as shown in Figure 14(h). Each color in Figure 14(h) represents a 5–6 dB amplitude range. Examination of the processed data in color-coded format provides rapid assessment of the ballast condition from the top of the ties to a depth of approximately 30 in. Three important features are in the color-coded data that will be examined in detail in the data analysis section: (1) the color versus depth; (2) the rate of color transition versus depth; and (3) color reversals versus depth. Each of the three features is easily extracted from the color-coded data using automated routines. This methodology was initially implemented to process the TTC data discussed in Section 5.1.

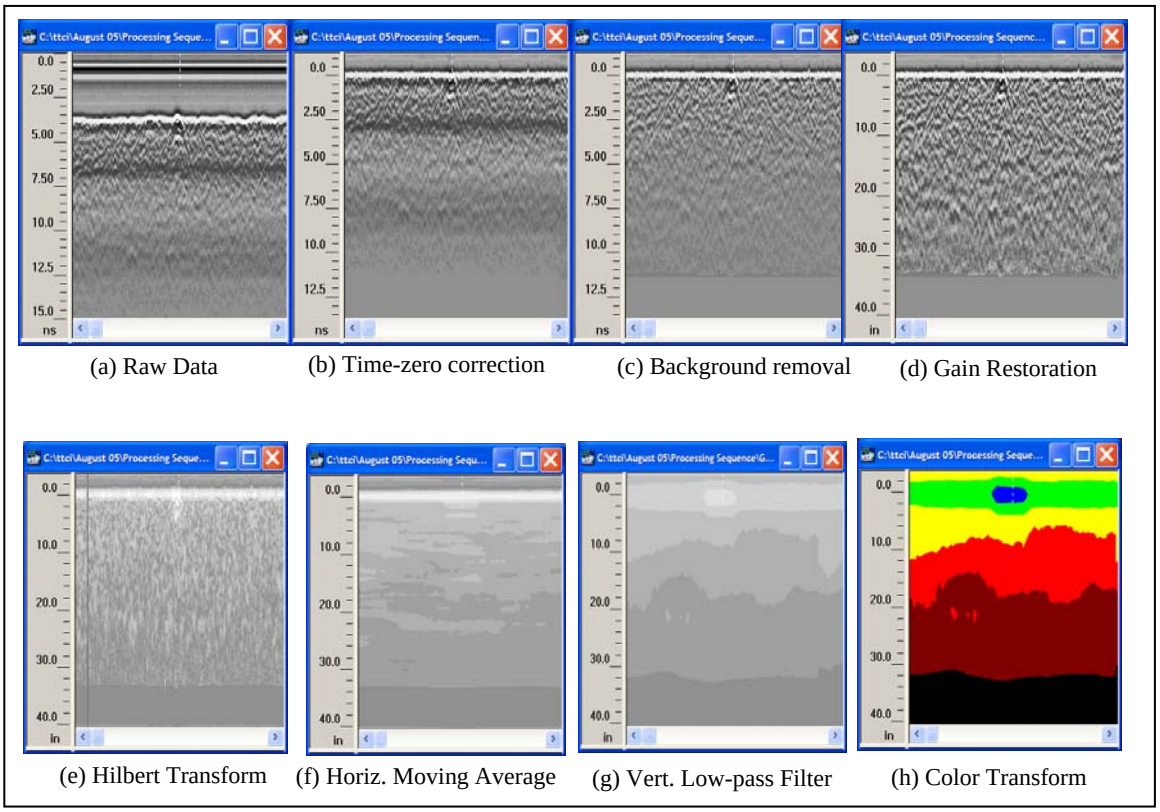

Figure 14. Data processing and display steps applied to TTC 2 GHz GPR data.

Data presented in Sections 5.2–5.5 were processed using a slightly different methodology whereby the horizontal low pass filter was replaced by a 1,000 MHz high pass FIR filter, which was implemented as the first post-processing step. The 1,000 MHz high pass filter effectively removes the low-frequency dark band in the data without impacting significant layer reflections that could be, for example, associated with trapped moisture.

A second difference in the data processing associated with Sections 5.2–5.5 was the last step applied to the data—a transformation to ballast condition color-coding. Three significant developments were implemented: (1) a highly-desirable self-calibrating feature, (2) the signal-to-noise level monitoring of the data, and (3) both the rate of scattering amplitude decay and total scattering amplitude decay were accommodated in the color transformation. These processing changes were introduced after data from Amtrak and BNSF track were obtained in 2006. All data presented in sections 5.2–5.5 were processed using this color transform step.

4.2. 500 MHz Horn Antenna Data

The 500 MHz data were processed differently than the 2 GHz data. After initial decimation of the data from a 13.2 scans/m (4 scans/ft) data collection density to 0.3 scans/m (1 scan/ft), a time-zero correction was applied. Next, a horizontal background removal was performed, where the background scan was obtained by averaging all the scans in the file. File lengths were typically 8–16 km (5–10 miles). Subsequently, a 6 m (20 ft) horizontal moving average

was applied to the data to improve layer reflection continuity. Finally, a 0–42 decibels (dB) 2 point gain was applied to accommodate for natural signal propagation loss. This correction was empirically derived from visual inspection of the data from the Orin Subdivision and Alaska Railroad. After implementation of the amplitude correction, anomalous amplitude reflections can be easily detected irrespective of their depth. Figure 15 shows the data processing steps applied to the 500 MHz data after decimating it to 1 scan/ft density. The fact that the same amplitude correction has been applied to data obtained from two very diverse track substructures is indicative that the correction values may be usefully applied to data obtained from other track substructures.

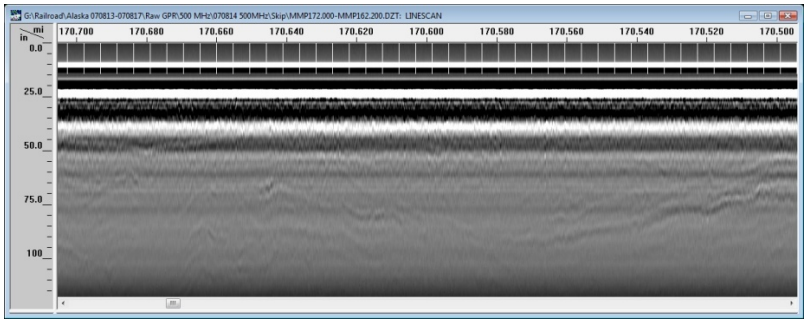

(a) Unprocessed 500 MHz data, 1 scan/ft data density

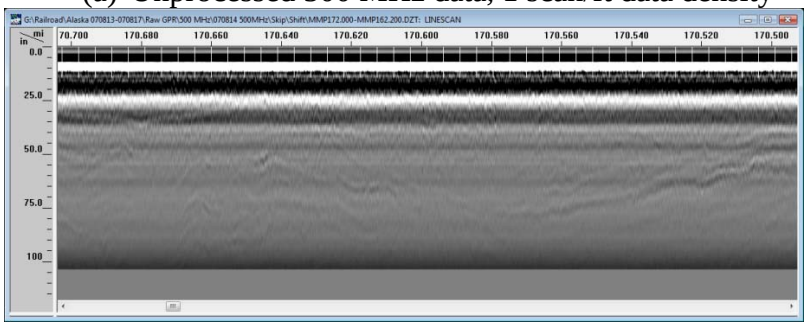

(b) Time-zero Correction

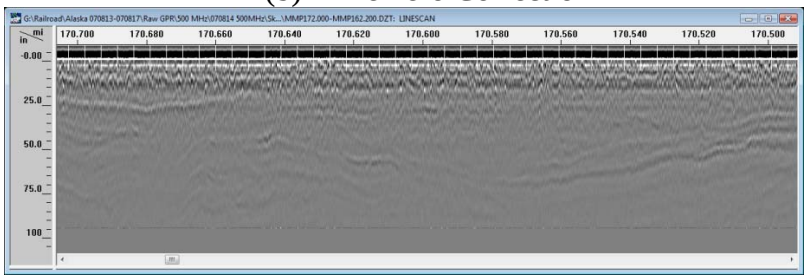

(c) Background removal

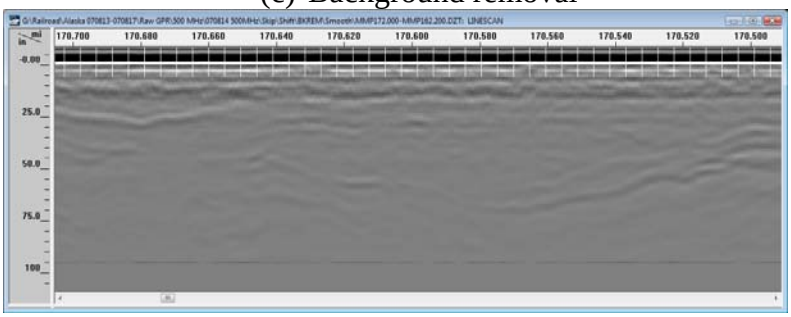

(d) Horizontal smoothing

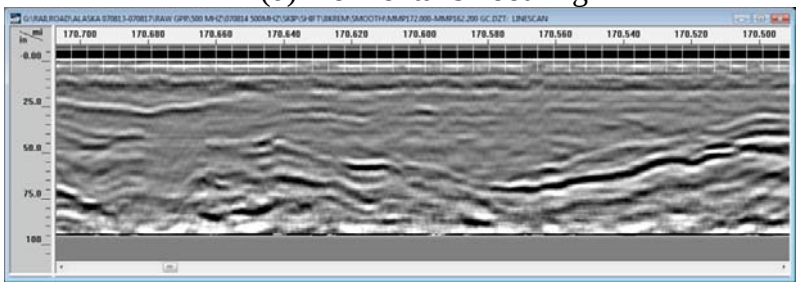

(e) 0-42 dB 2-Point Gain

Figure 15. Data processing and display steps applied 500 MHz data.

5. GPR Data Collection, Analysis, and Ground Truth

GPR data have been obtained at five different tracks. Fifteen miles of data were obtained on tracks in Pueblo, CO in August 2005. Ground truth collected at this location consisted of 15 cross trenches. Many ground truth methods, including dynamic cone penetrometer (DCP) data, visual inspection, and ballast sampling, were implemented at 14 of these cross trenches. The GPR data and ground truth from 12 trenches were subsequently used to develop the automatic data processing methodologies. Twenty-eight miles of GPR data were collected on Amtrak's tracks between Providence, RI and Sharon, MA in March 2006. Ground truth data consisted of five locations along the track where mud splashes were apparent on the ballast, ties, and rails. GPR data and ground truth are analyzed in detail in the following two subsections. GPR data were obtained on track in the Orin Subdivision, Wyoming and near Crawford, NE in June, 2006.

GPR data have been obtained at five different tracks. Table 4 lists the data collection locations, dates, amount of data obtained at each location, subgrade type, and available ground truth.

Table 4. Summary of data collection areas and ground truth.

Location	Date	Miles Data	Subgrade Type	Samples and Cross Trenches	# Mudspots	Records of Undercutting And Shoulder cleaning (miles)
TTC	8/05	15	Sand	15	0	-
Providence, RI – Sharon, MA	3/06	29.5	Sand/Clay	0	5	29.5
West Bill, WY– Shawnee Junction, WY	6/06	75	Sand	5	260	21.9
Crawford, NE-Ardmore, SD	6/06	34.9	Expansive Clay	0	54	0.55
Gillette Area, Wyoming	7/07	131	Sand	20	-	-
Alaska Railroad	8/07	97	Sand/Clay	20	-	-

In 2007, 2 GHz and 500 MHz horn antenna data were obtained along 228 miles of track in the Orin Subdivision, Wyoming, and on the Alaska railroad. It was fortuitous that at both locations repeat data could be obtained along portions of the track before and after a rainfall.

5.1. Transportation Technology Center Incorporated Track, August 2005

TTC track provided the ideal setting to collect GPR data and detailed ground truth via cross trenches. Two miles of data were obtained on HTL in August, 2005. Subsequent to data collection, 15 cross trenches were dug for ground truth. The condition of the ballast at fourteen cross trenches was assessed using a combination of visual and statistical methods. Ballast samples from each visually identifiable layer were collected for sieve analysis. A fouling index was calculated from the sieve data. This fouling index value was then assigned to the visually discernable layer from which the sample was extracted.

A separate analysis was performed using the DCP data. Significant ballast fouling was identified based on the following two criteria: (1) there is a significant decrease in the slope of the DCP values with increasing depth; or (2) the calculated California Bearing Ratio (known as CBR), from DCP data, over an extended depth range is 75 percent or less. The DCP data may mainly provide insight into the location of layer interfaces.

The accuracy of the ballast ground truth measurements is limited by the nature of the ballast structure. Due to the presence of a transition area at interfaces, approximate measurements of ballast thickness may not be identified visually. Often no clear boundary can be observed between fouled ballast, clean ballast, and the subballast or subgrade. A second limiting factor in collecting the ground truth was the location relative to the position of the antenna during data collection. The backhoe used to dig the cross trenches could not effectively dig a vertical cross-section directly below the antenna that was positioned 6 in from the edge of the ties. The closest location yielding a vertical cross-section was right at the edge of the ties where some differences in ballast compaction and fouling relative to the actual data collection location would be expected.

Figures 16–17 show two end-member comparisons of 2 GHz data and the ground truth at the respective cross trenches. Ground penetrating radar data are compared to ground truth from a moderately fouled ballast layer in Figure 18. Figure 16 shows an exceptionally clean ballast layer. The minimally processed and fully processed GPR data in Figure 16(a) clearly reveal no loss in scattering amplitude down to a depth of 20–25 in. The pictures of the cross-trench, Figure 16 (c), reveal a clean ballast layer to an approximate depth of 17 in from the top of the ties. A thin 3-inch layer of crushed ballast containing some moisture is also evident in the figures. This layer lies on top of fine-grained subgrade. Three samples were extracted from the face of the cross-trench at depths of 11, 18, and 21 in. The sieve analyses from the deeper two samples yielded the fouling index and weight percent moisture values shown in Figure 16(b). The fouling boundary interpreted from DCP data obtained within several ties of the cross-trench is shown as an orange line in Figure 16(b). The large drop in the GPR scattering amplitude envelope observed in Figure 16(b) corresponds well with the approximate location of the clean ballast bottom.

Close inspection of Figure 17(b), which compares the scattering amplitude envelope to ground truth from a ballast section fouled starting at approximately 2-inches deep, reveals rapid attenuation with increasing depth. A less steeply dipping scattering amplitude envelope is observed in Figure 18(b) from the cross-trench with intermediate fouling.

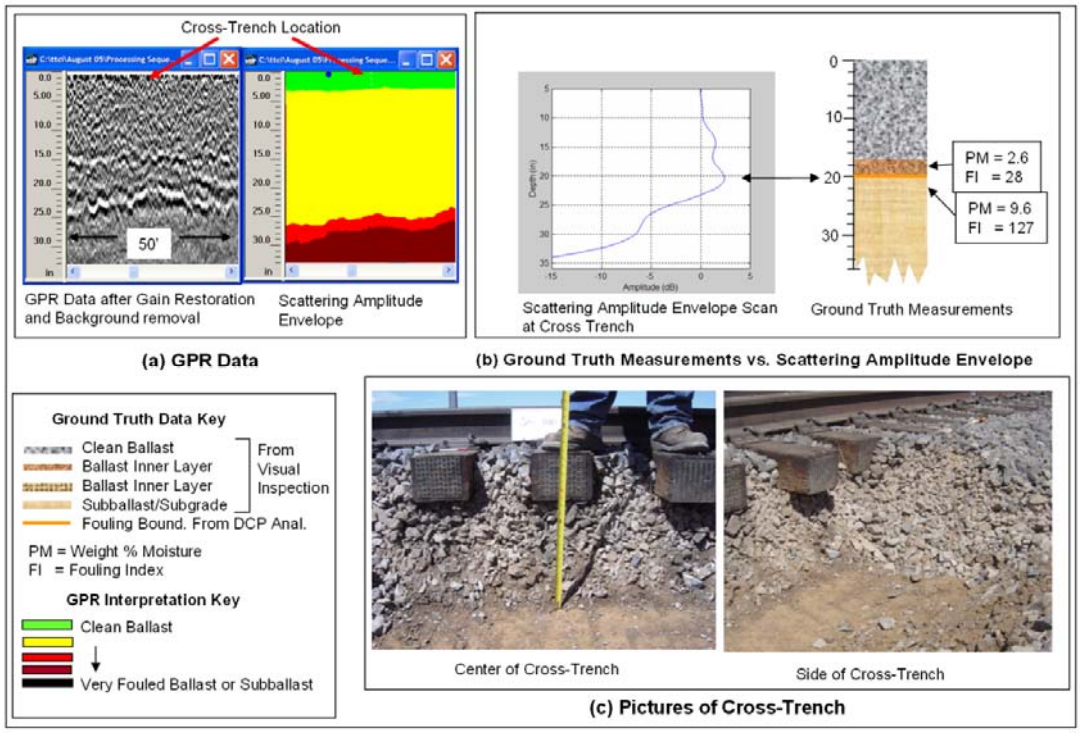

Figure 16. Comparison between GPR and ground truth data from section of thick, clean ballast layer.

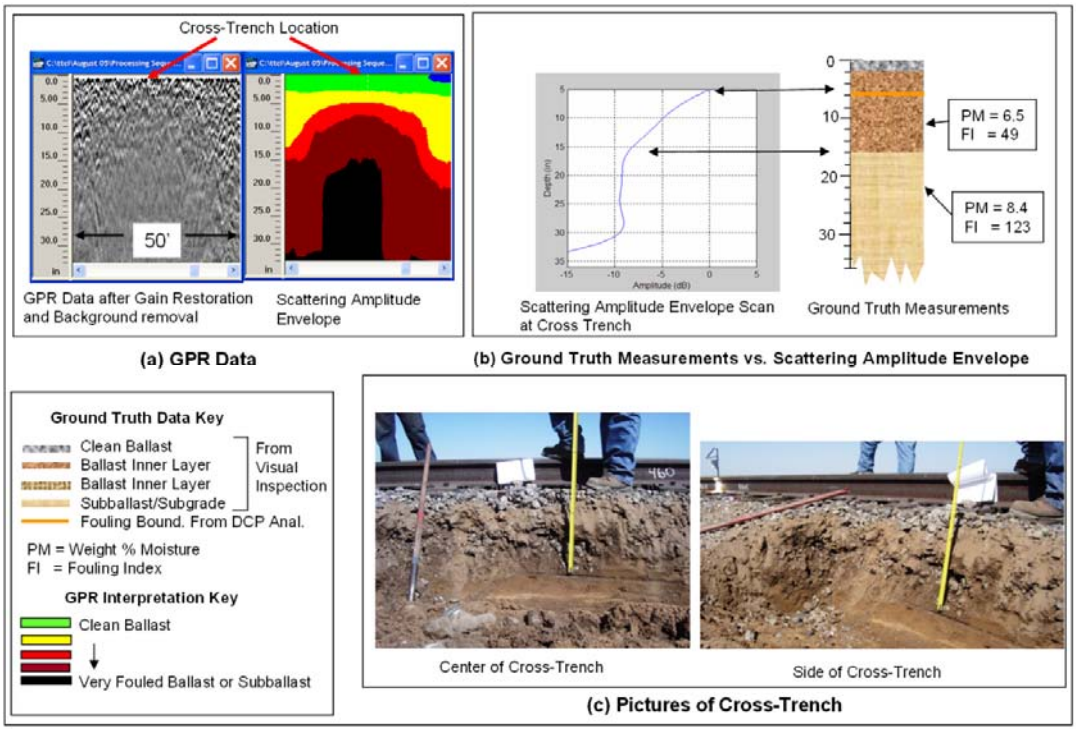

Figure 17. Comparison between GPR and ground truth data from section of thin, fouled ballast layer.

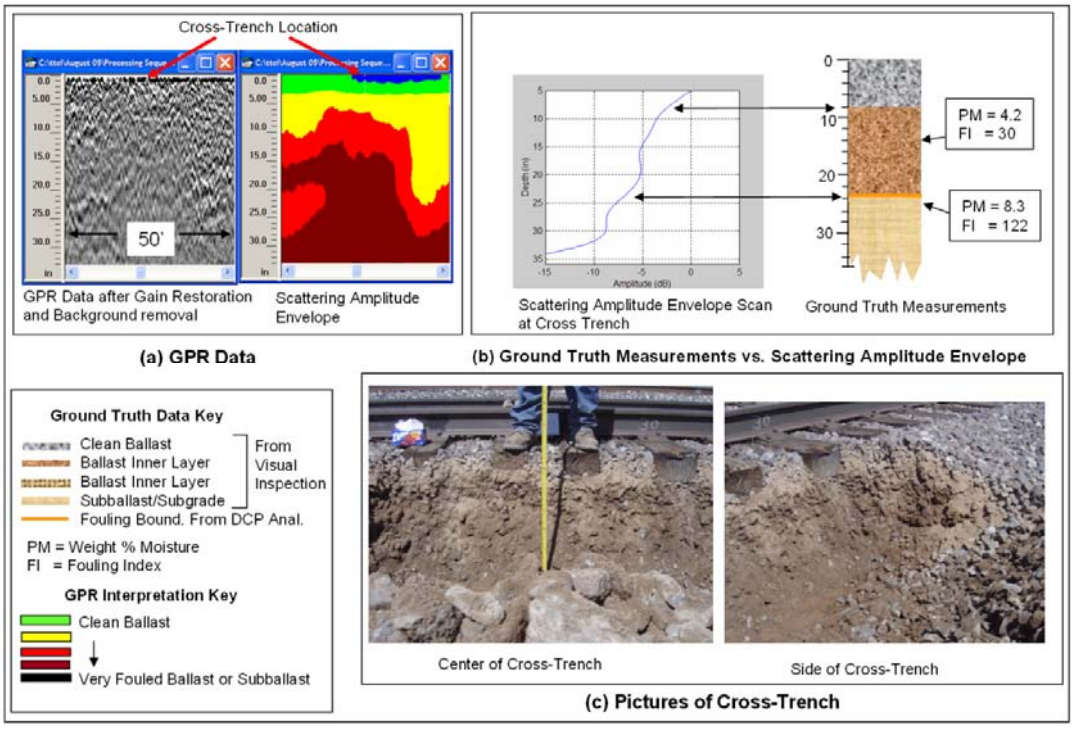

Figure 18. Comparison between GPR and ground truth from section of moderately fouled ballast layer.

Figure 19 presents the scattering amplitude envelopes of scans obtained at the locations of cross trenches. Focusing on the depth range from 5 to 25 in, two dominant trends in the amplitude curves are: (1) steady slope as illustrated by the red line in Figure 19; and (2) a stepped curve as illustrated by the green line in Figure 19. One might initially infer increased gradational ballast fouling with increasing depth from the red line and a constant ballast fouling followed by an abrupt transition from the green line.

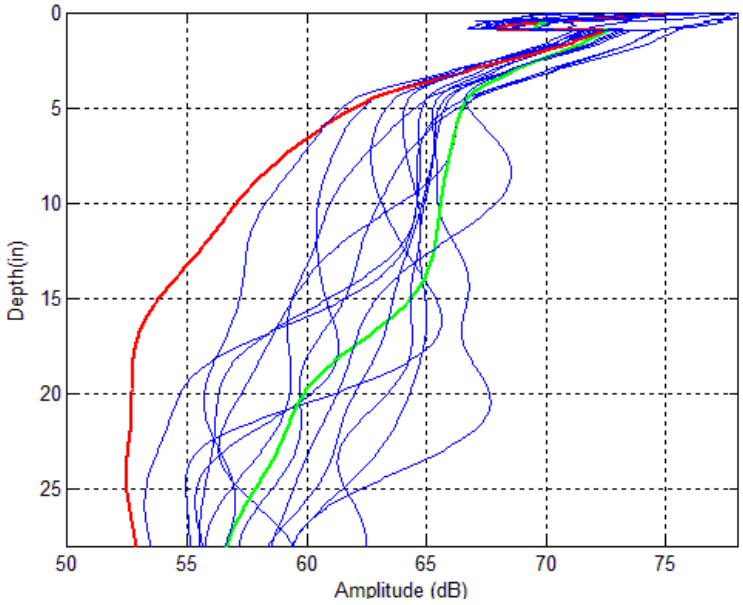

Figure 19. Scattering amplitude envelope at each cross-trench location. Red and green lines indicate end-member amplitude decay characteristics.

Figure 20 presents the scans from Figure 19 with the depth corresponding to the subballast or subgrade layer indicated by a red asterisk. A constant permittivity of 4 was used to construct the depth scale in Figure 20. The major layer boundary plots near the top or along the steep slope of curves with abrupt boundaries (black lines) and at different locations along the decay curves with consistent slopes (blue lines).

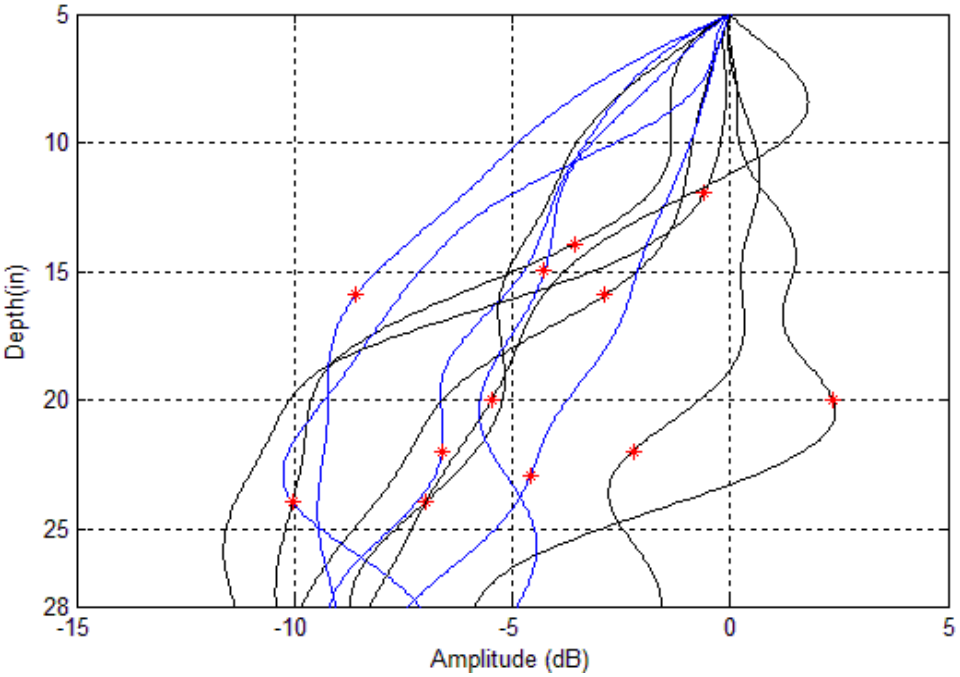

Figure 20. Scattering amplitude envelope at cross-trench locations with the location of the first major layer boundary indicated by red asterisks. Black lines are stepped-type decay curves and blues lines represent relatively steady slope amplitude decay. (Data from 3 cross-trench locations excluded due to incomplete or inconsistent sampling).

The relationship between the relative decay of the scattering amplitude envelope with increasing depth and the fouling index can be quantified by charting the average scattering amplitude envelope decay rate between 5 in and the top of the subballast or subgrade layer versus the weighted average fouling index of samples obtained within the ballast layer, as shown in Figure 21. This calculation was used for comparison with the fouling index because it does not require any amplitude calibration and minimizes the effect of local amplitude disturbances in the GPR data. A general trend of higher decay slopes versus increasing fouling index is observed. In keeping all other variables fixed, this relationship would be expected considering that the proportional void volume decreases with increasing fouling, hence, the scattering from the voids would also decrease. The rate of GPR scattering amplitude attenuation is also significantly influenced by moisture content. The colors of the points plotted in Figure 21 represent the relative moisture content of the samples. A general trend of lower-to-higher moisture content versus lower-to-higher fouling index is observed.

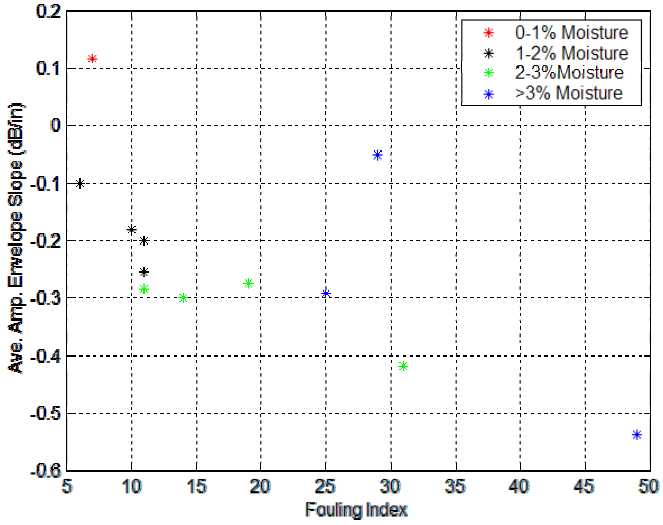

Figure 21. Average amplitude envelope slope in ballast layer versus weighted fouling index from sieve analysis of ballast sample. Colors indicate relative weighted percent moisture content.

The fouling index versus moisture content is plotted in Figure 22. A nearly linear relationship is apparent between moisture content and fouling index. The average scattering amplitude envelope slope versus fouling index is plotted in Figure 23, with the sloping amplitude envelopes plotted in blue and the stepped amplitude envelopes plotted in black. Six of the seven sloping amplitude envelopes, which are the blue dots in Figure 23, correspond to all of the samples with average moisture content greater than 2 percent in Figure 22. A general relationship occurs between the shape of the scattering amplitude envelope (i.e., steady slope or stepped) and moisture content. The sloping amplitude envelopes may arise from a constant attenuation rate when associated with higher moisture content; whereas the stepped scattering amplitude envelopes possess a low attenuation rate and lower moisture contents.

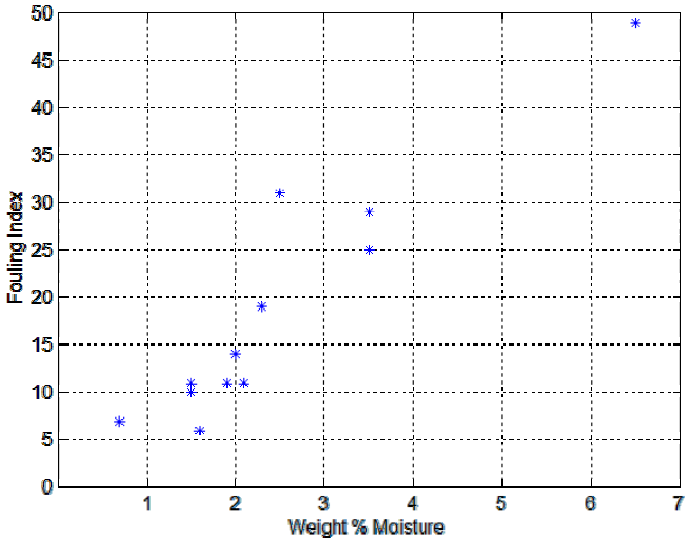

Figure 22. Weighted fouling index versus percent moisture of samples obtained within ballast.

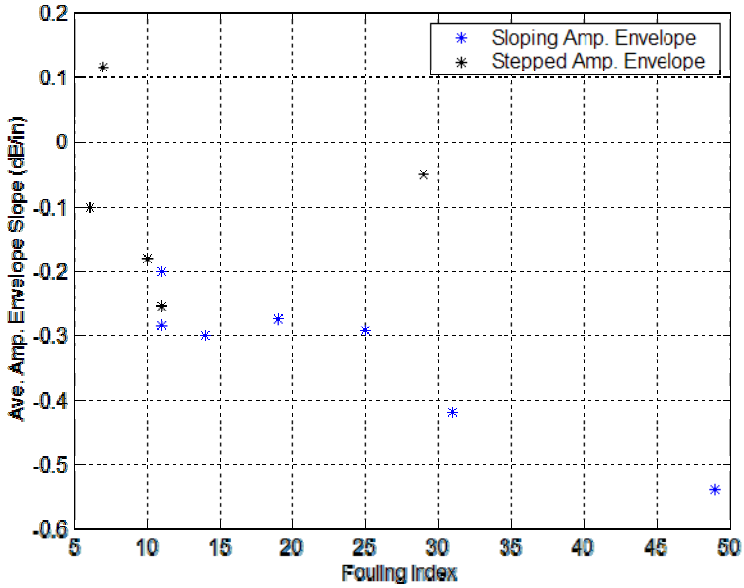

Figure 23. Average amplitude envelope slope in ballast layer versus weighted fouling index from sieve analysis of sample obtained within ballast. Blue and black points are from sloped and stepped scattering amplitude envelopes, respectively.

An expected increase in fines content would correspond to greater moisture retention capability. Because both fouling and moisture would increase the dielectric properties, although at different degrees, the research at this stage is not yet clear as to how much of the scattering amplitude envelope behavior is due strictly to moisture content versus progressive void filling with fouling material.

The general correlation between the scattering amplitude envelope characteristics, ballast fouling and moisture content presented in Figures 21–23 is a promising development with practical implications. First, the data processing strategy is very simple and easy to automate. Second, for this analysis, relative amplitudes are used, so no calibration is required. Third, the technique appears to be very sensitive to moisture content. Fourth, the technique can assess ballast condition without requiring reflecting boundaries in the data. Finally, the high vertical resolution provided by the 2 GHz horn antennas permits ballast evaluation in the depth range associated with the bottom of the ties.

One of the strengths of the scattering amplitude envelope approach is that it is scale-independent. The same processing sequence applied to data obtained at a scan density of 4 scans/ft can be applied to data obtained at 0.5 scans/ft. The desirable data collection density is thus dictated by the minimum resolvable ballast fouling area. Network level surveys at speeds up to 70 mph can be accomplished at lower scan densities to provide a large scale ballast condition assessment. Conversely, more detailed surveys can be conducted at speeds less than 25 mph to yield ballast condition on the scale of the tie-to-tie separation distance.

Figure 24(a) shows a section of processed TTC data at a data density of 6 scans/ft. The same data decimated to 0.5 scans/ft prior to processing are shown in Figure 24(b). Note the small scale features, such as the 10 ft wide pocket of thick clean ballast from 655–665 ft in Figure

24(a) are not observed in Figure 24(b). However, the thinning of clean ballast from the left side of the section to the right side of the section is evident in both figures.

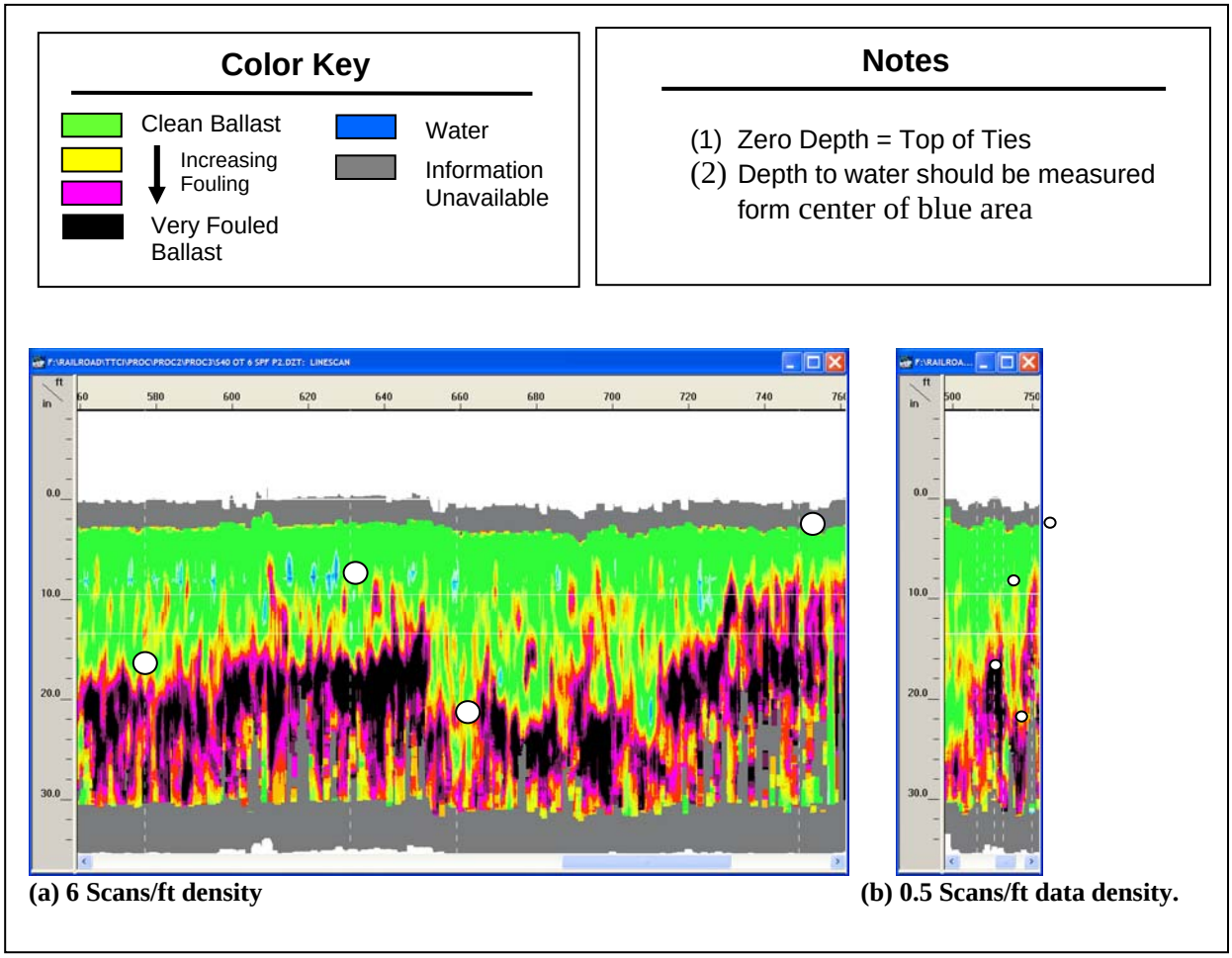

(a) 6 Scans/ft density **(b) 0.5 Scans/ft data density.**

Figure 24. Processed TTC data along a section with 4 cross trenches shown at a density of (a) 6 Scans/ft and (b) 0.5 scans/ft. The ballast fouling depths based on cross-trench data are represented by the white circles.

5.2. Amtrak Northeast Corridor, March 2006

A total of 29.6 miles of GPR data were obtained on Amtrak rails between Providence, RI and Sharon, MA on March 31, 2006. Areas of ballast distress were detected visually by staining on the ties and rails where the pumping action of saturated fouled ballast forced muddy water to the surface. These stained sections, often termed “mudspots” were clearly evident in the video data obtained at the same time as the GPR data. Five stained sections of track have been identified. No undercutting or shoulder cleaning has been performed along this section of track for at least 10 years. The GPR data were decimated from the data collection density of 4 scans/ft to 0.5 scans per foot before processing. Subsequent to processing, the data were further decimated to a density of 0.1 scan/ft to permit display of 5 mi of data per page. Figures 25–31 show the processed GPR data from the right shoulder from Milepost (MP) 189 to MP 218.6.

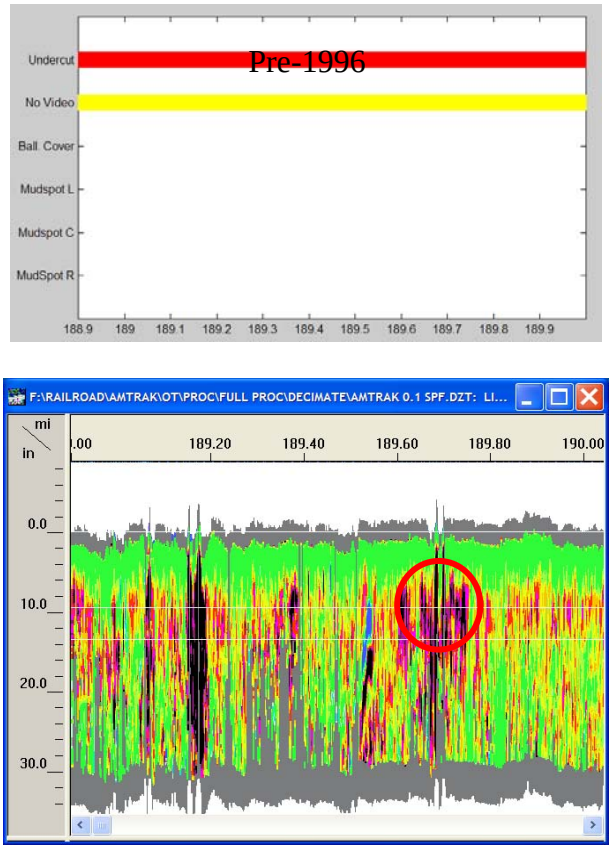

Figure 25. Available ground truth data (top) and automatically processed GPR data on right shoulder from MP 189-190 on Amtrak track (bottom). Red ovals denote large areas of significant fouling near the bottom of the ties

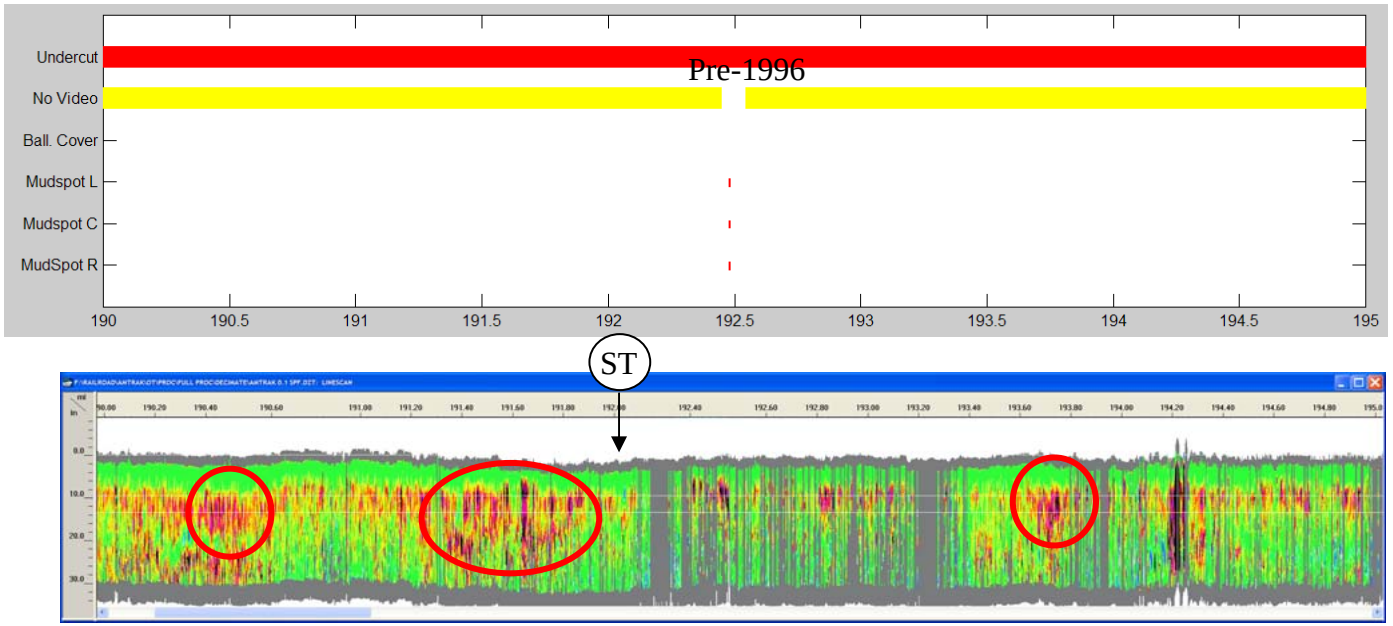

Figure 26. Available ground truth data (top) and automatically processed GPR data on right shoulder from MP 190-195 on Amtrak track (bottom).Red ovals denote large areas of significant fouling near the bottom of the ties. "ST" denotes passenger platform location.

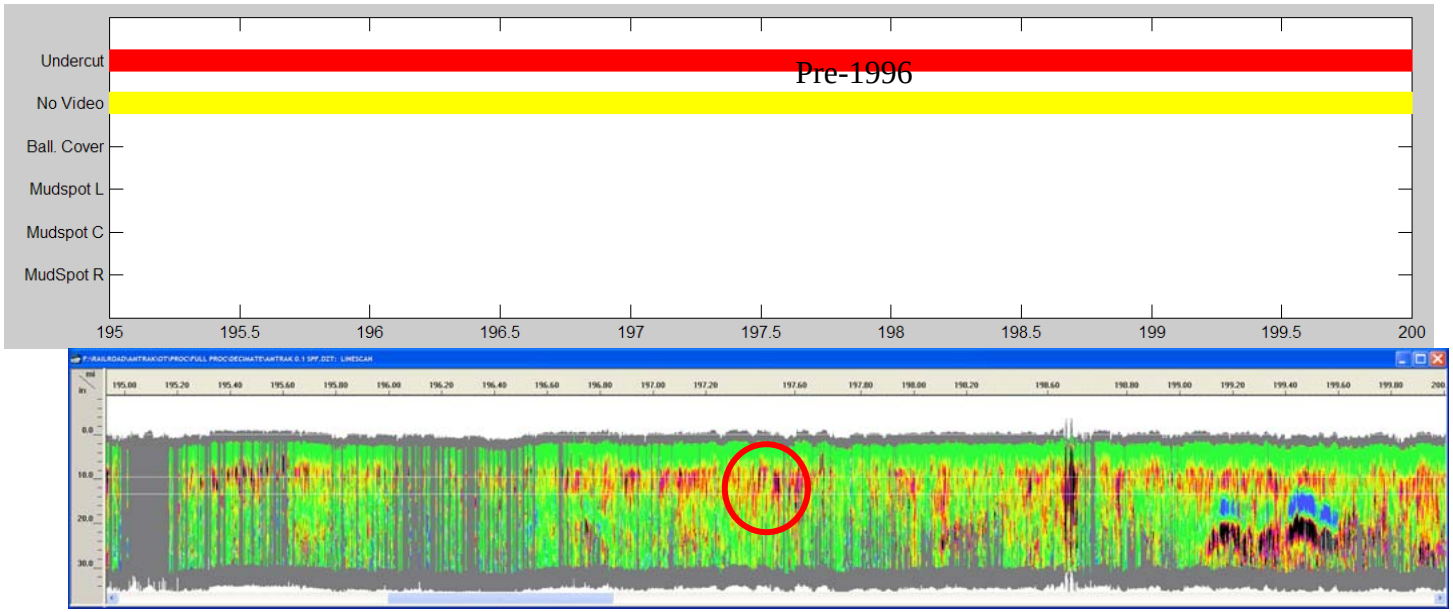

Figure 27. Available ground truth data (top) and automatically processed GPR data on right shoulder from MP 195-200 on Amtrak track (bottom). Red ovals denote large areas of significant fouling near the bottom of the ties.

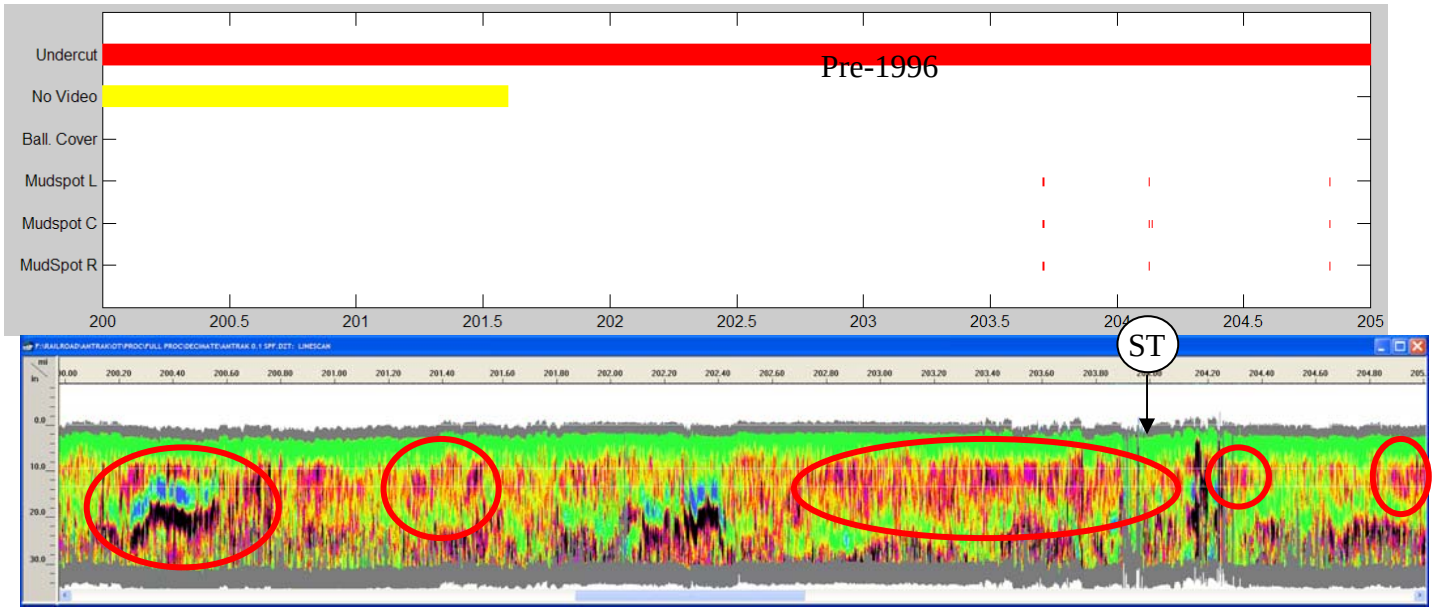

Figure 28. Available ground truth data (top) and automatically processed GPR data on right shoulder from MP 200-205 on Amtrak track (bottom). Red ovals denote large areas of significant fouling near the bottom of the ties. "ST" denotes passenger platform location.

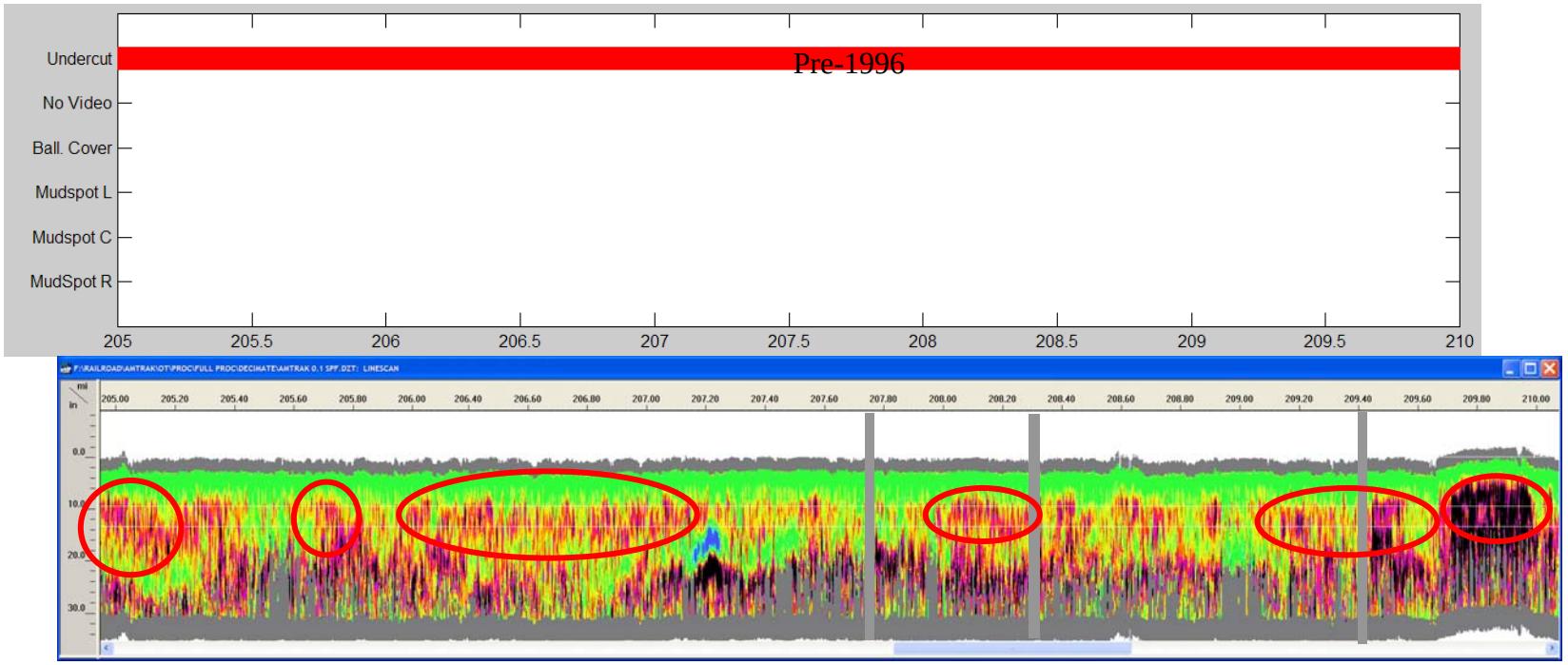

Figure 29. Available ground truth data (top) and automatically processed GPR data on right shoulder from MP 205-210 (bottom) on Amtrak track.Red ovals denote large areas of significant fouling near the bottom of the ties.

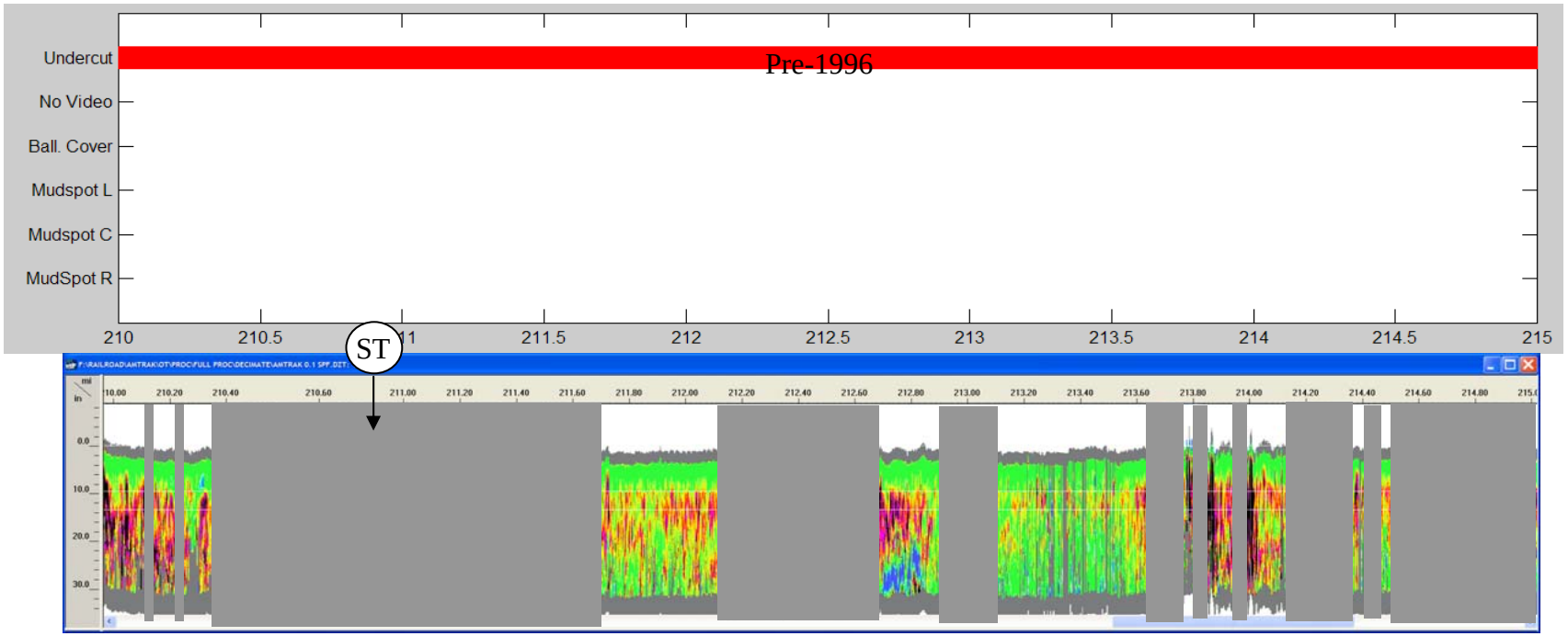

Figure 30. Available ground truth data (top) and automatically processed GPR data on right shoulder from MP 210-215 on Amtrak track (bottom). The large areas with missing data are associated with a replaced rail being too close to the antenna on the shoulder. "ST" denotes passenger platform location.

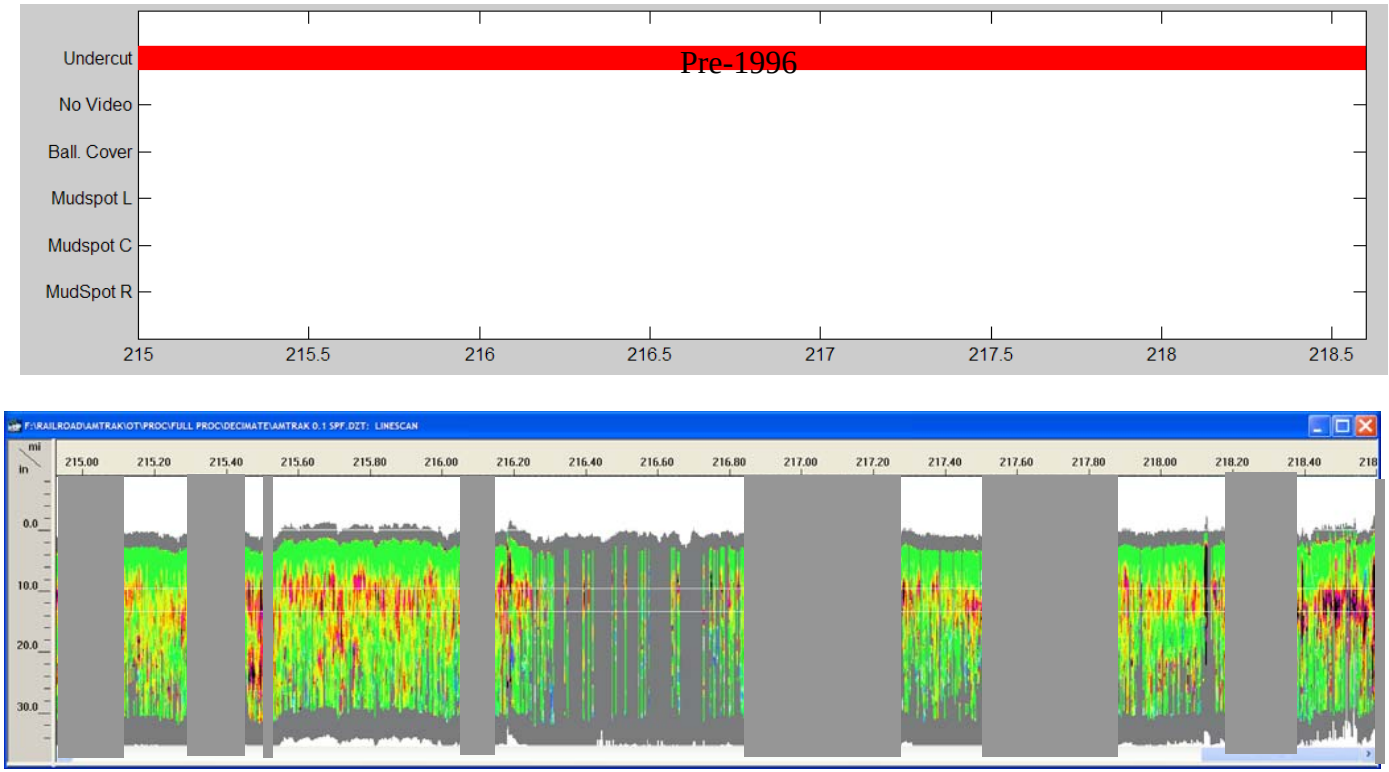

Figure 31. Available ground truth data (top) and automatically processed GPR data on right shoulder from MP 215–218.6 on Amtrak track (bottom). The large areas with missing data are associated with a replaced rail being too close to the antenna on the shoulder.

The ground truth section of each figure contains a number of categories. The top category refers to undercutting information. If the segment is left blank, then no undercutting information was obtained. Otherwise, the segment above the relevant section of GPR data is colored red or green and the year in which the undercutting was performed is indicated. The second category "No Video" is yellow over the sections of GPR data where no video data were obtained. The "Ball. Cover" category is colored black over sections of track that are covered with ballast. Along these sections the ballast cover typically prevents mudspot detection. The last three categories refer to mudspots. The last letter of each category refers to the location where the mudspot was detected based on inspection of the video data, where "L", "C", and "R" refer to the left side, center, and right side of the track facing in the direction of increasing MP. A red line is drawn at each mudspot location. The length of the line is a relative indicator of the severity of the mudspot. The shortest lines indicate staining and the longest lines are indicative of fouling so severe that the fouling material covers the ties.

GPR data should be interpreted using the color key and notes shown in Figure 24. Note, the data from the other two antennas are not shown. The GPR data from the antenna located between the rails does not yield acceptable results when the data are obtained over concrete ties. The data from the left side antenna was compromised by external radio-frequency noise. Fortunately, the right-side antenna was manufactured prior to FCC transmission regulations, so the signal strength ratio of this antenna is 6 dB greater than the signal strength of the other two antennas. This difference in signal strength was sufficient to yield acceptable data from the pre-FCC regulation antenna in most of the data collection area.

Examination of Figures 25–31 reveals that the processed GPR data indicates much of the data collection section is fouled at depths less than 10 in. More severe fouling is indicated in certain areas. These areas of concentrated fouling are circled. Four out of 5 of the mudspot locations are concentrated between MP 203.5–205 in a zone indicated by the GPR data to be heavily fouled. GPR data containing strong reflecting horizons can infer the presence of an interface between media containing different water saturation levels. These strong reflecting horizons are represented by blue in Figures 25–31. Concentrated blue areas at MP 200.55 and MP 202.35 infer high saturation levels within several in of the bottom of the ties.

Figure 32 shows processed data at a 4 scans/ft density from a mudspot at MP 203.71. Although the processed data in the vicinity of MP 203.71 infers significant fouling, the extent of fouling at 203.71 is even greater as shown by the black color in the figure.

Large sections of the GPR data from MP 210–218.6 are not shown due to the presence of a replaced rail very near the antenna mounted on the shoulder. The near proximity of the rail is observed in the GPR data as a strong reflector, thereby impacting the scattering amplitude envelope.

The GPR data on the Amtrak track were obtained and processed without knowledge of the undercutting and shoulder cleaning history in the data collection area. The processed GPR data may indicate the correct ballast condition based on the fact that neither undercutting nor shoulder cleaning has been done in the past decade. Unfortunately, the data collection area didn't include a section of track that had recently been undercut or subject to shoulder cleaning so as to clearly differentiate between known clean and fouled ballast.

(a) Mudspot location at MP 203.71. Antenna data shown below from left side of track

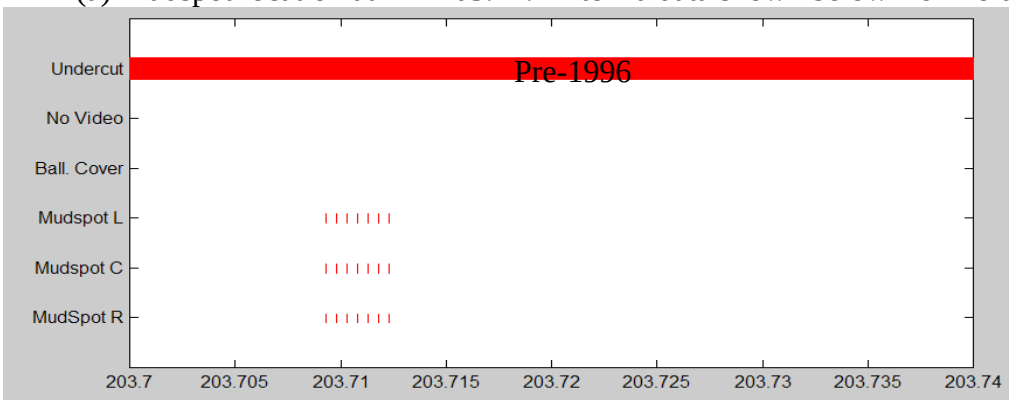

(b) Ground truth information

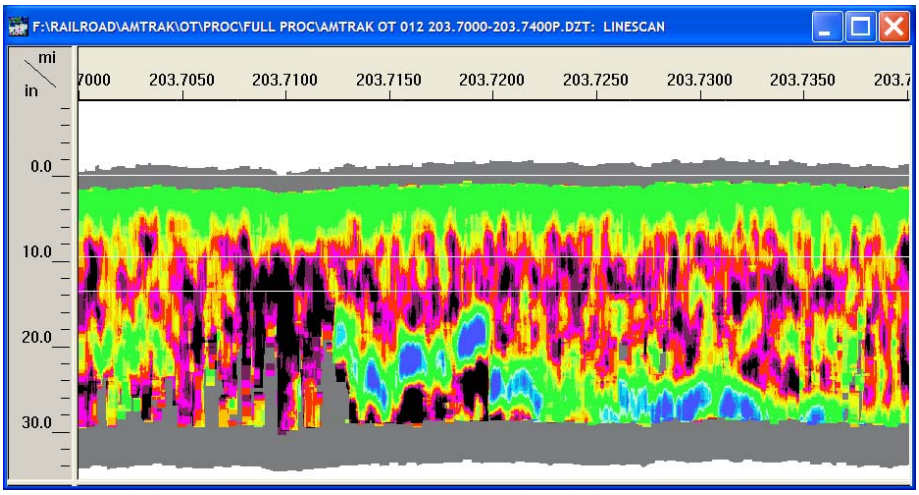

(c) Processed GPR data

Figure 32. Mudspot data: (a) Picture of mudspot on Amtrak track at MP 203.71; (b) corresponding ground truth; and (c) processed GPR data.

5.3. BNSF June 2006

More than 104 mi of GPR data were obtained on BNSF tracks June 6–8, 2006. Data were obtained on Main Tracks 2 and 3 between MP 82 and 118, starting at West Bill, WY and ending at Shawnee Junction, WY. The second data set was collected on Main Tracks 1 and 2 between MP 433 and 451, starting north of Crawford, NE and ending in Ardmore, SD.

5.3.1 West Bill, WY–Shawnee Junction, WY Data

The GPR data were obtained at scan densities ranging from 4 to 18 scans/ft. Video data were obtained over most of the data collection area. The video data are missing along approximately 7 miles because of video camera overheating problems.

A significant amount of ground truth verification in the form of surface mudspots and undercutting records was used to assess the accuracy of this processed GPR dataset for ballast condition evaluation. Additionally, the ballast was sampled at five locations. The ballast samples were extracted between the rails. Only processed data from the two outer antennas is provided in this report. The ties in most of the data collection area were concrete. The processing algorithm does not perform adequately on center antenna data obtained on tracks with concrete ties. Nonetheless, visual observation of mudspots and close examination of GPR data indicate that in most cases a general relationship occurs between the ballast condition immediately outside the ties and between the rails.

Figures 33–40 show processed GPR data and currently available ground truth along BNSF track Main 2 from MP 82.9–117.4. Some sections of the track were completely covered with ballast to the top of the rails. As a result the bottoms of the antennas were too close to the ballast surface and most of the GPR data could not be processed. This is the reason why there are large gray sections in Figure 33.

Available undercutting records from 2004–2006 are provided as part of the ground truth data in Figures 34-40. In general, the extent of ballast fouling predicted by the GPR data is much less in these recently undercut areas than areas where undercutting has not been performed in the past 2 years. For example, undercutting performed in 2005 from MP 92.3–92.6 (Figure 35) is clearly indicated by a clean section of ballast which is adjacent to a much fouled ballast section from MP 91.3–92.3. The section from MP 96.3–98.5 (Figure 36) was undercut 2 months prior to data collection. This section appears as very clean ballast in the processed GPR data. The section from MP 103.6–106.5 (Figures 36 and 37) was undercut in 2004 and appears as very clean ballast in the processed GPR data. The subsequent section from MP 106.5–110.6 was also undercut in 2004 but the GPR data indicates a higher amount of fouling. Numerous mudspots, observed in video data along this section, support this interpretation. Clean ballast is inferred from the GPR data from MP 110.6-117.4 (Figures 39 and 40). This section of track was undercut in 2005. Comparison of the undercut sections reveals that there are different levels of fouling between the different sections. The most significant fouling among the recently undercut track

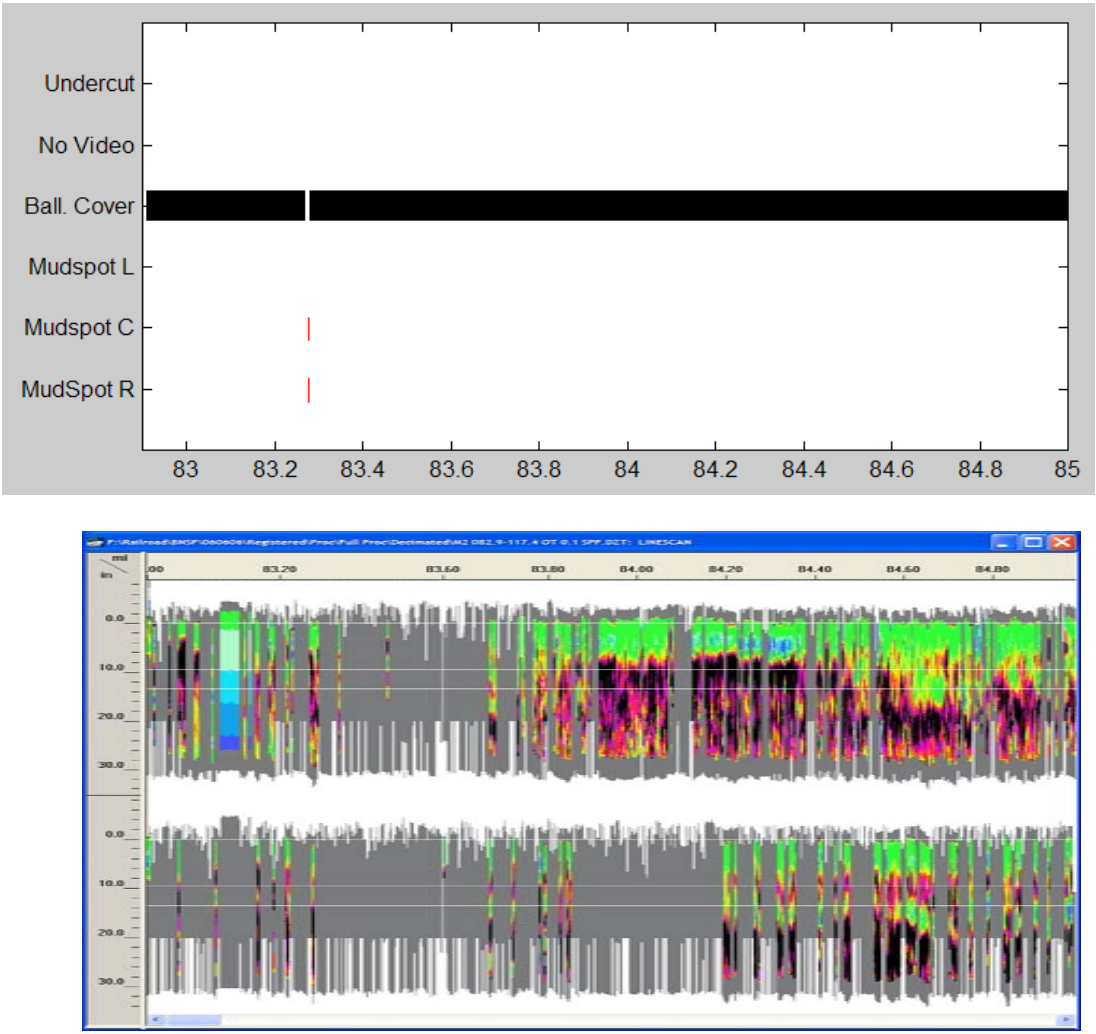

Figure 33. Available ground truth data (top) and automatically processed GPR data (bottom) from Main 2 MP 82.9-85 on BNSF track.

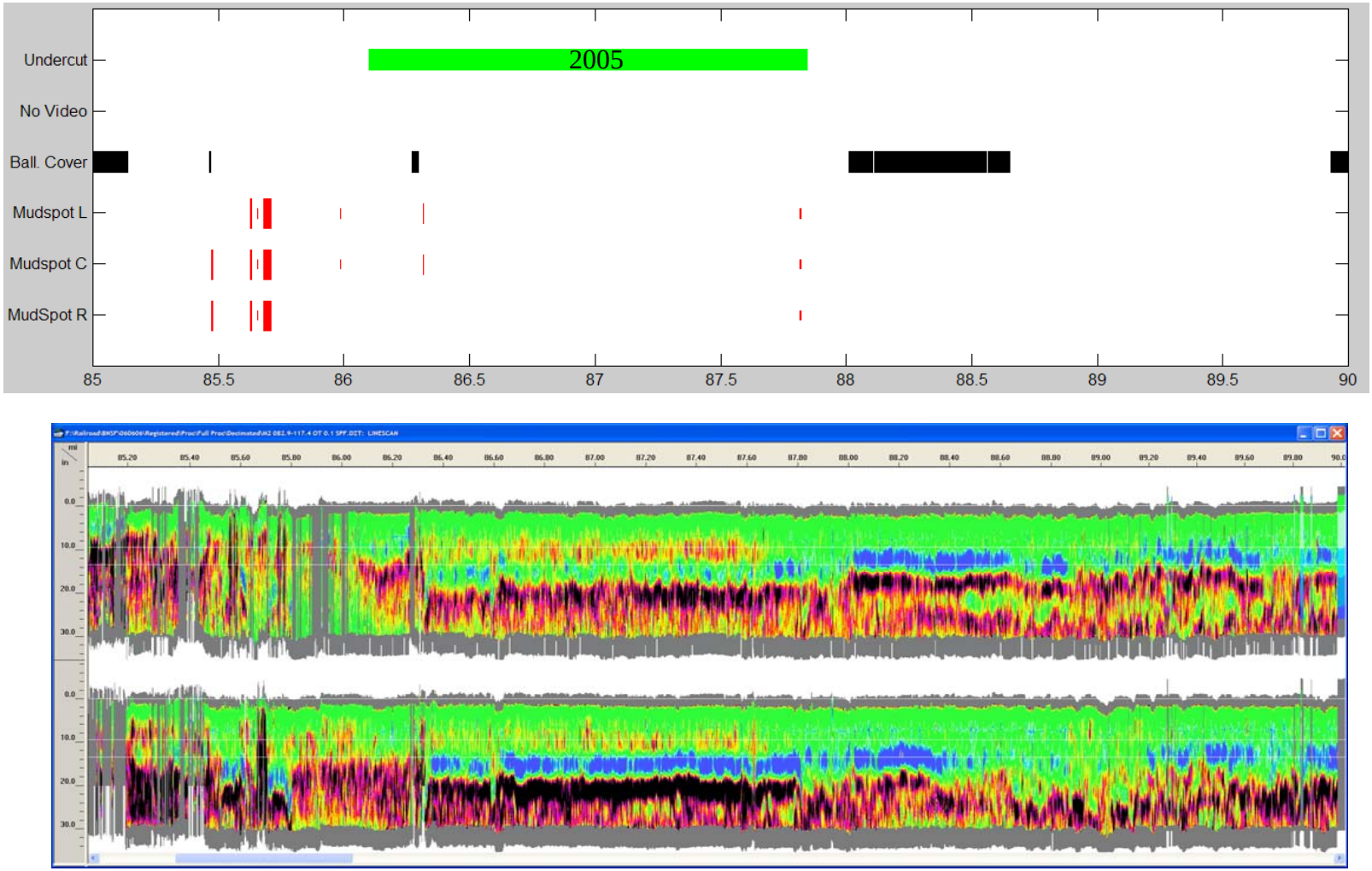

Figure 34. Available ground truth data (top) and automatically processed GPR data (bottom) from Main 2 MP 85-90 on BNSF track.

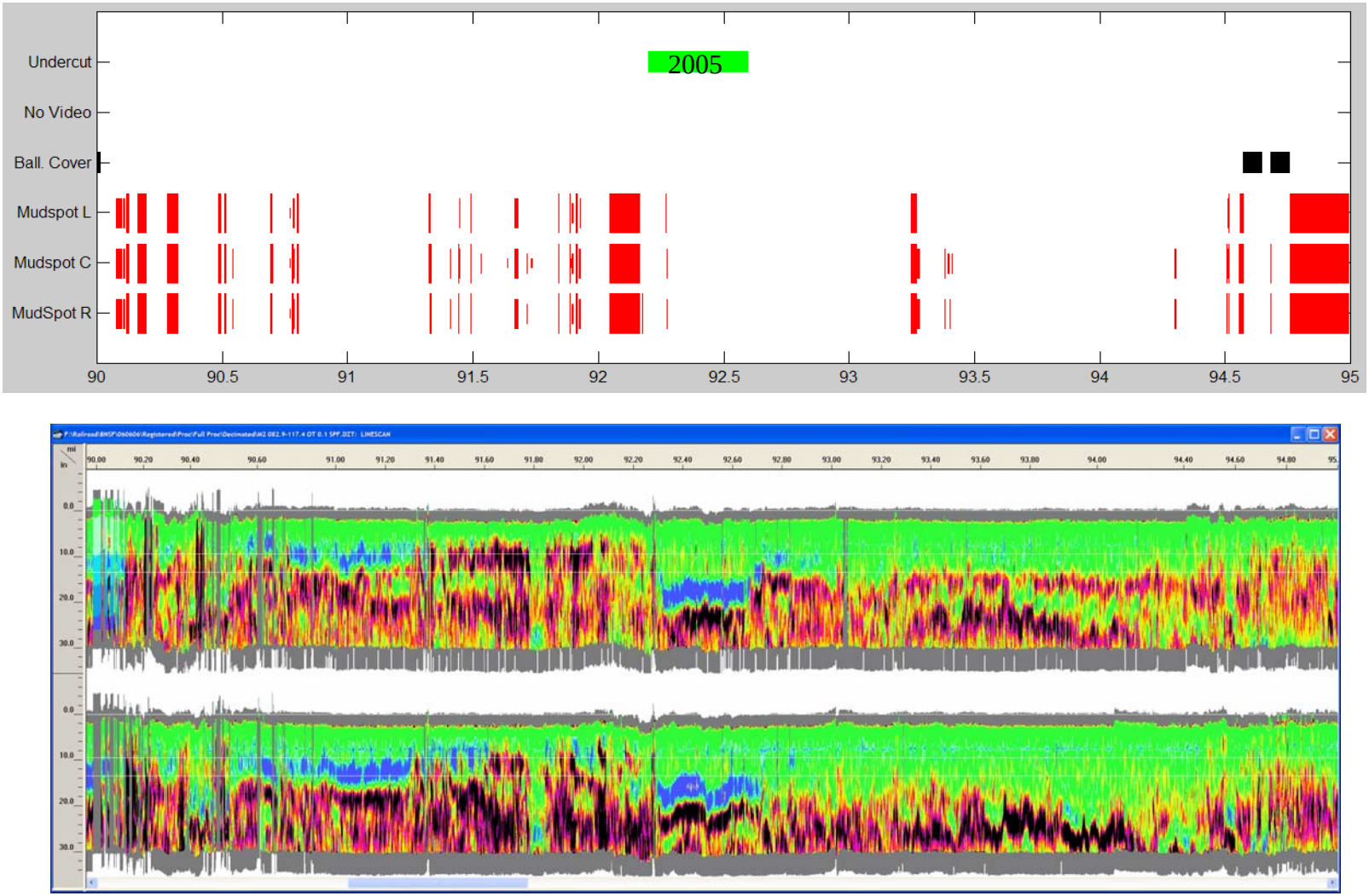

Figure 35. Available ground truth data (top) and automatically processed GPR data (bottom) from Main 2 MP 90-95 on BNSF track.

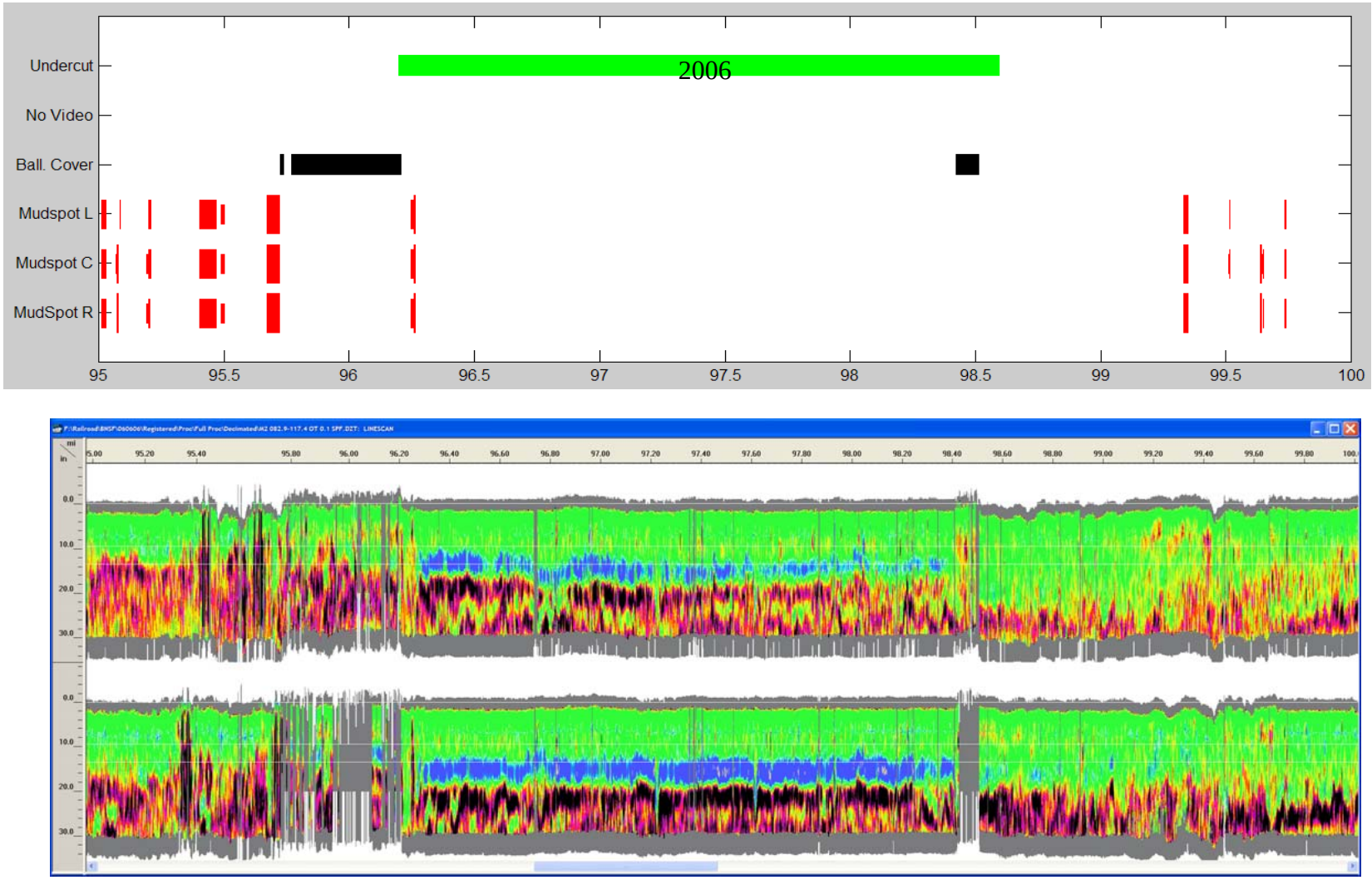

Figure 36. Available ground truth data (top) and automatically processed GPR data (bottom) from Main 2 MP 95-100 on BNSF track.

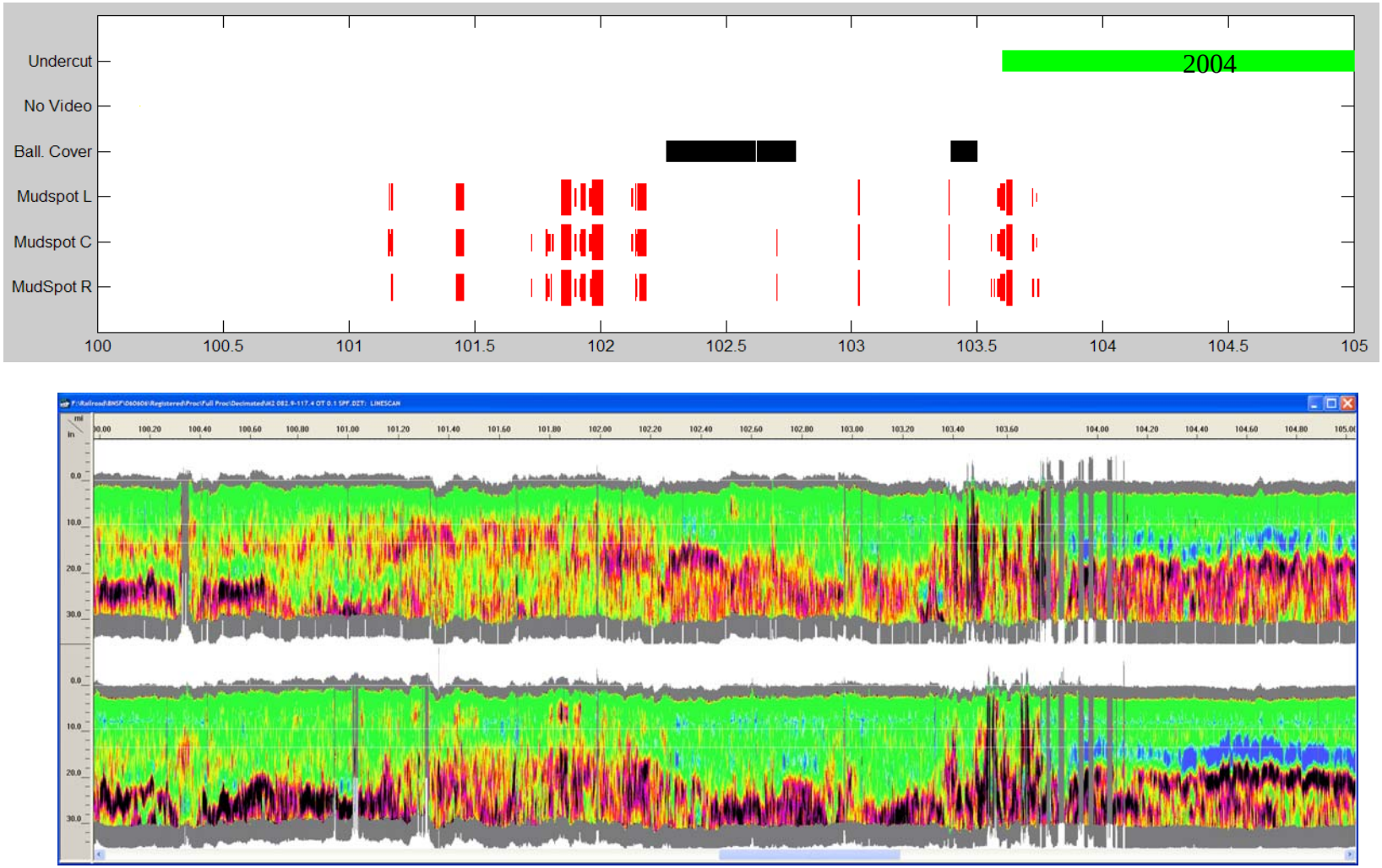

Figure 37. Available ground truth data (top) and automatically processed GPR data (bottom) from Main 2 MP 100-105 on BNSF track.

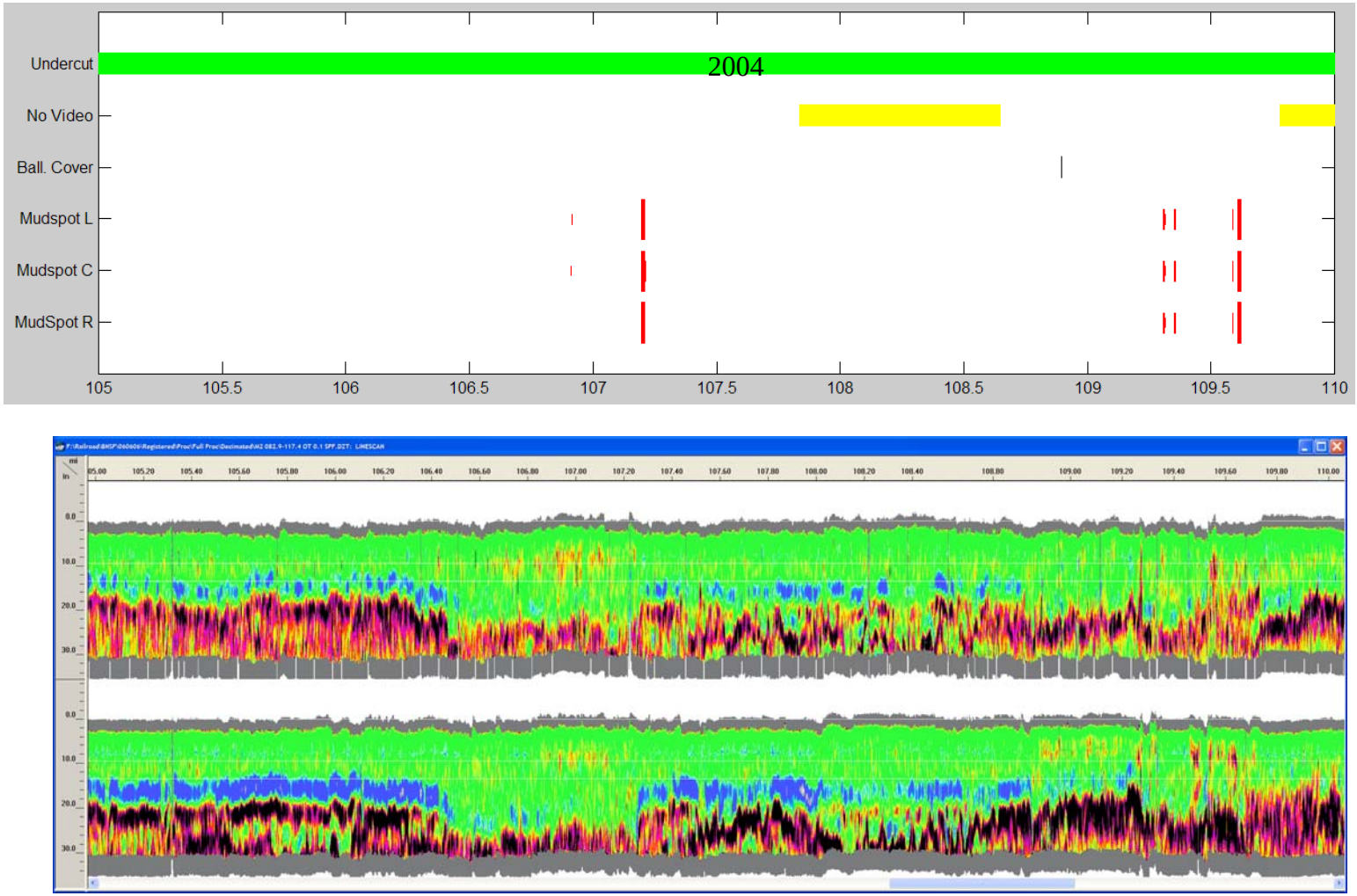

Figure 38. Available ground truth data (top) and automatically processed GPR data (bottom) from Main 2 MP 105-110 on BNSF track.

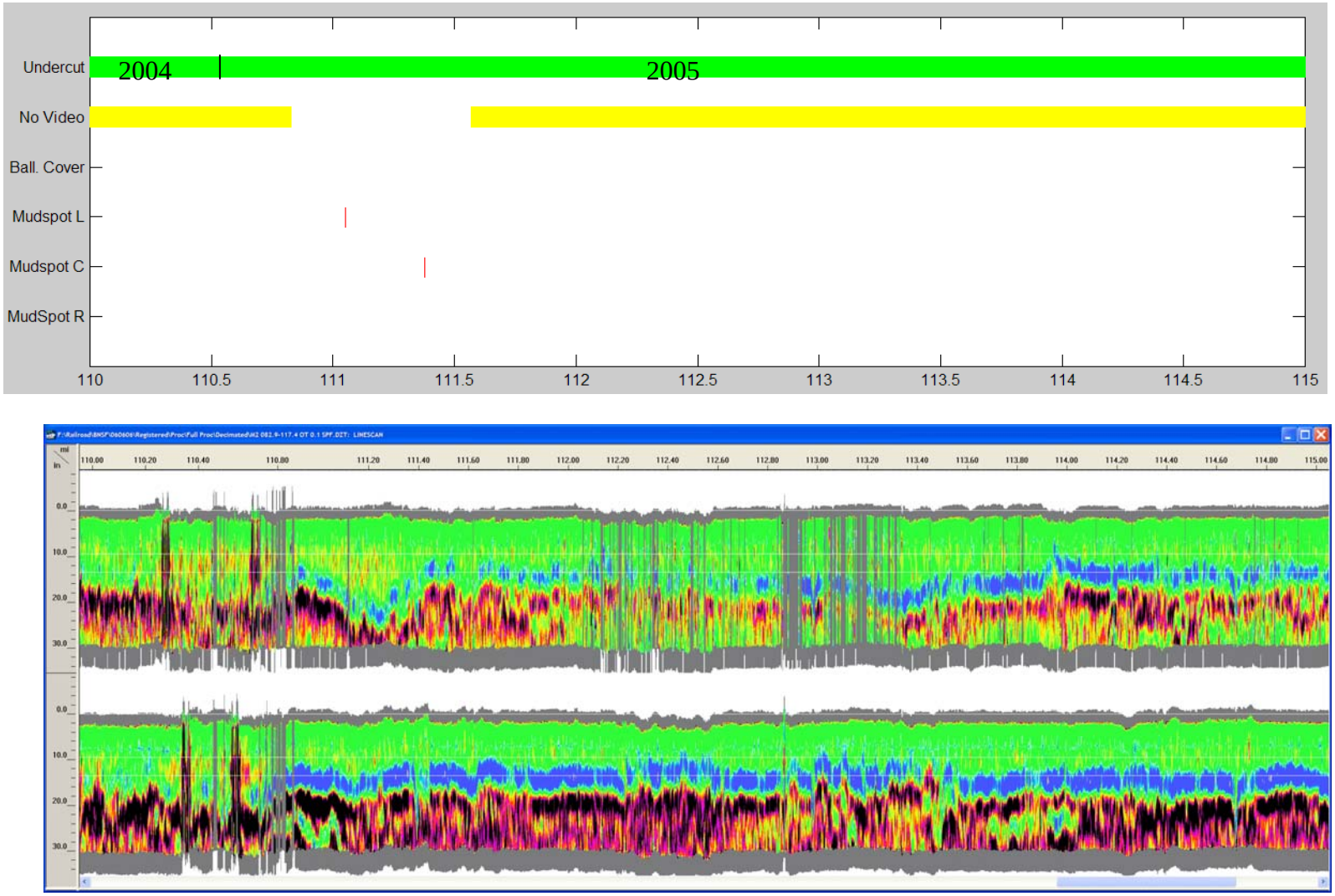

Figure 39. Available ground truth data (top) and automatically processed GPR data (bottom) from Main 2 MP 100-115 on BNSF track.

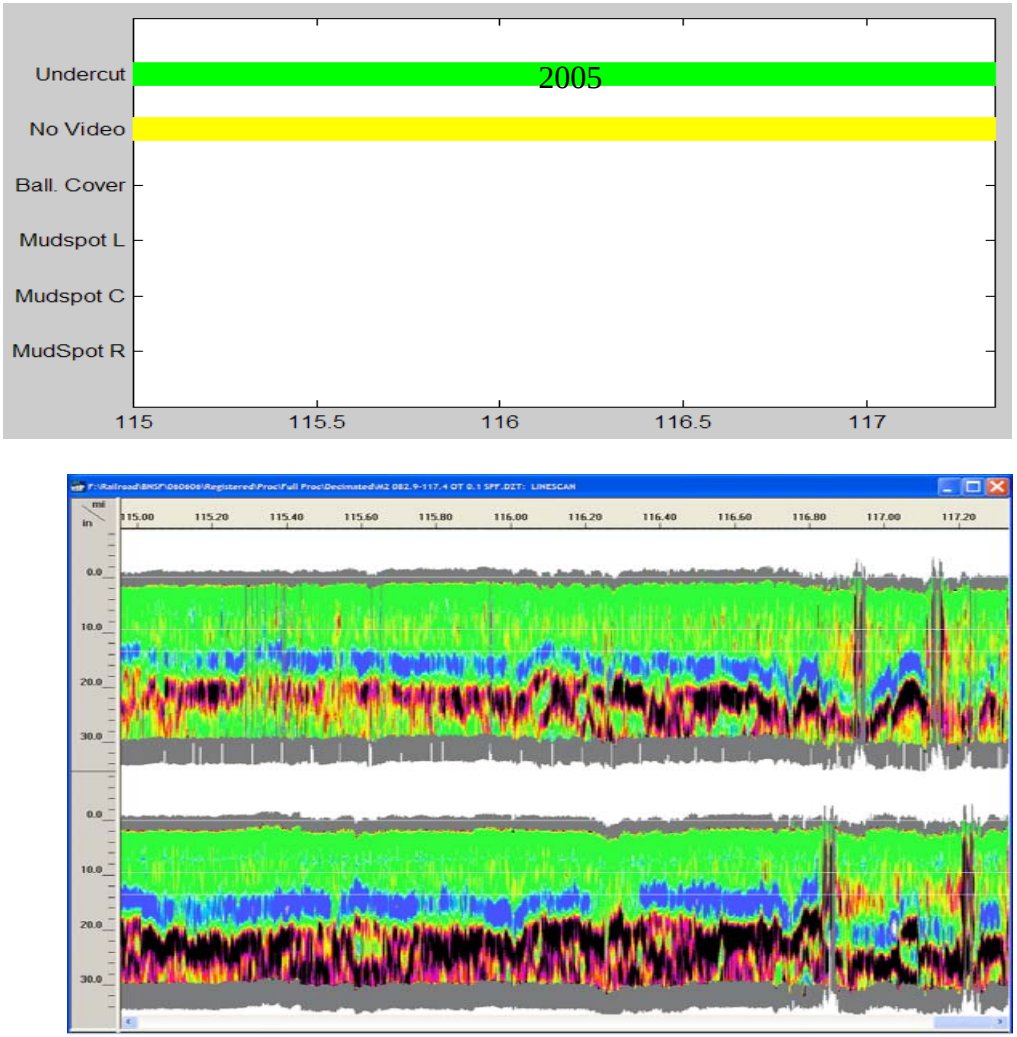

Figure 40. Available ground truth data (top) and automatically processed GPR data (bottom) from Main 2 MP 115-117.4 on BNSF track.

sections is observed in the data along the section from MP 86.2–87.6 (Figure 34). In this section there is considerable fouling approaching the bottom of the dies ties on the left side of the track. All other sections of recently undercut track appear as relatively clean ballast in Figures 34-40.

A total of 148 separate mudspots were identified based on inspection of video from Track Main 2 MP 82.9–111.5. There is exceptional agreement between mudspot locations and severe shallow fouling indicated by the processed GPR data. The most striking comparison is illustrated in the section from MP 90-95 (Figure 35). Concentrated shallow fouling from MP 90–90.75 and 91.3–92.3 inferred from GPR data is clearly confirmed by many mudspots. Significantly, there are no mudspots in the section from MP 90.75–91.3 where the GPR data indicate clean ballast.

Figure 41 shows high resolution mudspot data from MP 109.61. This portion of the track was undercut in 2004. The mudspot captured by the video camera clearly reveals fouling extending to the ballast surface. This was inferred from examination of the GPR data presented in Figure 41(c). The most severe fouling indicated by the GPR data corresponds to the physical location of the mudspot. The entire section of GPR data in addition to the mudspot appears to be severely fouled near the surface. Additional GPR data were obtained along a parallel track between MP 82.9–117.4. The data and ground truth are in good agreement.

The undercutting and mudspot ground truth data are supplemented by five ballast samples that were dug between the rails. Comparisons of processed data to ground truth at three of these sample locations are presented in Figures 42 and 43. The sample shown in Figure 42 was obtained at MP 97 on Main Track 2, which was undercut two months before GPR data collection. Very clean ballast was measured to a depth of 15 in between the rails. A sample extracted between 15- and 18-inches in depth was very moist, as shown by the mud on the spade in Figure 42(a). This moisture corresponds well to the blue band in the GPR data centered at approximately 16-inches in depth.

A local pocket of clean ballast was inferred from the GPR data presented in Figure 43 from MP 91.8 to MP 91.8 plus 400 ft. Two samples were extracted in close proximity. The sample from the fouled section is clearly fouled to the surface as shown in Figure 43(a). The local pocket of clean ballast inferred from GPR data was confirmed by the sample extracted between the rails, which was clean to a depth of 10 in (Figure 43(c)). The data from outside the ties matched the condition of the ballast sampled between the rails. GPR and ground truth comparisons of the remaining two samples were in good agreement.

(a) Mudspot location at MP 109.61. Left side of track corresponds to right side of video.

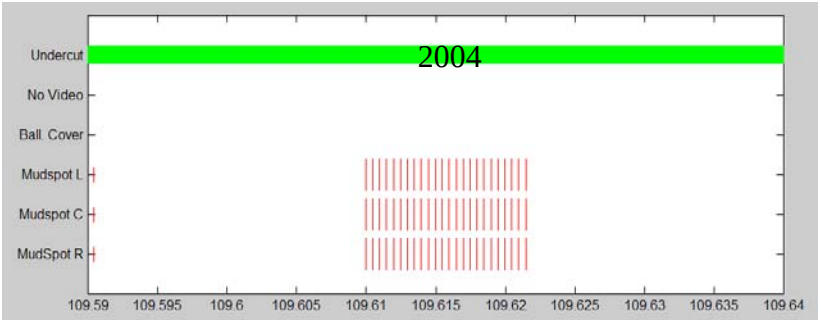

(b) Ground truth information

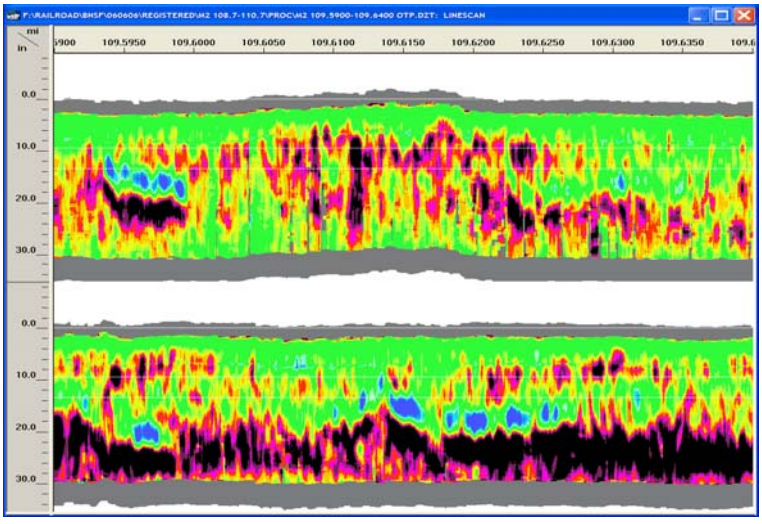

(c) Processed GPR data from left (top) and right (bottom) sides of track.

Figure 41. Mudspot data: (a) Picture of mudspot on BNSF track Main at MP 109.61; (b) corresponding ground truth; and (c) processed GPR data.

(a) Pictures of sample location. Note the moisture on the spade in the left picture.

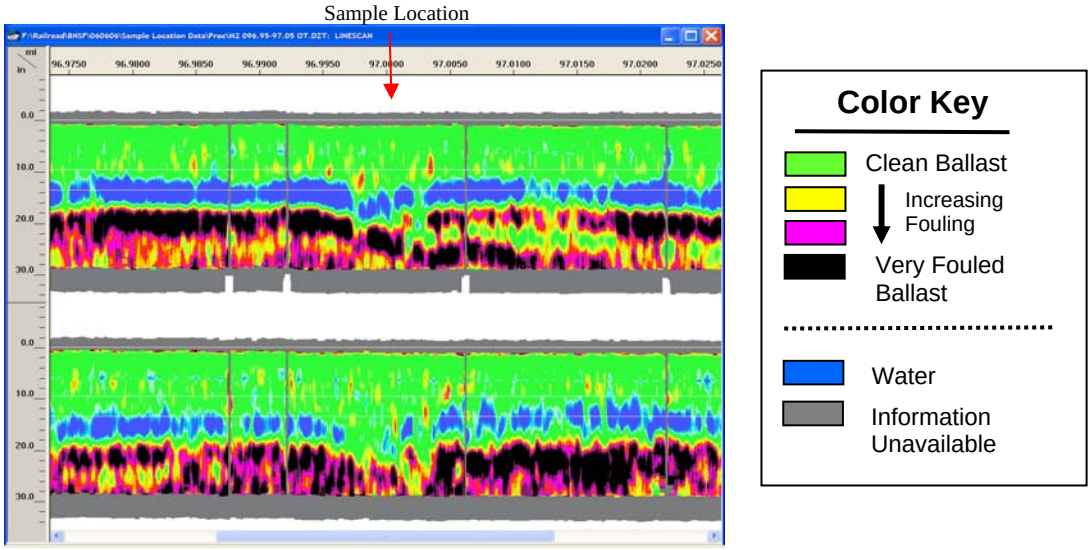

(b) Processed GPR data from antennas outside ties.

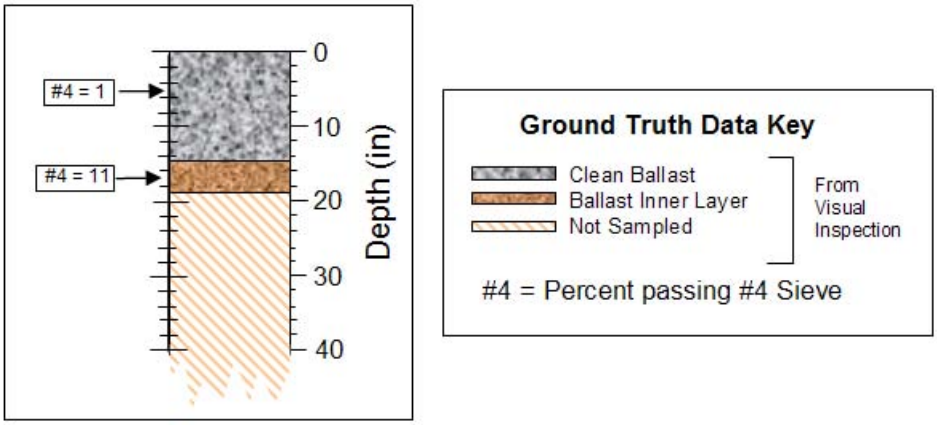

(c) Ground truth analysis from sample extracted between rails.

Figure 42. Ground truth data from MP 97 on Main 2: (a) Pictures of sample location; (b) Processed GPR data; and (c) analysis of ground truth sample.

(a) Picture of sample location #1.

(b) Picture of sample location #2.

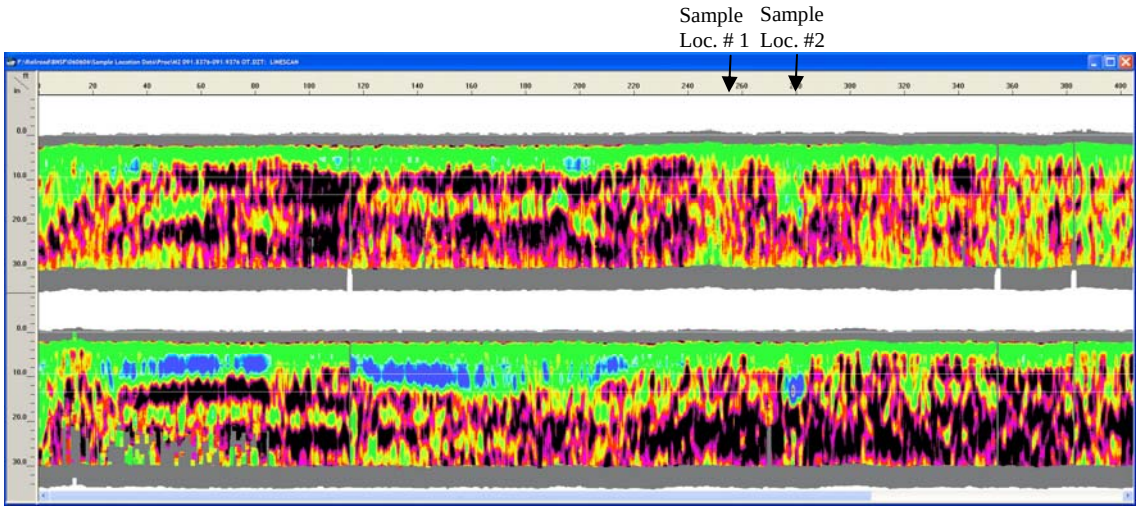

(b) Processed GPR data from antennas outside ties. Use color key in Figure 42 to assess ballast condition.

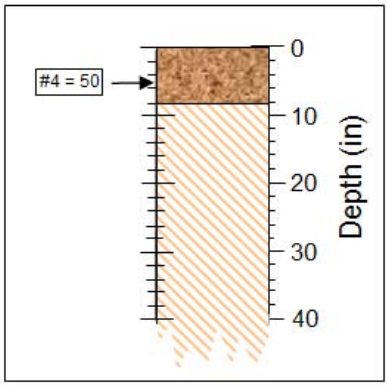

Sample #1 Analysis

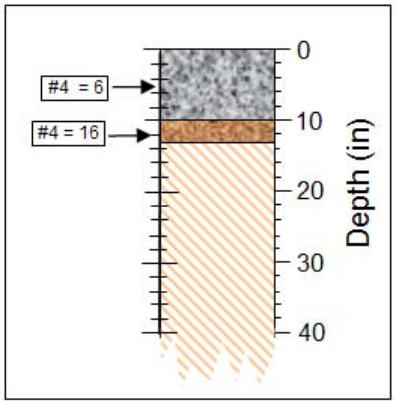

Sample #2 Analysis

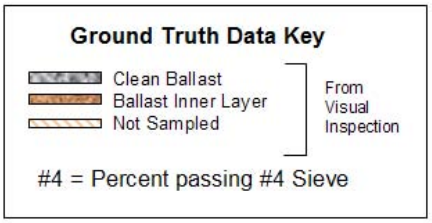

(c) Ground truth analysis from sample extracted between rails.

Figure 43. Ground truth data from Main 2 at MP 91.8 + 255 ft and 280 ft: (a) and (b) Pictures of sample locations; (c) Processed GPR data; and (d) analysis of ground truth.

Very good agreement between the GPR data and available ground truth is observed along the 69 miles of GPR data obtained on tracks south of West Bill, WY. The GPR data clearly revealed the extent of ballast fouling associated with mudspots, demarcated the extents of undercutting, and inferred the condition of the ballast where undercutting has not been recently done and no mudspots are present.

5.3.2 Crawford, NE–Ardmore, SD Data

The data along tracks north of Crawford, NE to Ardmore, SD were obtained at scan densities ranging from 6 to 12 scans/ft. Video data were obtained over the entire data collection area. Most of the track contains concrete ties. Consequently, only data from antennas mounted outside the ties are presented. Ground truth obtained at the data collection area consists of two sections of track which were undercut in 2006 prior to GPR data collection and 54 mudspot locations identified from the video data.

Figures 44–48 show the processed GPR data and available ground truth from the section of track identified as Main 2 between MP 433.0 and MP 451. Only 23 separate mudspots were identified along this section. Most of the GPR data in this section infers little ballast fouling. Much of the fouling that is present is apparently localized. For example, the fouled ballast section from MP 437.5–-437.7 is surrounded on both sides by clean ballast (Figure 45). Localized fouled areas are also apparent in Figure 46 at MP 440.3, MP 440.85, MP 441.4, MP 441.7, MP 443.0, and MP 444.7. Mudspots were identified at two of these locations and the center of the track was covered with 2–4 in of ballast at four other locations. The four locations with covered ballast can reasonably be assumed to be areas requiring maintenance in the form of tamping.

The one section of track that is known to be recently undercut, MP 436.95- MP 437.15 in Figure 45 shows very clean ballast in the GPR data from the right side antenna and interestingly, some significant spot fouling within the undercut section in the left side antenna. This discrepancy is currently unexplained. Detailed records of the undercutting along this section have not been obtained. There is, however, a turnout located along the left side antenna on this section of track. The most fouled sections of ballast on the left side antenna correspond to the beginning and ending locations of the turnout. It is likely that the undercutting operation was impacted by proximity of the turnout at these locations.

The very localized mudspot location at MP 446.02, shown in Figure 47, is explored in more detail in Figure 49. The picture of the mudspot in Figure 49(a) clearly shows significant fouling to the surface in the middle of the track. The corresponding GPR data from outside the rails in Figure 49(c) are in good agreement. Significant fouling, extending to the near surface, is clearly observed in the GPR data between MP 446.01 and 446.03. The processed GPR data and ground truth comparison—along track Main 1 between MP 433.6 and MP 450.5—is similar to the data from track Main 2.

A reasonable relationship between the GPR data and available ground truth is observed from the data obtained north of Crawford, NE and Ardmore, SD. Some discrepancy

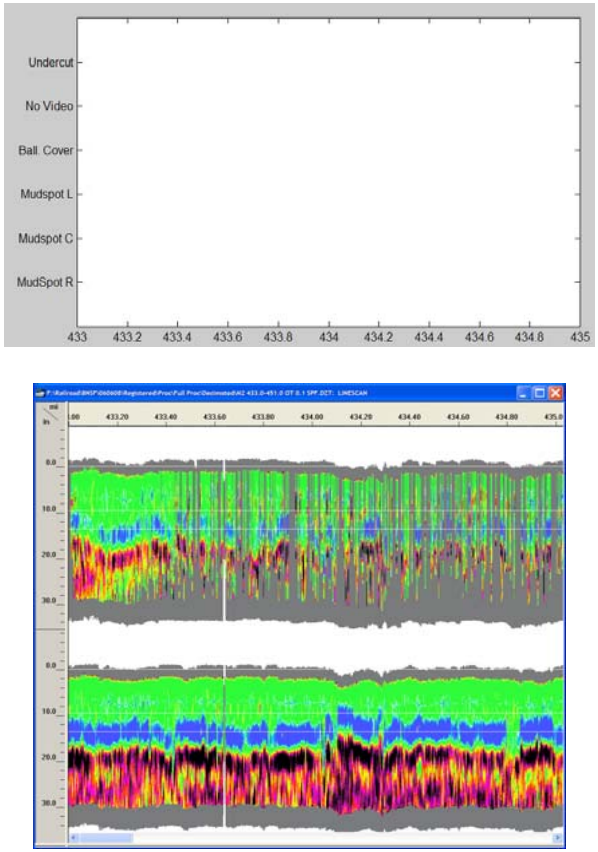

Figure 44. Available ground truth (top) and automatically processed GPR data (bottom) from Main2 MP 433–435 on BNSF track.

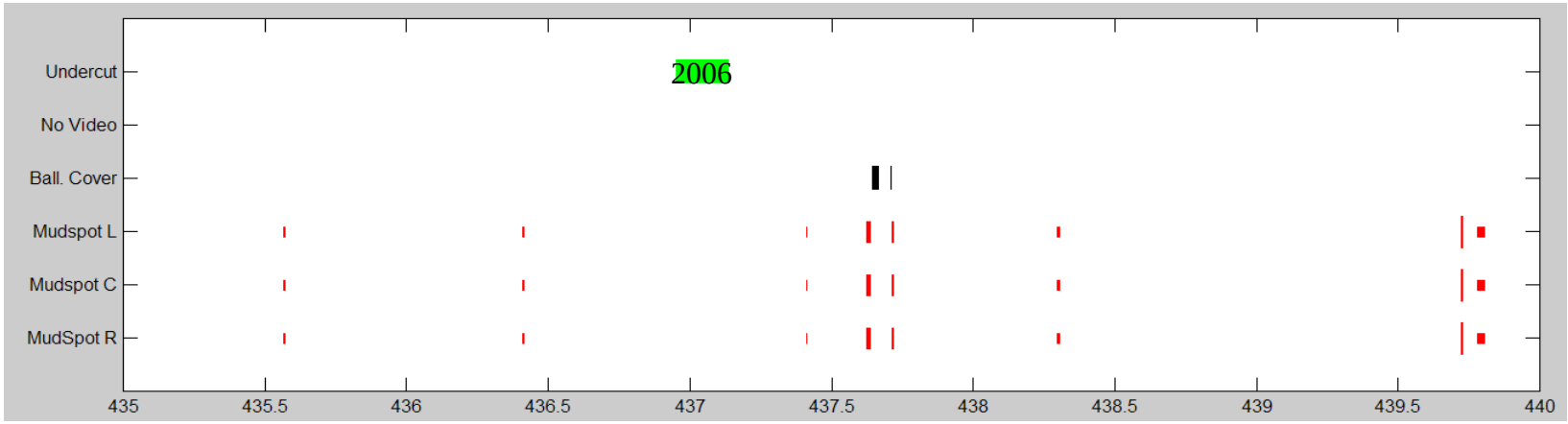

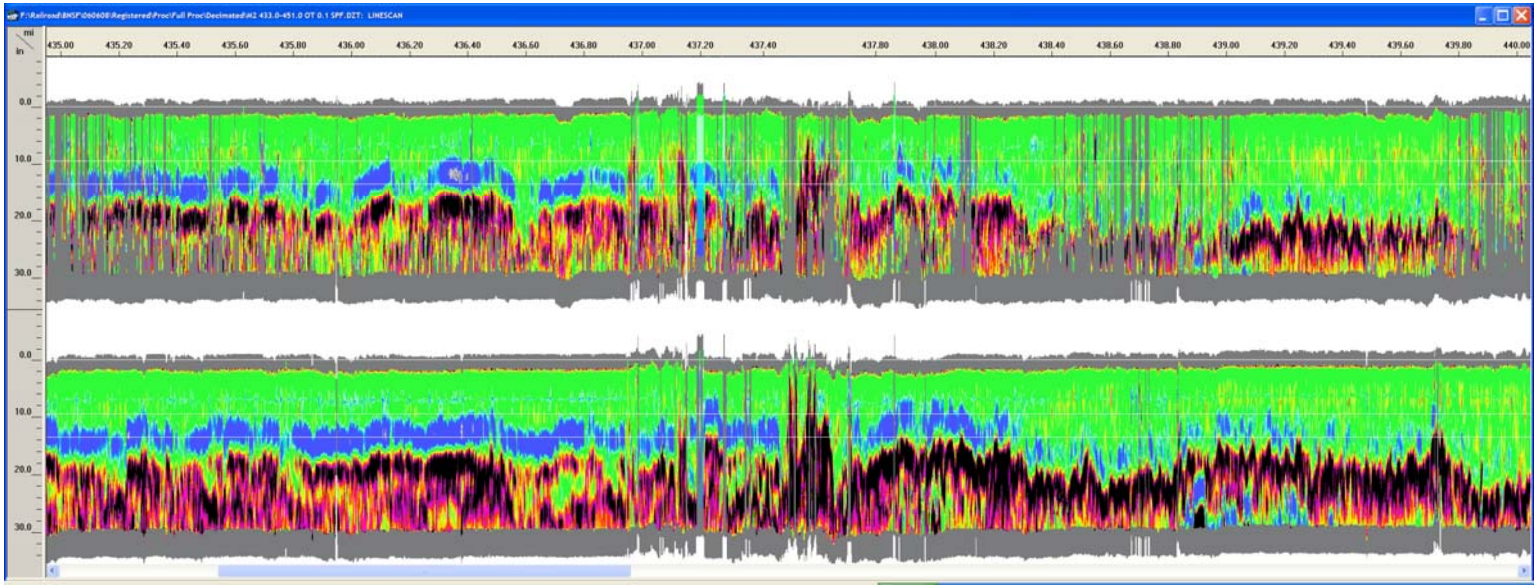

Figure 45. Available ground truth (top) and automatically processed GPR data (bottom) from Main 2 MP 435–440 on BNSF track.

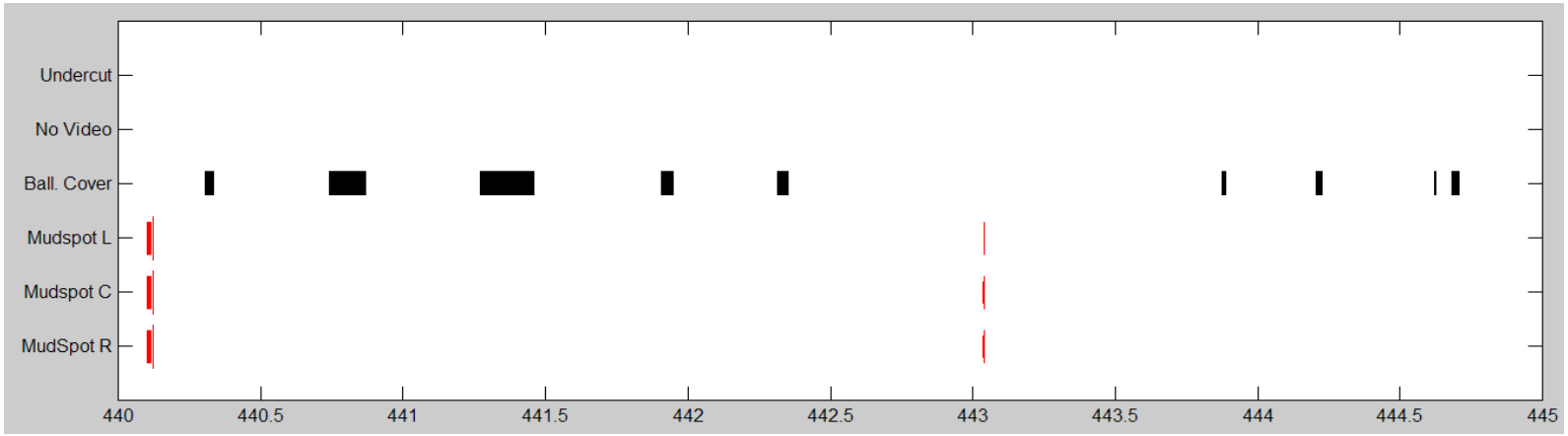

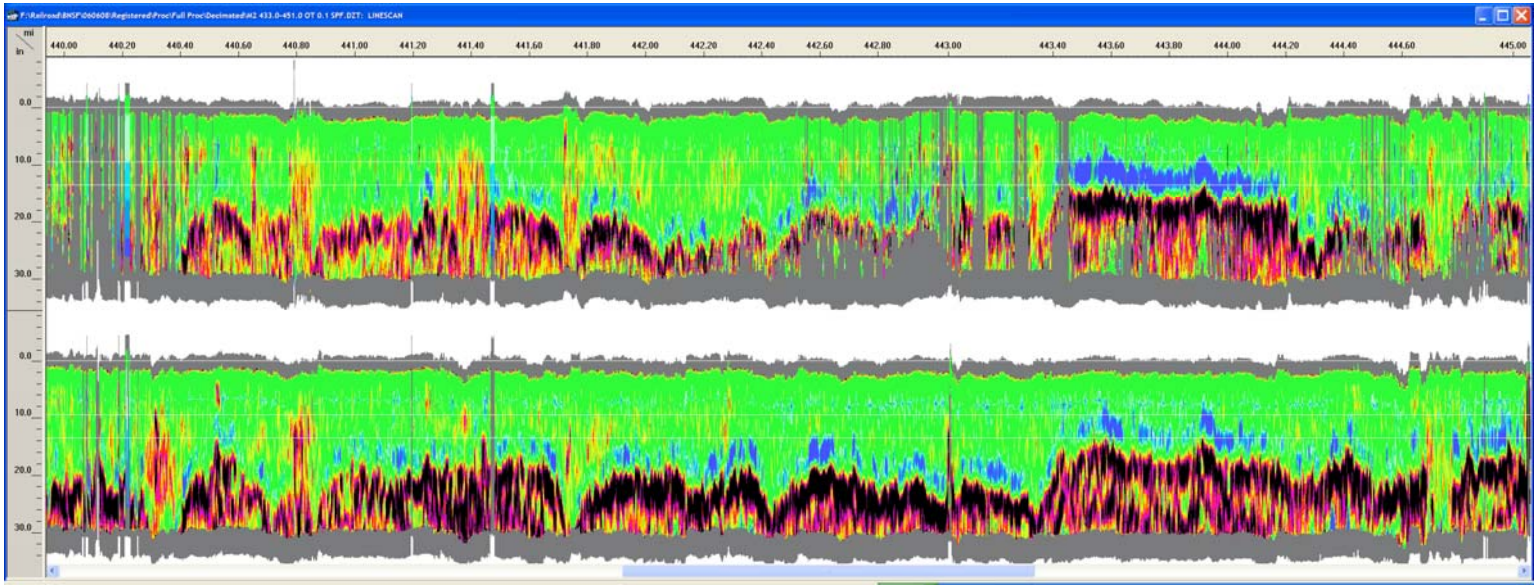

Figure 46. Available ground truth (top) and automatically processed GPR data (bottom) from Main 2 MP 440–445 on BNSF track.

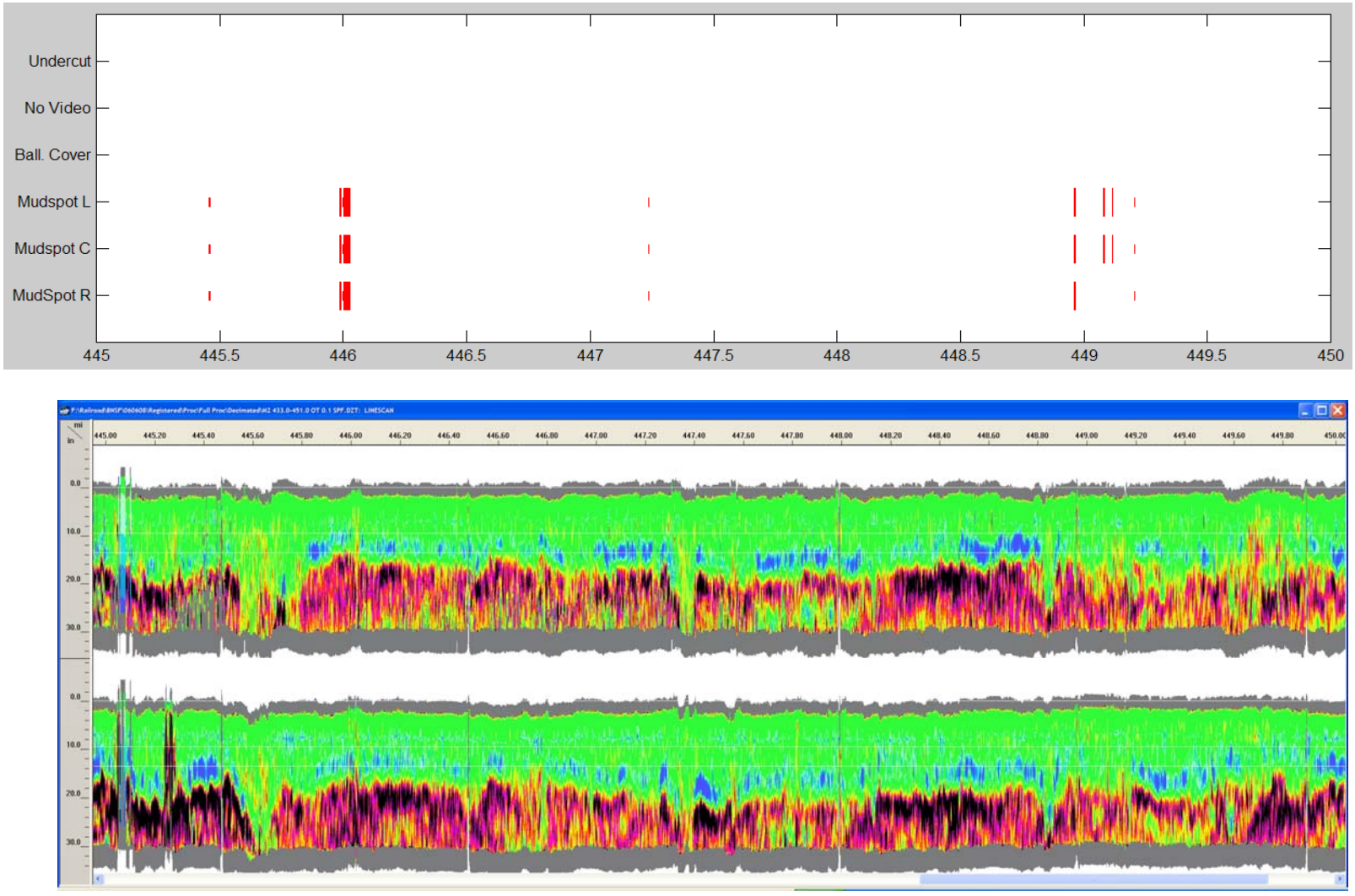

Figure 47. Available ground truth (top) and automatically processed GPR data (bottom) from Main 2 MP 445–450 on BNSF track.

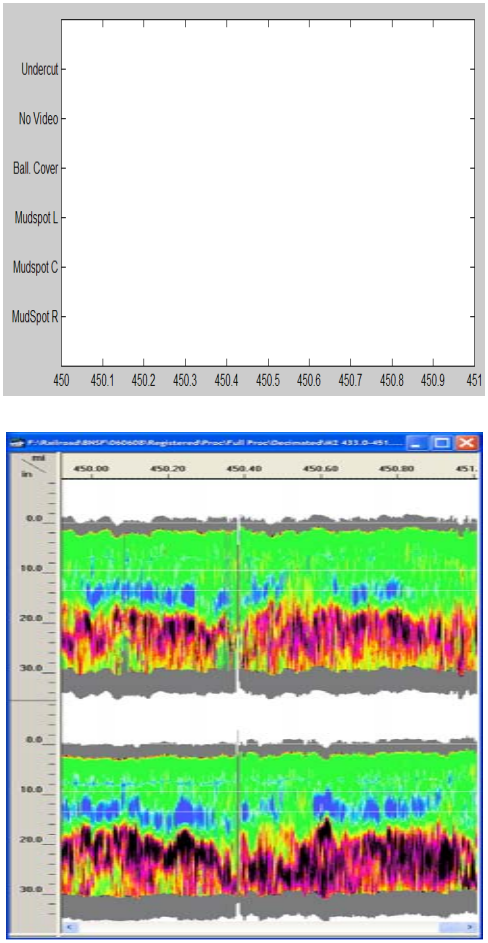

Figure 48. Available ground truth (top) and automatically processed GPR data (bottom) from Main 2 MP 450–451 on BNSF track.

(a) Mudspot location at MP 446.02. Left side of track corresponds to right side of video.

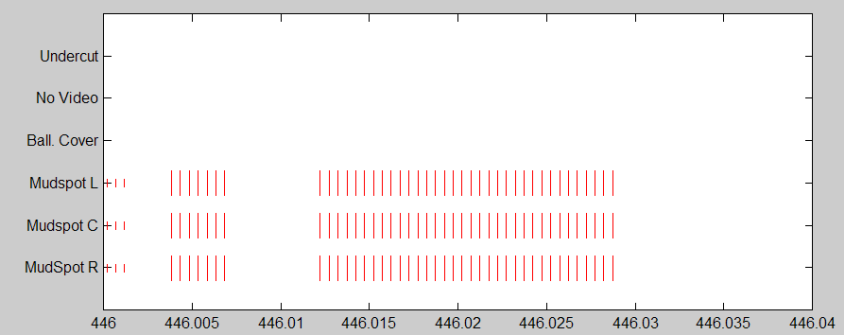

(b) Ground truth information

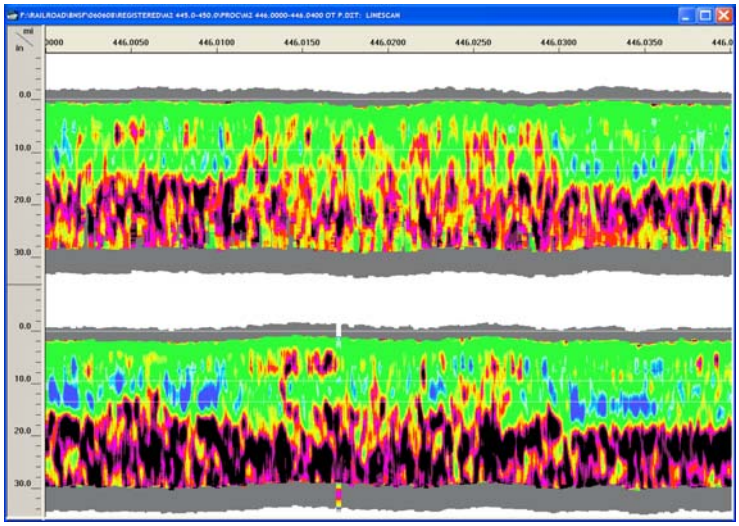

(c) Processed GPR data from left (top) and right (bottom) sides of track.

Figure 49. Mudspot data: (a)Picture of mudspot on BNSF track Main 2 at MP 446.02; (b) corresponding ground truth; and (c) processed GPR data.

exists between recent undercutting data and inferred ballast fouling based on GPR data along one side of the track that is currently unexplained. The mudspots are limited, but correlate well to fouling inferred from processed GPR data.

5.3.3 Orin Subdivision, Wyoming, July 2007

Ground penetrating radar (GPR) data were obtained on tracks in the Orin Subdivision between July 23 and July 26, 2007. The data were obtained using a 500 MHz air-launched antenna centered between the rails and two 2 GHz horn antennas mounted on the shoulders.

5.3.3.1 Data Collection

BNSF provided a hi-rail vehicle to mount the GPR horn antennas. The data collection setup is shown in Figure 50.

Figure 50. Data collection setup. Two 2 GHz horn antennas were mounted on the shoulders and a 500 MHz horn antenna was mounted between the rails.

Table 5, below, summarizes the GPR data collection. There was significant rainfall in Gillette the evening of July 25 and during the day of July 26. The precipitation recorded at Gillette Airport on July 25 and 26 was 0.29 and 0.43 in, respectively. On July 26, most of the data was obtained while it was raining. The rainfall was fortuitous in that it permitted data collection under moist conditions. It was also possible to recollect data on 5-mile (Main 2 MP34.8 – 40), 18-mile (Main 2 MP 43.3-62), and 0.2-mile (Main 4 MP -0.2 – 0) segments of track that data were also obtained on July 23 and July 25, before the rainfall. Historical precipitation records at Gillette airport indicate relatively dry conditions with no rainfall events greater than 0.1 in during the 2 weeks prior to data collection. Gillette Airport is approximately 12 mi and 35–62 mi from the shortest and two longer sections of track, respectively, where the repeat data were obtained. Local variations in weather can occur, and it is likely, but not certain, that the moisture condition in the ballast over the data collection area July 23–25 and was much drier than after the rainfall on the evening of July 25 and during data collection on July 26.

Table 5. Data Collection Summary on BNSF Railroad

Date	Track	MP Start	MP End	Total Miles
7/23/07	Main 2	62	43.3	18.7
7/23/07	Main 1	43.5	34.9	8.6
7/23/07	Main 2	34.8	40	5.2
7/23/07	Main 3	40	54	14.0
7/25/07	Main 4	-0.2	0	0.2
7/25/07	Main 2	0	14.2	14.2
7/26/07	Main 4	-0.2	0	0.2
7/26/07	Main 3	0	14.7	14.7
7/26/07	Main 2	14.7	62	47.3
7/26/07	Main 4	-0.2	0	0.2
7/26/07	Main 3	0	8	8

5.3.3.2 Ground Truth

Ground truth in the form of hand-dug holes was obtained at 20 locations on the shoulder of the track. Ground truth holes were dug concurrent with the data collection. All ground truth holes were located near road crossings or other well-registered locations along the track that could be accurately correlated with the GPR data. Near these registered locations, specific ground truth locations were chosen for the purpose of sampling the widest range of ballast and subballast conditions based on visual inspection of the GPR data. Figure 51 shows a typical hand-dug ground truth hole. Two groups obtained ground truth. One group sampled the aggregate at 6-inch depth increments. The other group sampled the aggregate at within each visually identifiable layer, the depth of which varied from one ground truth location to another. At each sampling depth interval, two samples of aggregate of about 2–3 lbs weight were collected and triple-bagged in zip-lock bags. All samples were subsequently analyzed for moisture content and aggregate size distribution.

The two largest factors affecting the accuracy of the samples were their locations perpendicular to the edge of the ties, and the fact that discrete samples were obtained. The fouling condition of the ballast can change rapidly along a cross-section of the road bed. This is important because the radiation pattern of the horn antenna is relatively narrow. The center of the 2 GHz antenna was mounted 6 in off the end of the ties. Very careful sample gathering would ensure that the sample was always obtained 6 in off the end of the tie. However, some of the samples likely were obtained closer to the end of the tie because that corresponds to the wall of the hole that was generally the most stable. The samples that were obtained were representative of the 6-inch depth increment. Any change in ballast fouling over this 6-inch range would be registered in the sample bag as a mixture of the different fouling materials. How accurate, then, is the ground truth from the samples? In general, it is believed that most of the samples provide an accurate measure of the fouling index at the location of the GPR data. The implication is that several samples could be marginally inaccurate due to their sample location or a mixture of two different fouling conditions (i.e. very clean and much fouled ballast) over the 6 in depth interval. For the purposes of this report, the sample fouling is assumed to be constant over 6 in depth increments.

Figure 51. Typical ground truth hole. Pink material at bottom is top of the subballast.

The top of the subballast layer shown in Figure 51 was typically observed at 18–25 in below the top of the ties. In areas where the ballast was clean, the moisture contrast between the clean ballast and the subballast was substantial. Correspondingly, a significant layer typically is reflected in the GPR data associated with the interface between the ballast and subballast.

The subgrade layer was located in only two of the 20 ground truth holes. At both locations the subballast layer was approximately 10-12-inches thick. The ballast fouling material was often visually identifiable as coal dust. The coal on the cars is piled above the top of the car and blows off while the train traverses along the tracks. Figure 52 shows one location near Donkey Creek Junction where a 4-inch thick layer of coal dust was just beneath the top of the ballast that was not identifiable from the surface.

(a) Surface at Donkey Creek Junction (b) Coal dust just beneath top of ballast

Figure 52. Donkey Creek Junction ground truth location exhibiting no fouling based on surface inspection, but 4-inch thick layer of coal dust just beneath the top of the ballast.

5.3.3.3 Two GHz Horn Antenna Data

The 2 GHz horn antenna data obtained on the shoulders of the track were processed using the same methodology as the data obtained in 2006. The graphic display of the processed data has been finalized and is shown in Figure 53. The color-coded data are shown on the top in Figure 53. The calculated shoulder ballast height—relative to the top of the ties, clean ballast thickness, and depth to significant moisture—are shown in graph the middle section of Figure 53(a). The bottom section Figure 53(a) contains colors representing clean ballast thickness along a thin bar. The color key to the bar is shown in Figure 53(b). The color bar display is very intuitive and allows the user to quickly locate areas of significant fouling. All of the following figures of processed 2 GHz data in this report are displayed with the format shown in Figure 53.

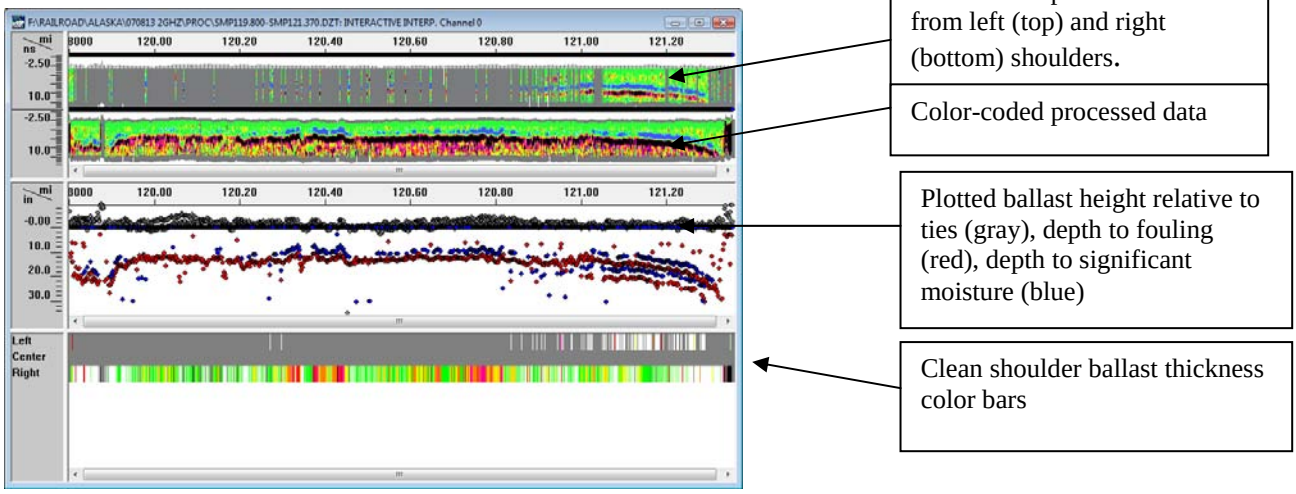

(a) Processed data: top–color coded data indicated degrees of fouling (green–clean, blue–moisture, red-black fouled; middle–red dots = depth to fouling, blue dots = depth to moisture; bottom–color coded ballast fouling depths fro shoulders;

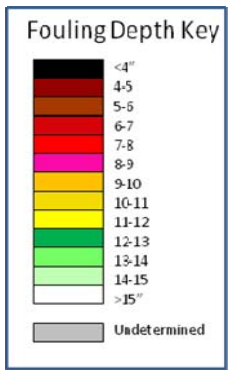

(b) Fouling depth color key for color bar data.

Figure 53. Processed 2 GHz horn antenna data showing degrees of processing: (a) Processed data; (b) color key for bar data at the bottom of (a).

Inspection of the processed 2 GHz GPR data reveals areas of clean ballast, moderately fouled ballast, and severely fouled ballast. The severely fouled ballast sections are typically less than 0.4 miles in extent. Examples of typical processed data from clean and fouled ballast in the Orin Subdivision are shown in Figures 54 and 55, respectively. Some sections of the track were recently built, thus contained clean ballast, while other sections were significantly fouled. Sudden changes in fouling conditions, as shown at MP 45.6 in Figure 55, were common.

Before comparing the GPR calculated fouling depth to the ground truth data, considerations must be taken. It is unclear what fouling index constitutes significant fouling. On the basis of data obtained during this project, a fouling index between 20 and 30 is suggestive of substantial fouling. The relationship between fouling index and track structural integrity depends on several factors. Clearly, increased fouling also increases the likelihood of track instability. The potential for track instability is further compounded by certain types of fouling material and/or increased moisture content (Tutumluer, 2008). What minimum fouling depth presents potential track stability issues? Research indicates that as the fouling depth approaches the bottom of the ties, the potential for track instability increases substantially. Given this, a fouling depth within several inches of the tie thickness would warrant attention (Wenty, 2007).

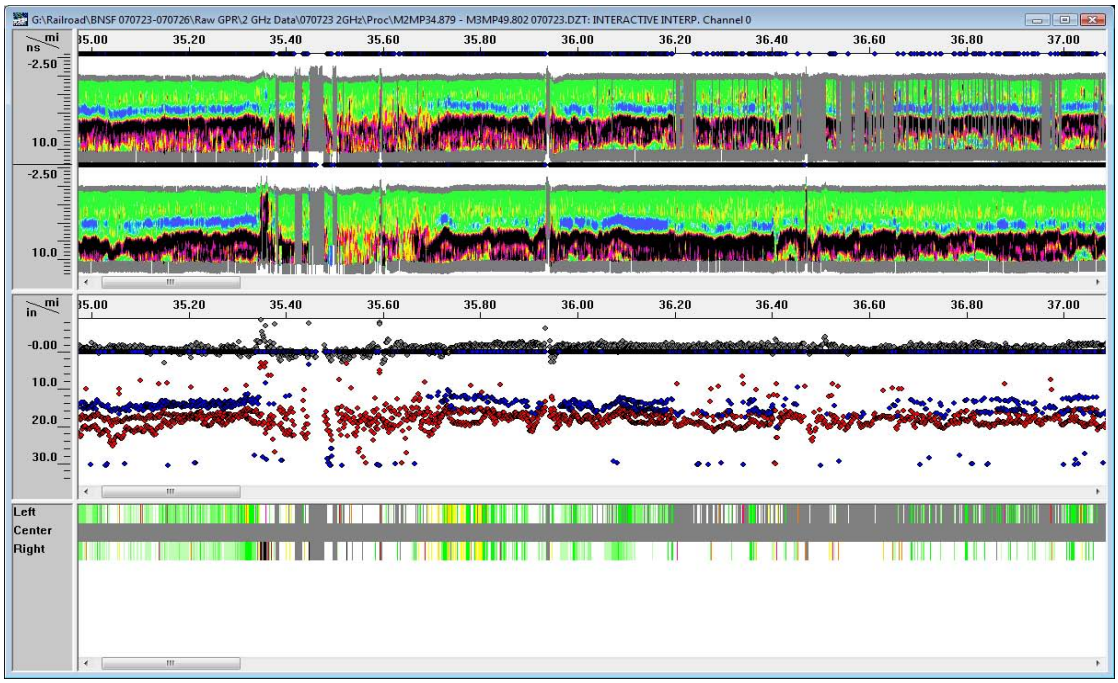

Figure 54. Processed 2 GHz horn antenna data from section of track with predominately clean ballast between M2 MP 35.0–MP 37.0.

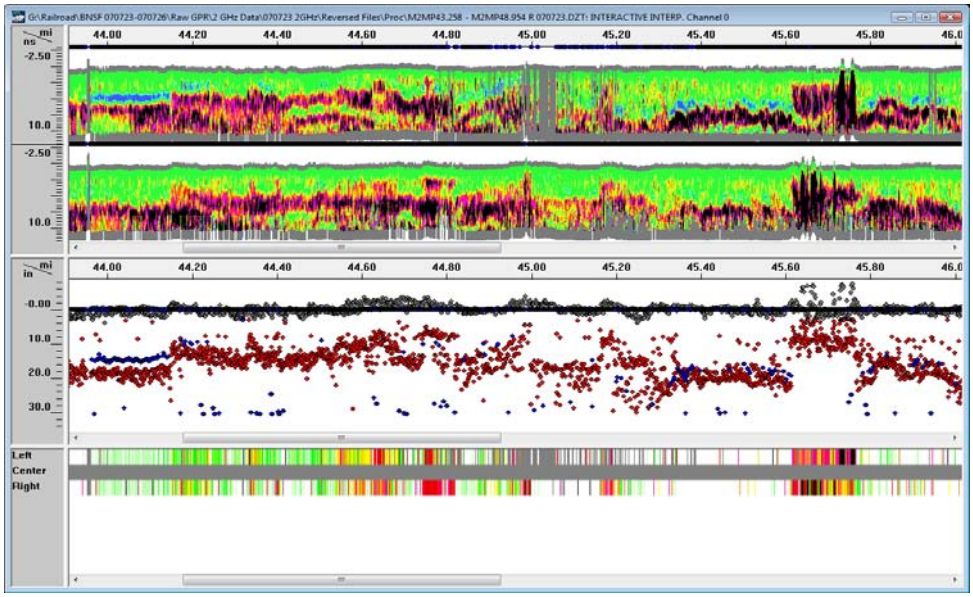

Figure 55. Processed 2 GHz horn antenna data from section of track containing severely fouled ballast M2 MP 44.6–MP 44.8 and MP 45.6–MP 45.8.

In Figure 56, the fouling depth, obtained from GPR data analysis, is compared with the fouling index for each sample depth at each ground truth location. The close correlation between the location of the GPR-calculated fouling depth and transition from green to yellow or red at most ground truth locations in Figure 56 leads to the conclusion that a reasonable agreement between the GPR-predicted calculated fouling depth and the depth of the sample corresponding to the transition from a fouling index less than 20 to greater than 20.

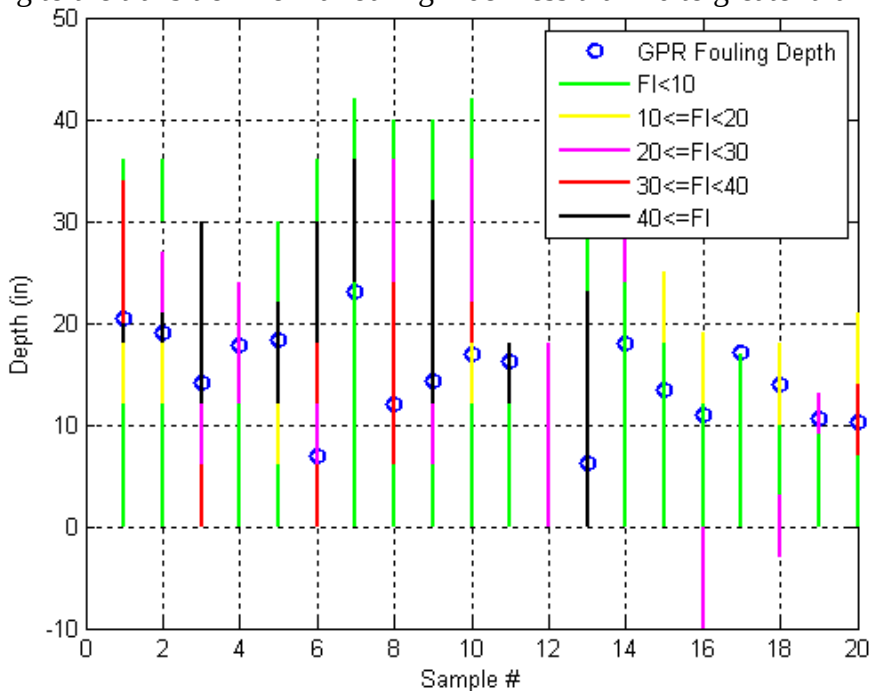

Figure 56. Comparison of the GPR predicted fouling depth and the fouling index calculated from sieve analysis of samples.

An observed agreement exists between the depth intervals corresponding to changes in ballast fouling and the GPR-calculated fouling depth. In hindsight, a better ground truth sampling interval would have incorporated gathering a sample at a 9-inch depth, to better assess the accuracy of the GPR data at this important depth. Assessing the accuracy of the GPR-calculated fouling depths requires a major assumption that may not be valid for all of the ground truth samples. This assumption is that the fouling index is constant throughout the depth interval from one sample to the next. This is very likely not the case for one or more samples. However, there should be an overall agreement between the GPR-calculated fouling depth and the fouling indexes of the samples. A second consideration is value of the GPR-calculated fouling depth in relation to maintenance priority. For example, the accuracy of the GPR-calculated clean ballast thickness is most important in the vicinity of the bottom of the ties. Therefore, whether the GPR-calculated clean ballast thickness is 2 in or 6 in it will not affect the ballast cleaning priority. The same reasoning is applicable for a very thick clean ballast, say 16 or 20 inches in thickness. The maintenance priority is not affected by GPR-calculated ballast thickness errors for depths less than the tie thickness and much greater than the tie thickness. This is important because the scattering attenuation method is inherently less accurate for very thin clean ballast layers and very thick clean ballast layers.

Using this reasoning, the accuracy of the GPR-calculated ballast thickness for maintenance priority assignment will be as follows:

- Full agreement: GPR depth in first 6-inch depth interval with fouling index greater than 20.
- Likely agreement: GPR depth within 2 in of the first 6-inches depth interval with fouling index greater than 20.
- Moderate fouling agreement: GPR Depth in Fouling Index greater than 10 and less than 20.
- Thick ballast agreement: GPR depth greater than 12 in and ballast 12 in or less in thickness has fouling index less than 10.
- Disagreement: None of above conditions apply.

Table 6. GPR accuracy related to ground truth fouling data

Sample #	Full Agreemenet	Likely Agreement	Moderate Fouling Agreement	Thick Ballast Agreement	Disagreement
1	Yes				
2	Yes				
3					Yes
4	Yes				
5	Yes				
6		Yes			
7		Yes			
8	Yes				
9					Yes
10			Yes		
11	Yes				
12*					
13		Yes			
14				Yes	
15				Yes	
16					Yes**
17	-			Yes	
18	-				Yes**
19	Yes				
20	Yes				
	-				

***Signal-to-noise of GPR data too low to provide accurage GPR-calculated fouling depth.**
****A thin layer of fouled ballast was located above the ties with a thick clean ballast layer beneath.**

A close examination of Table 6 reveals that 79 percent of GPR-calculated fouling depths show agreement or likely agreement with the ground truth. Four ground truth locations are where there is disagreement. At two of these locations there was a thin layer of heavily fouled ballast above the ties and a thick layer of very clean ballast beneath. The GPR calculated fouling depth didn't accommodate the thin layer on top. Overall, the results are considered to be very reasonable. Personnel at BNSF railroad were pleased with the GPR data.

An obvious correlation exists between percent moisture and fouling index. The higher the fouling index, the greater the capacity to store moisture. The calculated fouling depth is compared to the percent moisture in the samples at the ground truth locations in Figure 57. The correlation between calculated fouling depth and the first sample exhibiting moisture greater than 2 percent is clear.

The percent moisture versus fouling index is plotted for all the ground truth samples in Figure 58. Clearly, a trend in increasing moisture with increasing fouling index exists. Also, a wide

range is occurring in moisture content, even at low fouling indexes. This is surprising. Recent ground truth data obtained from the Alaska Railroad (see section 5.5) and at TTC showed a moisture content that rarely exceeded 15 times the fouling index for fouling indexes greater than 20. For example, the maximum percent moisture between fouling indexes of 20 and 30 did not exceed 4 percent at those other locations. On the Orin line, however, several samples with fouling indexes between 20 and 30 have percent moisture over 8 percent. Although compositional analyses were not performed on the BNSF samples, it is likely that the cause for this is the high moisture retention ability of coal dust (Tutumluer et al., 2008).

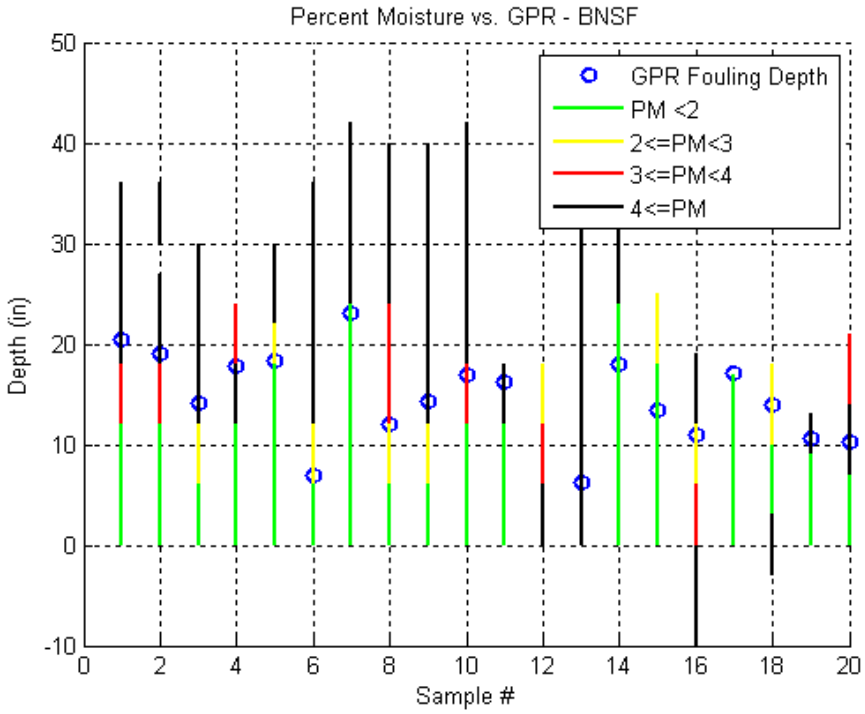

Figure 57. Comparison between GPR-calculated fouling depth and percent moisture.

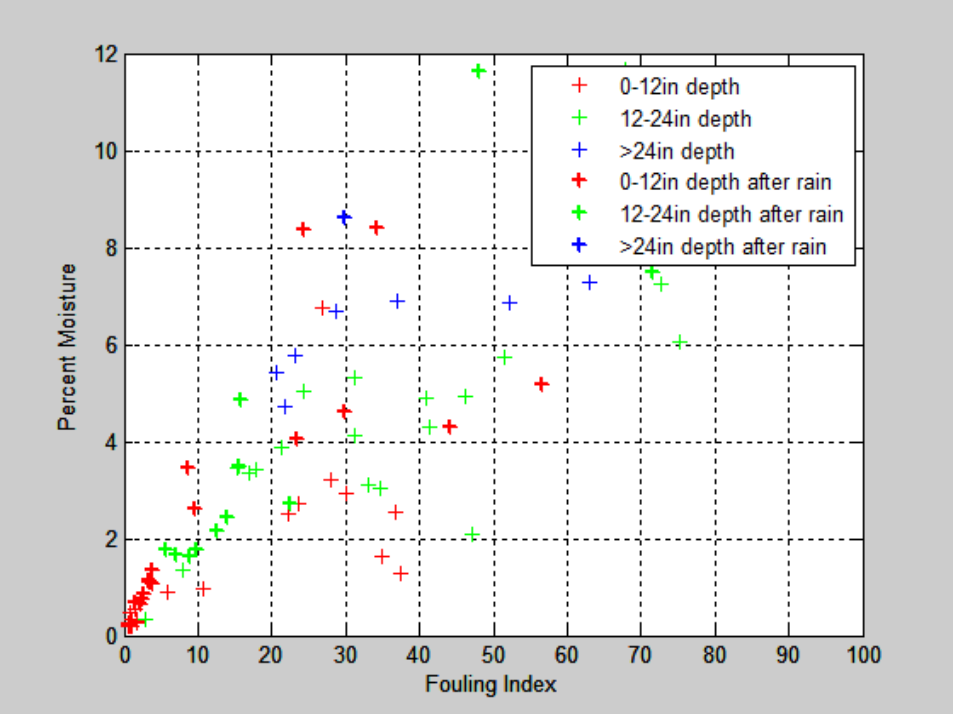

Figure 58. Plot of percent moisture versus fouling index from all the ground truth samples. The sample points are color-coded based on the depth they were extracted. Bold symbols indicate samples extracted 1–2 days after rainfall (0.3 -0.5 in).

The high moisture retention ability of coal dust and the observed sensitivity of the GPR to moisture content can be examined in relation to GPR data obtained under different moisture conditions. Figures 59 and 60 show GPR data obtained on track Main 2 between MP 37 and MP 39. The data in Figure 59 were collected before a rainfall and the data collected in Figure 60 were obtained during a rainfall event. At the time of data collection (mid-afternoon on July 26) most of the rainfall had already occurred. A noticeable increase in the calculated fouling extent and decrease in clean ballast thickness is observed in Figure 60 (during rainfall) compared to Figure 59 (pre-rainfall). A change in calculated fouling extent is also observed in areas with moderate to heavy fouling. Figure 61 shows a section of Main 2 track between MP 44 and MP 46 that contains mostly heavily fouled ballast with pockets of clean ballast at MP44.0-44.15, MP 45.4–45.6 and MP45.8–46.0. The processed data shown in Figure 62 was obtained along the same section of track during the rainfall event. A pronounced increase in calculated fouling occurs over most of the section except for two locations corresponding to the cleanest calculated ballast—MP44–44.15 and MP45.846.0 (left track side in Figure 61 corresponds to the right track side in Figure 62) .

The preliminary conclusion regarding the effect of precipitation on the GPR-calculated fouling is that significant precipitation events generally result in a noticeable increase in calculated fouling except in some locations with the cleanest ballast. The increased moisture in the ballast layer results in greater signal attenuation that appears in the processed data as a decrease in clean ballast thickness. It is suspected that most of this effect is associated with the fact that coal dust is a major fouling material along the data collection route and coal dust

has an anomalously high absorption capacity. This conclusion is supported by other recent data collected in Alaska and obtained under two different moisture conditions that didn't show nearly this level of calculated fouling sensitivity to precipitation (see Figure 79 in Section 5.5.3). The average percent moisture versus fouling index ratio for the samples extracted from the Alaska Railroad track was significantly lower than the Orin Subdivision samples (see Figure 78 in Section 5.5.3).

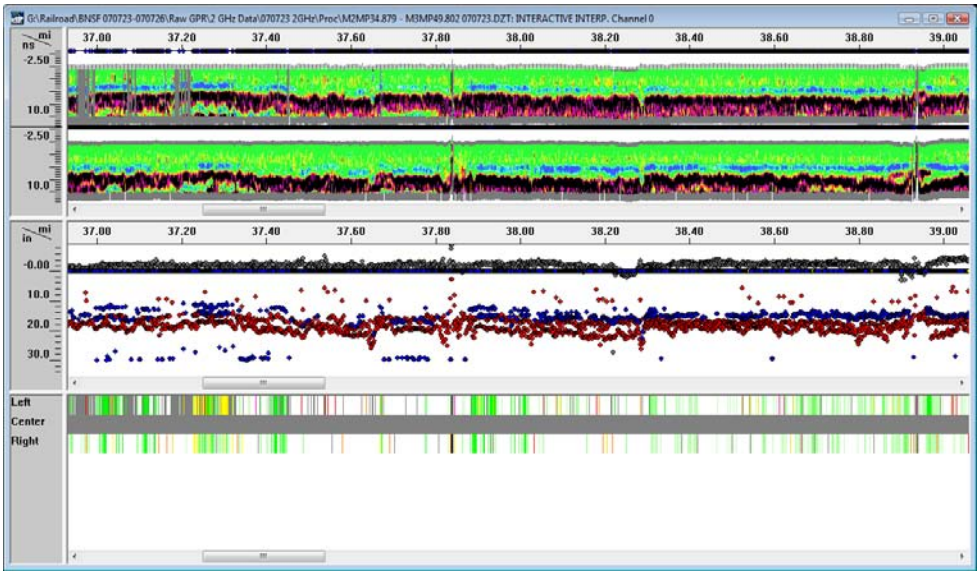

Figure 59. Processed 2 GHz data obtained between MP37 and 39 on track Main 2 before a rainfall event.

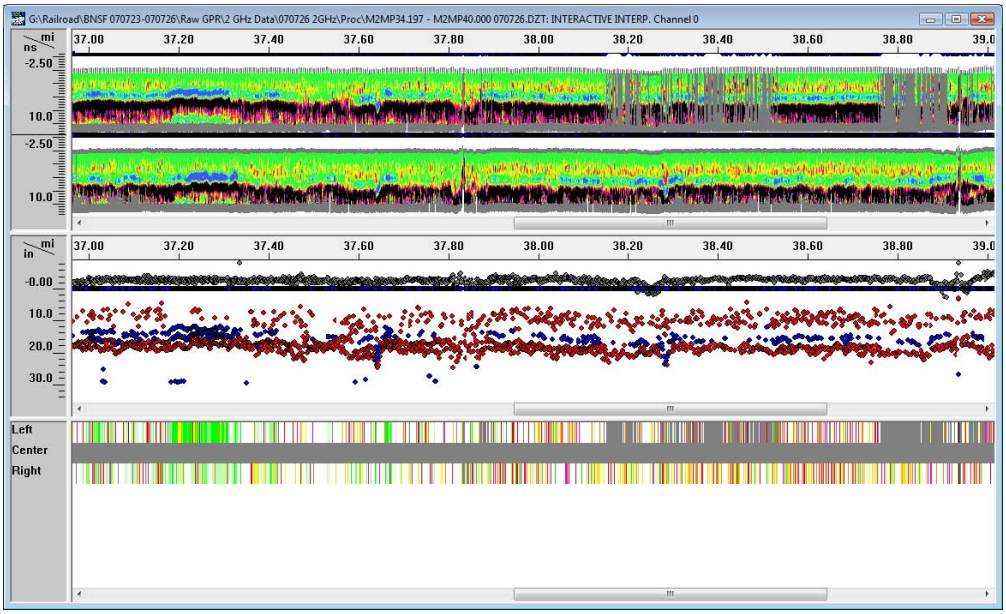

Figure 60. Processed 2 GHz data obtained between MP 37 and 39 on track Main 2 during rainfall event.

Figure 61. Processed 2 GHz data obtained between MP 44 and 46 on track Main 2 before a rainfall event. Data has been reversed relative to data collection direction. As a result the left track side data in this figure corresponds to the right track side data in Figure 62.

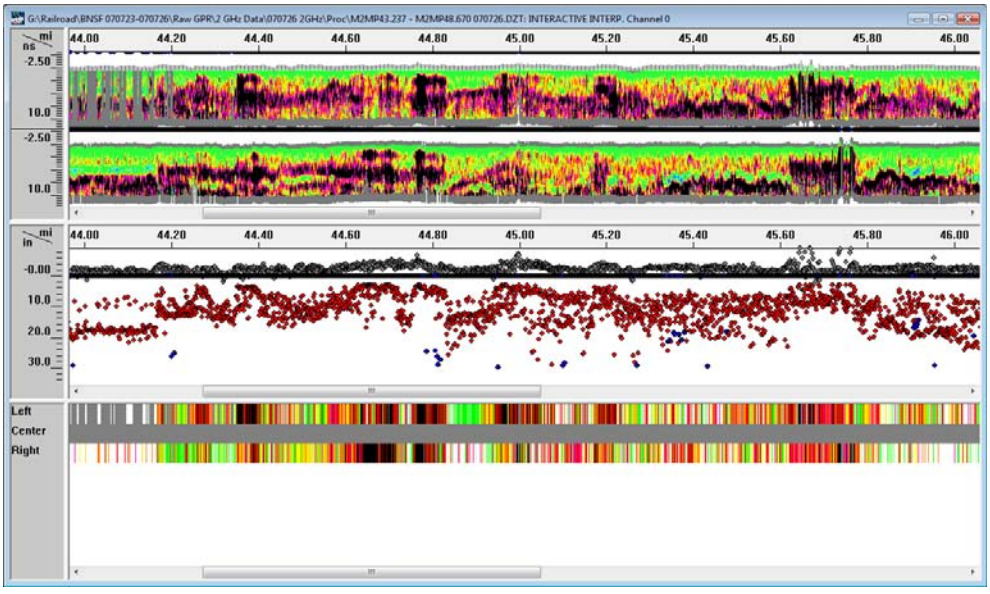

Figure 62. Two GHz data obtained between MP 44 and 46 on track Main 2 during rainfall event.

5.3.3.4 Five Hundred MHz Horn Antenna Data

The 500 MHz data were processed differently than the 2 GHz data. Processing was performed to remove banding in the data associated with reflections from the rails and ties with minimal impact to the layer interface reflections.

A layer reflection was often observed in the 500 MHz data at 10–25-inches in depth. This reflection corresponds to the ballast bottom. Areas where this reflection is most visible, often correspond to the cleanest ballast as shown in Figure 63, which compares 500 MHz data to processed 2GHz data between MP 50 and 49. The strong reflection between MP 50 and MP 49 observed in the processed 500 MHz data corresponds to a thick layer of clean ballast at the shoulders calculated from the 2 GHz data.

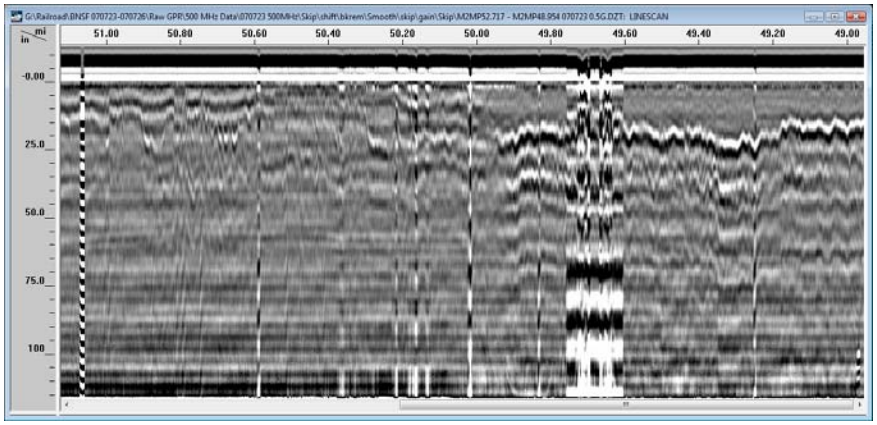

(a) Processed 500 MHz data on track Main 2 between MP 51 and MP 49. A relative permittivity of 4.0 was used to calculate depth.

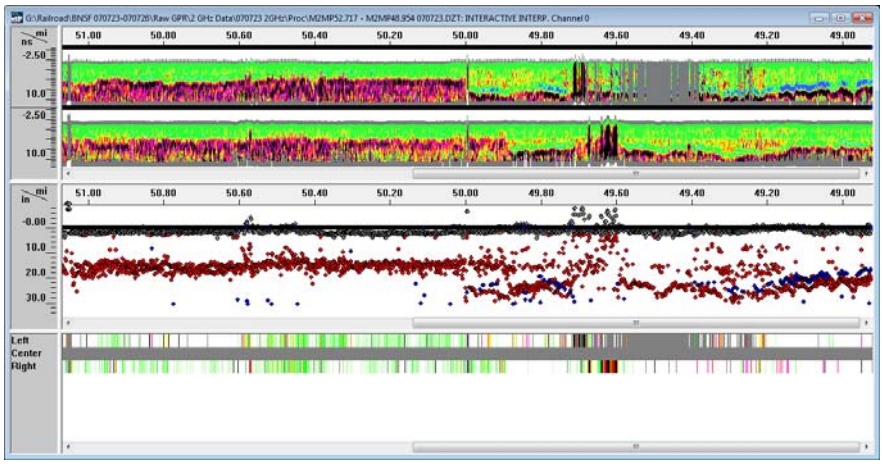

(b) Processed 2 GHz data on track Main 2 between MP 51 and MP 49.

Figure 63. Processed GPR data between MP 51 and MP 49 on track Main 2: (a) 500 MHz data and (b) 2 GHz data. A significant reflection from the bottom of the ballast in the 500 MHz data the correlates to a thick clean section of ballast calculated from the 2 GHz data.

At ground truth locations where the subballast thickness could be measured, typically a reflection occurred between the subballast and subgrade interface. Exceptionally clean ballast is observed at the ground truth location shown in Figure 64. A significant moisture contrast occurred between the ballast and subballast layers as shown in Figure 64(c). Apparently a negligible moisture contrast occurred between the subballast and subgrade layers at the location of the ground truth hole. The 500 MHz data, shown in Figure 65, contains reflections that are in good agreement with the locations of the layer interfaces mapped at the hole's location.

(a) Location of ground truth (b) Cross-section of hole

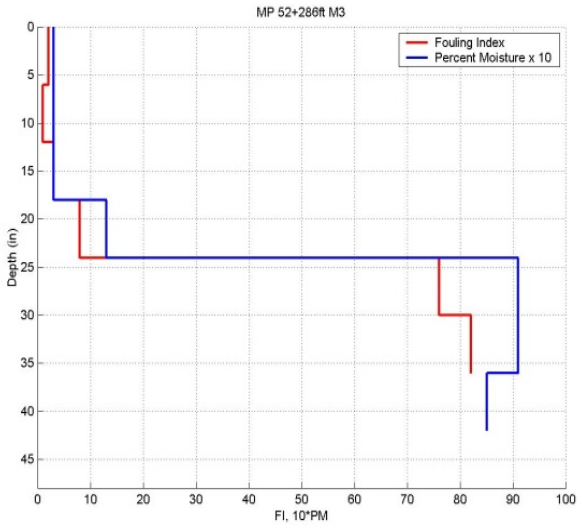

Visual Measurements:
Ballast thickness: 24”
Coal dust in ballast 21-24”
Subballast thickness: 11.5”

(c) Plot of fouling index (red) and percent moisture (blue) for each ground truth sample.

Figure 64. Ground truth of hole dug on track Main 3 at MP 52 +286 ft.

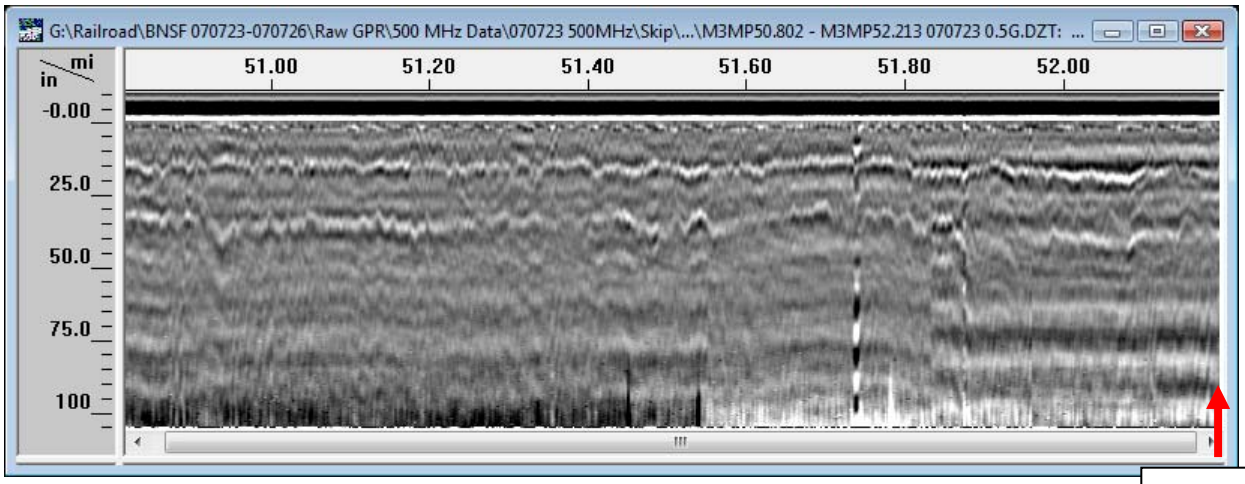

(a) Processed 500 MHz GPR data at core location. Note, ground truth hole dug on shoulder and 500 MHz data obtained between rails.

Ground Truth Location

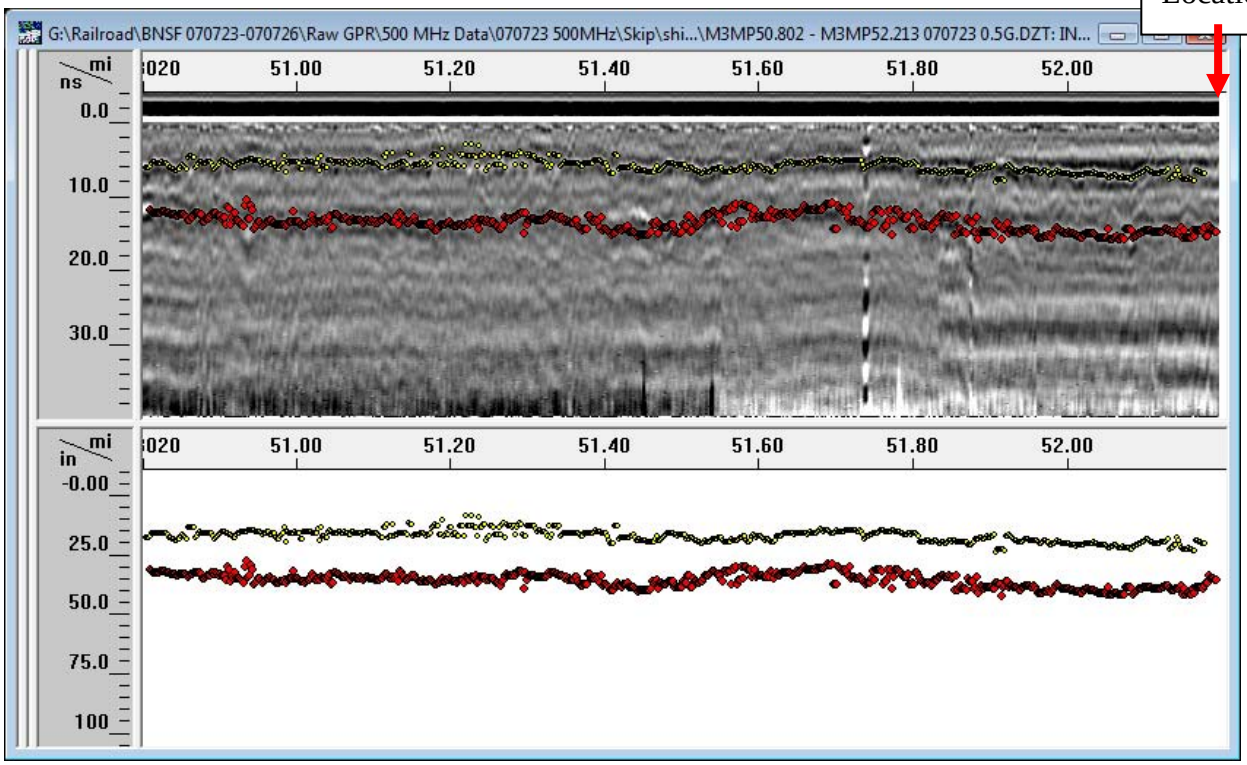

(b) Interpreted 500 MHz GPR data at core location. Relative permittivities used for ballast and subballast layers were 4 and 6.5, respectively.

Figure 65. Processed (a) and interpreted (b) 500 MHz GPR data at ground truth location on track Main 3 near MP 52. Mapped layers in (b) are in good agreement with the actual locations of the ballast-subballast and subballast-subgrade interfaces.

Layer reflections were also detectable in areas where the surface was significantly fouled. Figure 66 shows the ground truth from a hole located on track Main 1 measured 1,420 ft south

of the crossing at MP 37.8. The near-surface at this location was heavily fouled as shown in the pictures and the fouling index plot.

(a) Ground truth location

(b) Ground truth hole

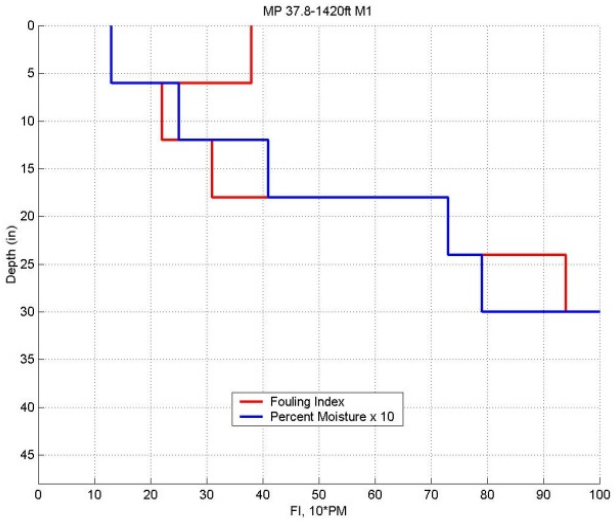

Visual Measurements:
Ballast thickness: 18.5”
Subballast thickness: 10”

(c) Plot of fouling index (red) and percent moisture (blue) for each ground truth sample.

Figure 66. Ground truth hole dug on track Main 1 at the crossing at MP37.8 + 1,420 ft.

The 500 MHz GPR data corresponding to ground truth in Figure 66 is shown in Figure 67. It is noteworthy that there was no discernable reflection from the ballast-subballast interface. This is not uncommon for scenarios where significant fouling occurs, which lowers the dielectric contrast at the interface between the ballast and subballast. The depth of the subballast-subgrade interface reflection interpreted from the GPR data, using a dielectric constant of 8.7 for the depth calculation, corresponds well with the location observed in the ground truth hole.

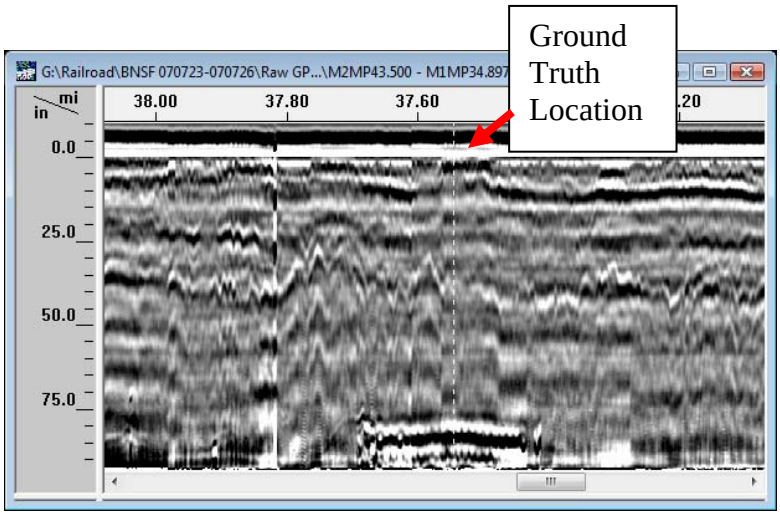

(a) Processed 500 MHz GPR data at core location. Note, ground truth hole dug on shoulder and 500 MHz data obtained between rails.

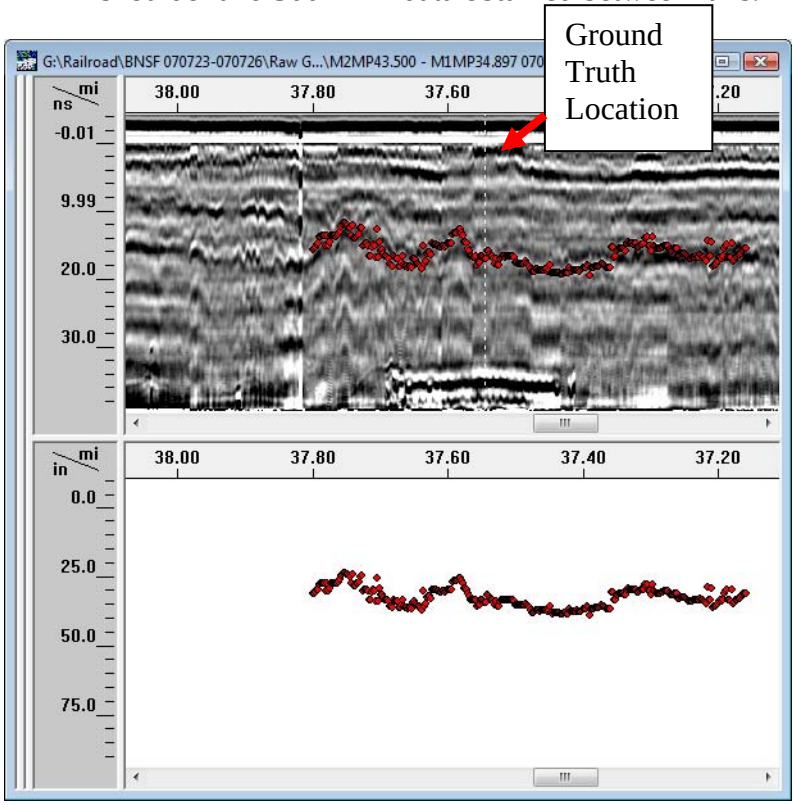

(b) Interpreted 500 MHz GPR data at core location. Relative permittivitiy used for ballast and subballast layers was 8.7.

Figure 67. Processed (a) and interpreted (b) 500 MHz GPR data at ground truth location on track Main 1, crossing at MP 37.8 + 1,420 ft south. Mapped layers in (b) are in good agreement with the actual locations of the ballast-subballast and subballast-subgrade interfaces.

Most of the 500 MHz reflections observed in the data from the Orin Subdivision were from the ballast-subballast and subballast-subgrade interfaces. Reflections from other, deeper, layers were not common. However, there was a segment on track Main 2 from MP 8 to MP 14.2, where numerous reflections extending beyond 6 ft in depth were observed. A segment of processed data from MP 8 to MP 10 is shown in Figure 68.

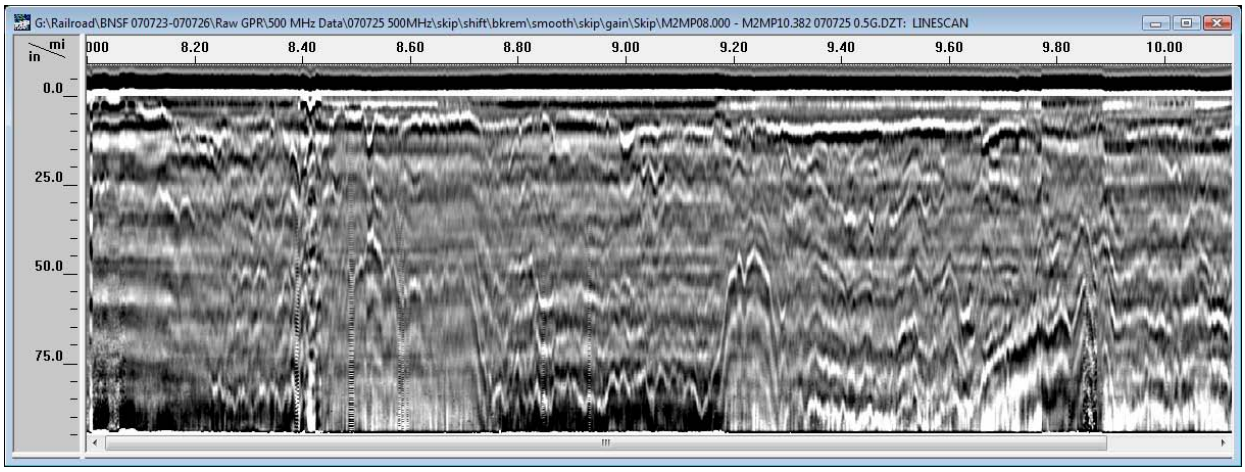

Figure 68. Processed 500 MHz data from MP 8.0–10.0 on track Main 2. Reflections from layers along this segment extend beyond 6 ft in depth. A relative permittivity of 6.25 was used to calculate depth from two-way travel time.

5.3.4 Alaska Railroad, August 2007

Ground penetrating radar (GPR) data were obtained on the Alaska Railroad between August 13 and August 15, 2007. The data were obtained using a 500 MHz air-launched antenna centered between the rails and two 2 GHz horn antennas mounted on the shoulders. Ground truth in the form of hand-dug holes was obtained at 20 locations on the shoulder of the track.

5.3.4.1 Data Collection

Table 7 summarizes the GPR data collection. Significant rains fell in Anchorage the evening of August 14, 2007. Consequently, a recollection of data occurred along the stretch between MP 172–151 on August 15, 2007. Subsequent to the data collection, rainfall records were obtained from two private weather stations located within 4 mi of the track between MP 154 and MP 160. The weather stations recorded 0.29 in and 0.50 in of rainfall the evening of August 14.

Table 7. Data Collection Summary on Alaska Railroad

Date	Track	MP Start	MP End	Total Miles (km)
8/13/07	Main	115.2	142.0	26.8 (43.1)
8/13/07	Siding	119.8	121.4	1.6 (2.6)
8/13/07	Siding	128.0	129.0	1.0 (1.6)
8/14/07	Main	203	162.2	40.8 (65.7)
8/14/07	Main	157.7	151.4	6.3 (10.1)
8/15/07	Main	172	151.5	20.5 (33.0)

5.3.4.2 Ground Truth

Ground truth holes were dug concurrent with the data collection. All ground truth holes were located near road crossings or other well-registered locations along the track that could be accurately correlated with the GPR data. Near these registered locations, specific ground truth locations were chosen for the purpose of sampling the widest range of ballast and subballast conditions based on visual inspection of the GPR data. Figure 69 shows a typical hand-dug ground truth hole. The aggregate was sampled at 6-inch depth increments. Two samples of aggregate of about 2–3 lbs weight were collected and triple-bagged in zip-lock bags at each 6-inch depth interval.

Additional ground truth in the form of frost heave locations and track geometry defects from geometry car data were obtained. The geometry car data were from the spring of 2008. Frost heave locations were identified by sections of the track where shims were added during the winter of 2008. These data were especially useful for providing a type of ground truth to compare with anomalous features observed in the 500 MHz data because the hand dug holes rarely exceeded 3.5 ft in depth. It is anticipated that track geometry defects, such as warping and buckling, should, to some degree, be the manifestation of some track structural problems arising from the subballast and/or subgrade. In those instances where the track geometry defects are indicative of substructure issues, the 500 MHz data would be useful to assess the characteristics of the problem, such as length and depth extent. The added knowledge gained would enable better maintenance planning, therefore resulting in savings to the railroad company.

Figure 69. Typical ground truth hole. The depth of this hole relative to the top of the tie was 3 ft.

The most distinctive feature observed in most ground truth holes was a layer of blue-gray stone varying from 18–24-inches deep. This stone layer typically yielded a lower fouling index and hence lower moisture content than the ballast above and subballast below. Figure 70 shows a close-up of the stone layer from the hole shown in Figure 69. The corresponding moisture and fouling index profile is shown in Figure 71. The blue-gray layer corresponds to the depth range from 18–24 in (Figure 71). Figures 72 and 73 reveal a similar layered structure at another ground truth location. The blue-gray layer at that location was located from 12-18-inches deep.

Figure 70. Layer of distinct blue-gray crushed stone that is typically near 24-inches deep at most ground truth locations. The moisture content of the subballast beneath this layer was substantially higher.

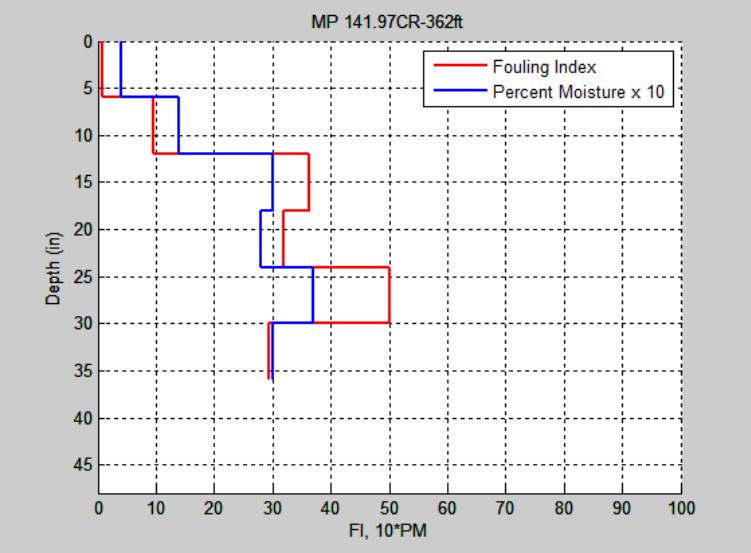

Figure 71. Fouling index and moisture content profiles at 6-inch deep increments at the sample location corresponding to Figure 70. Sample associated with blue-gray layer is 18–24-inches deep.

Figure 72. Another ground truth location exhibiting the layer of blue-gray stone.

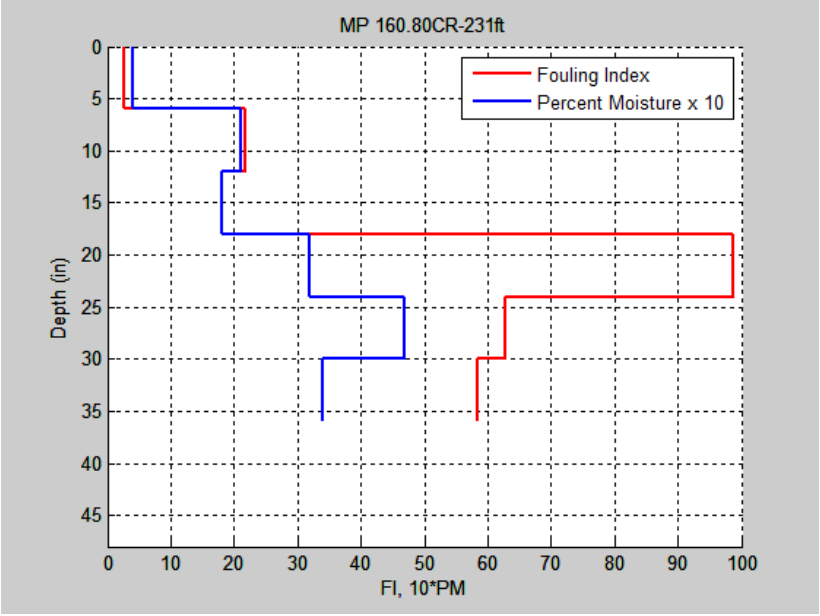

Figure 73. Fouling index and moisture content profiles at 6–inch depth increments at the sample location corresponding to Figure 72. Sample associated with blue-gray layer is 12–18-inches deep.

5.3.4.3 2 GHz Horn Antenna Data

The processed 2 GHz horn antenna data revealed that the ballast was fouled along most of the track over the data collection route. This was not unexpected because ballast cleaning is not

performed regularly. Some short sections of track did contain clean ballast. Examples of processed data from clean and fouled ballast are shown in Figures 74 and 75, respectively.

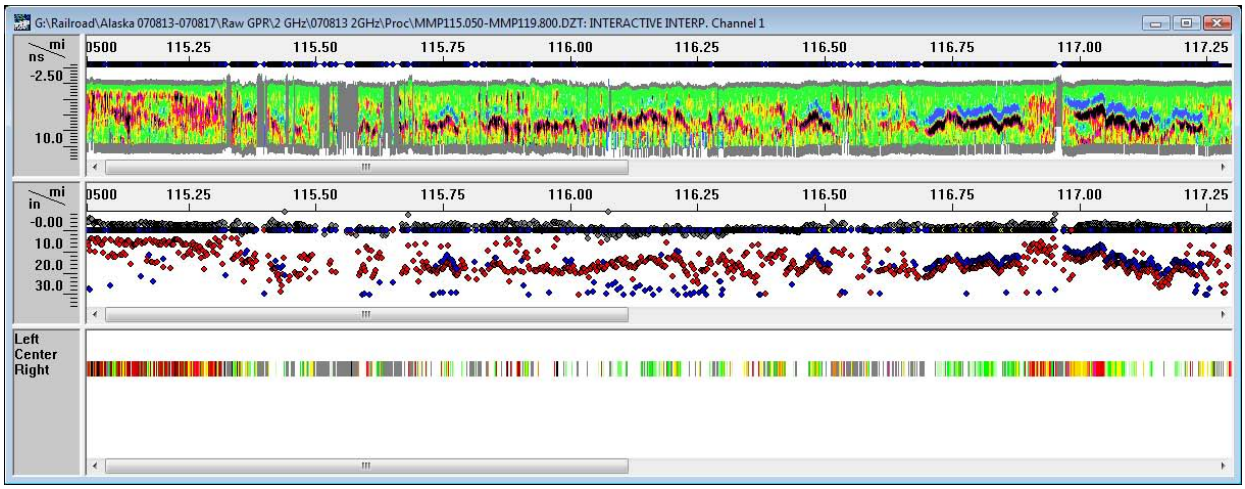

Figure 74. Processed data from the right shoulder from MP 115-117.25. The processed – data indicates that the shoulder ballast is generally clean to depths 12 in or greater along this segment of track.

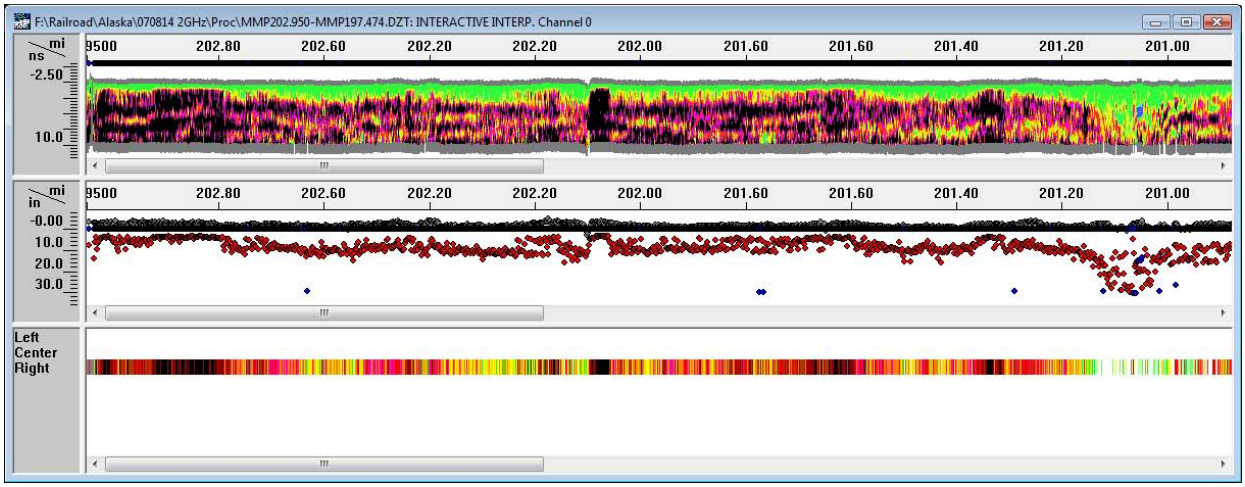

Figure 75. Processed data from right shoulder from MP 203–201. The processed data indicates the shoulder ballast is generally fouled at depths within 2 in relative to the bottom of the ties.

In Figure 76 the fouling depth obtained from GPR data analysis is compared with the fouling index for each sample depth at each ground truth location. Good agreement exists between the GPR-predicted fouling depth and the onset of significant fouling.

Close examination of Figure 76 shows that eight out of 20 of the ground truth locations have significant fouling less than 12 in below the top of the tie. In seven out of those eight

instances, the GPR-predicted fouling depth was less than 12 in. Likewise for the 12 instances where the onset of significant fouling is 30 cm (12 in) or more, the GPR-predicted fouling is greater than 25 cm (10 in) in seven cases and 22 cm (9 in) or greater in three out of the remaining five cases. There is good agreement between the GPR-predicted fouling depth and the onset of significant fouling.

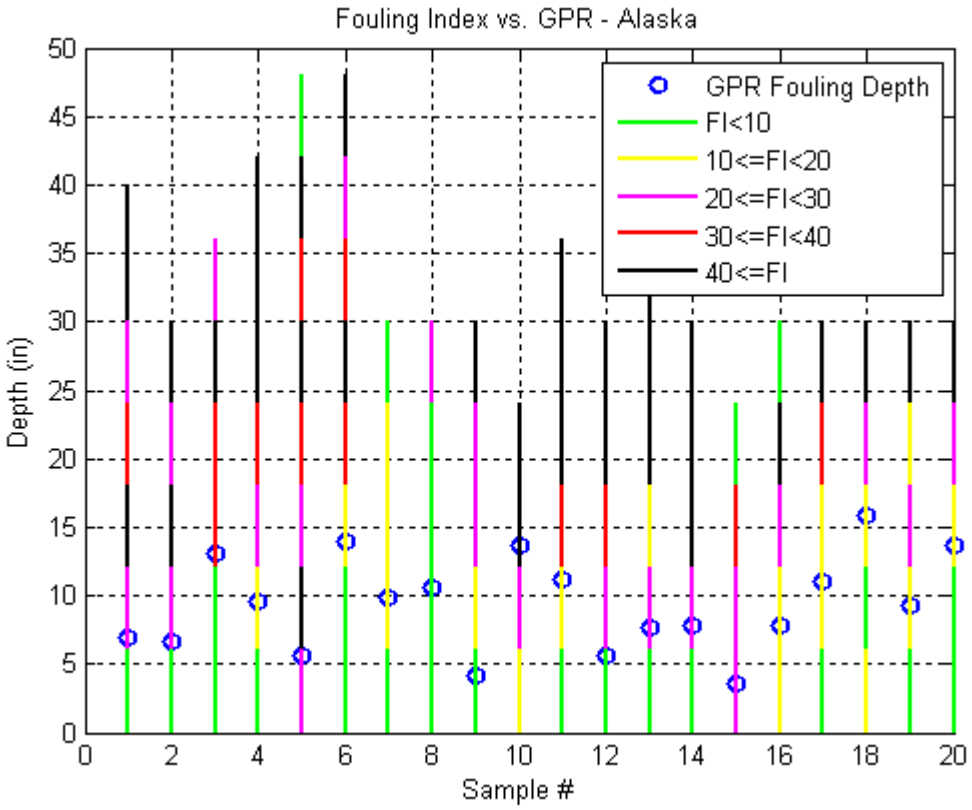

Figure 76. Comparison of the GPR predicted fouling depth and the fouling index calculated from sieve analysis of samples at 6-inch depth increments.

Table 8 shows the GPR-accuracy assessment using the methodology introduced in Section 5.4.3. There is 85 percent full and likely agreement between the GPR data and the ground truth. The similar level of agreement with the Orin Subdivision track is encouraging considering the huge differences between the track structure and maintenance history on the Alaska track versus the Orin Subdivision track. A great deal more moderate fouling occurred with fouling indexes between 10 and 20 from the Alaska railroad track versus the Orin Subdivision track. The moderate fouling attenuates the GPR-void scattering at a higher rate relative to clean ballast, resulting in shallower GPR-calculated clean ballast thicknesses. This is observed in Figure 76 where many of the GPR-calculated clean ballast thicknesses are in the 9-12-inch range because of the moderate fouling condition of the ballast.

A correlation exists between percent moisture and fouling index. The higher the fouling index is, then the greater the capacity to store moisture. The calculated fouling depth is compared to the percent moisture in the samples at the ground truth locations in Figure 77. The correlation

between calculated fouling depth and the first sample exhibiting moisture greater than 2 percent is clear.

Table 8. GPR accuracy related to ground truth fouling data

Sample #	Full Agreemenet	Likely Agreement	Moderate Fouling Agreement	Thick Ballast Agreement	Disagreement
1	Yes				
2	Yes				
3	Yes				
4			Yes		
5	Yes				
6			Yes		
7			Yes		
8					Yes
9					Yes
10					Yes
11			Yes		
12		Yes			
13	Yes				
14	Yes				
15	Yes		Yes		
16			Yes		
17	-		Yes		
18	-		Yes		
19	-		Yes		
20	-		Yes		

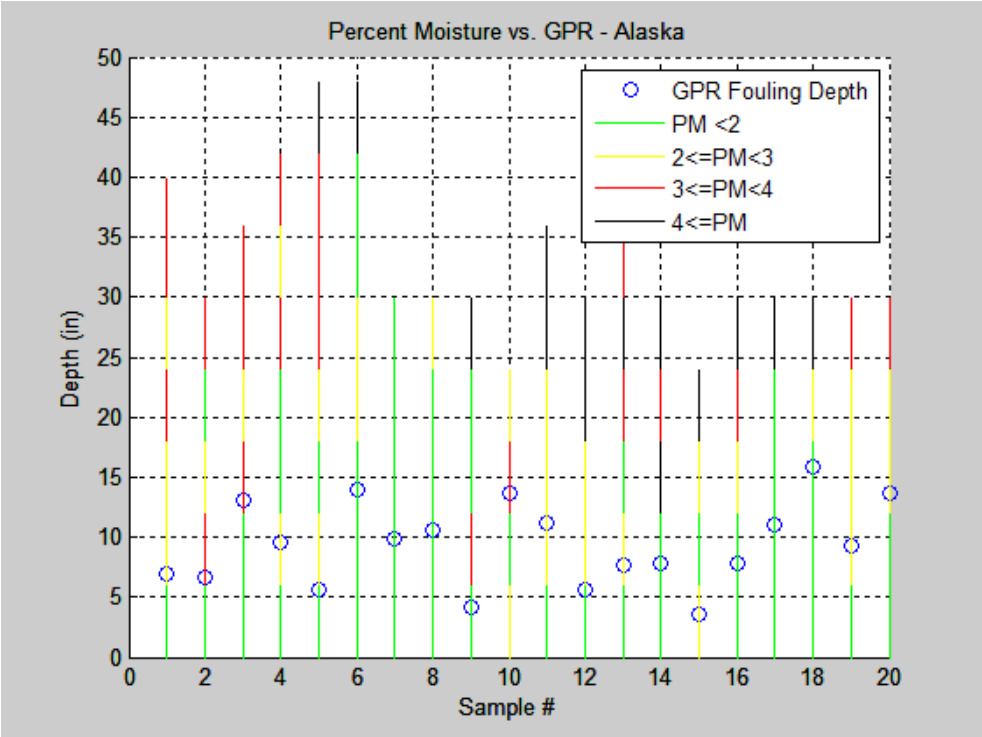

Figure 77. Comparison between GPR-calculated fouling depth and percent moisture.

The percent moisture versus fouling index is plotted for all the ground truth samples in Figure 78. There is a clear trend in increasing moisture versus increasing fouling index.

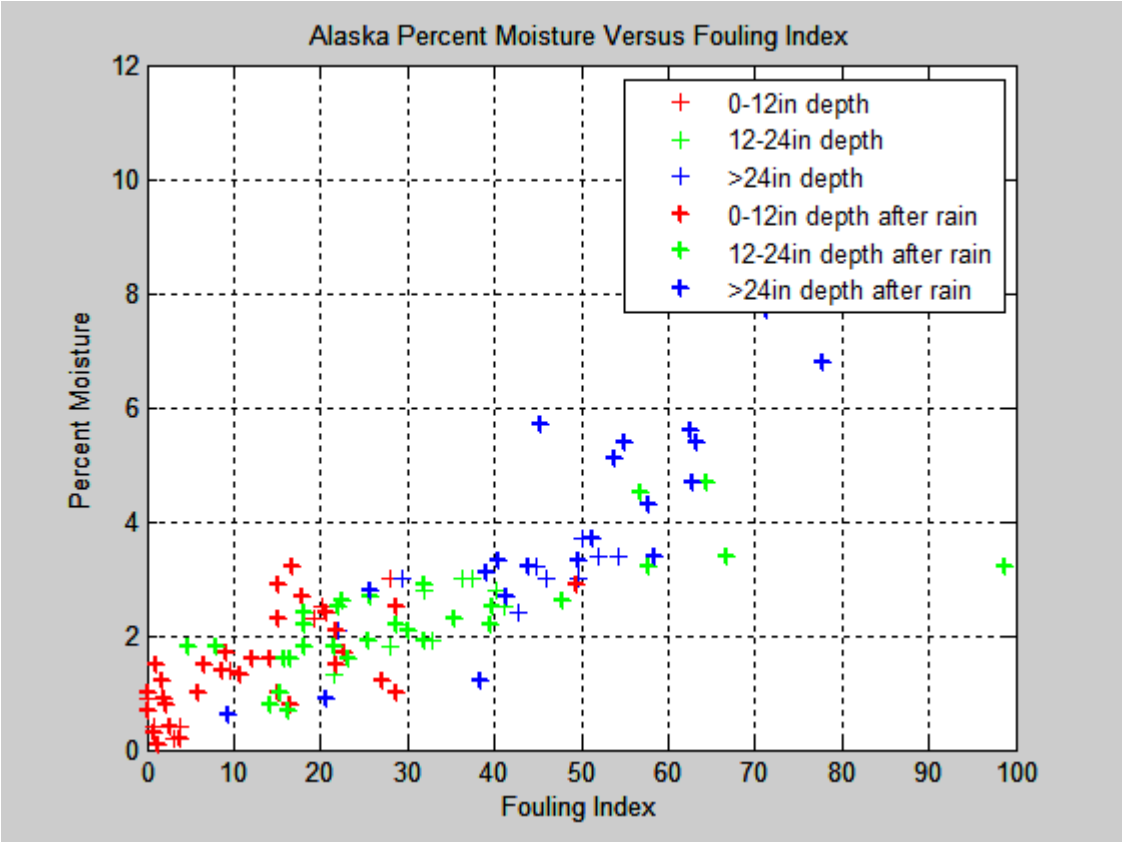

Figure 78. Plot of percent moisture compared to fouling index from all the Alaska ground truth samples. The sample points are color-coded based on the depth they were extracted. Bold symbols indicate samples extracted 1–2 days after rainfall between 0.3–0.5 in.

A fortuitous rainfall event provided the means to obtain repeat data over a section of track with different moisture conditions. Repeat data were collected along a 20-mile segment of track between MP 172–152 before and after a rainfall event likely between 0.3–0.5 in. Figure 79 shows (a) processed data obtained prior to the rainfall and (b) processed data obtained after the rainfall event. The fact that the data are very similar indicates the method is robust to some change in moisture. Clearly, moisture in the ballast layer existed prior to the rainfall the evening of August 14. One of the local weather stations reported approximately 0.5 in of rainfall 10 days before data collection. (No data were available from the other weather station.)

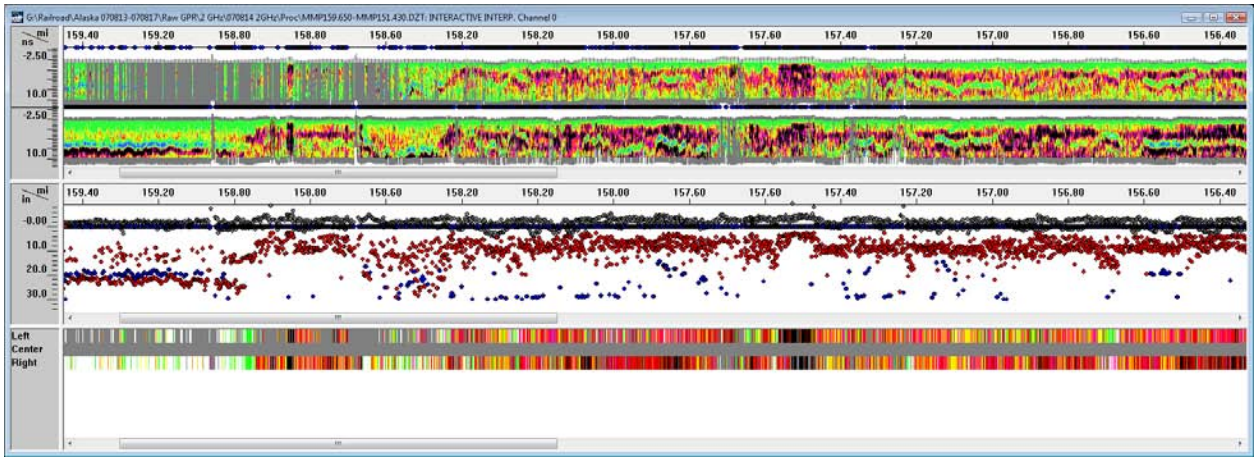

(a) Data obtained prior to rainfall between MP 159.4–156.4

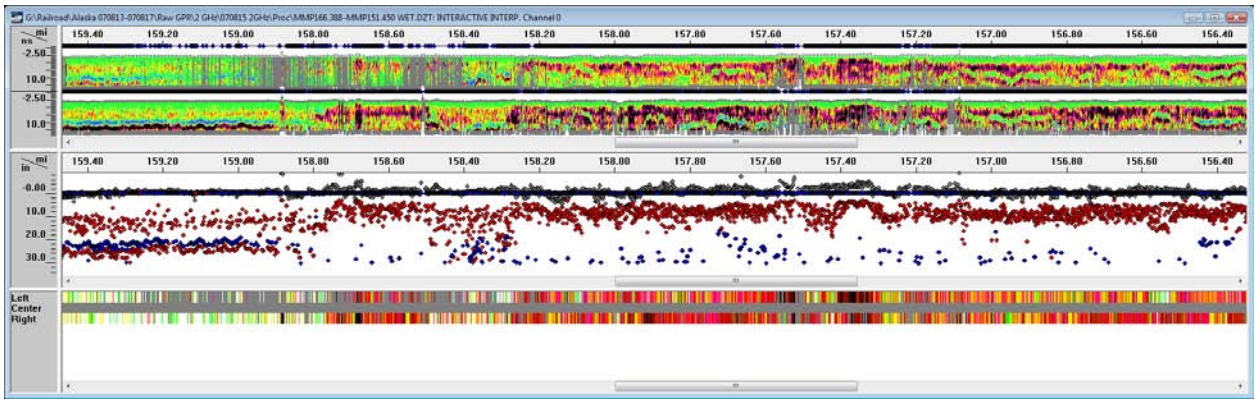

(b) Data obtained day following rainfall of 0.3 and 0.5 in between MP 159.4–156.4.

Figure 79. Comparison of processed 2 GHz data before and the day after a rainfall estimated to be 0.3 and 0.5 inches

5.3.4.4 500 MHz Horn Antenna Data

A layer reflection was often observed in the 500 MHz data at 15–25-inches in depth. Comparison between the 500 MHz data and ground truth indicates this reflection is likely associated with a moisture increase at the bottom of the blue-gray stone layer. A good example of this layer reflection is shown in Figure 80.

(a) Picture of ground truth location of samples

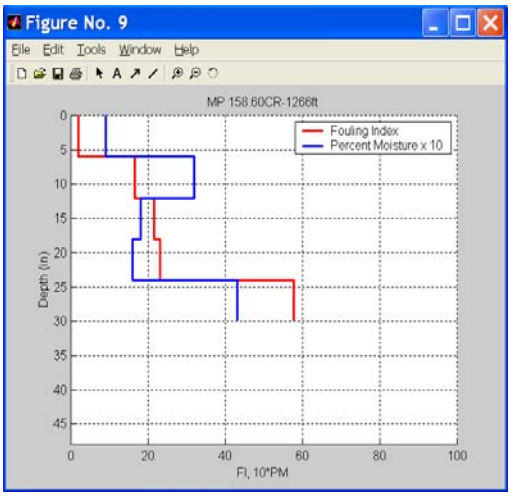

(b) Sieve and moisture analyses

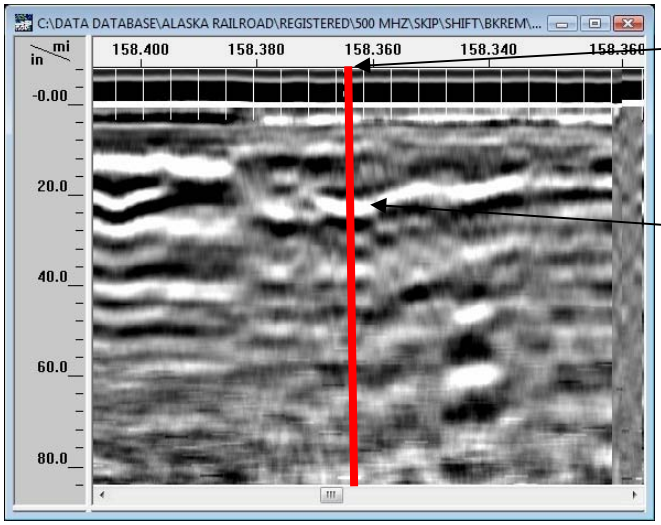

Sample location (sample obtained outside edge of ties and 500 MHz data obtained between rails)

Reflection likely associated with bottom of blue-gray crusted stone

(c) Processed 500 MHz data. Note the strong reflection at 20–25-inches deep.

Figure 80. Comparison of 500 MHz data and ground truth at one location.

The reflection between 15–25-inches in depth was generally most prominent in the data from MP 115–132, which corresponds to a section of track with generally clean ballast. This is anticipated because there would be a greater moisture contrast between clean ballast and subballast.

Numerous sections of 500 MHz data that contained high subballast or subgrade reflections were at depths 3–7 ft. These high-amplitude reflections often are associated with a material change that traps moisture. Anomalous high-amplitude reflections can easily automatically be located in the data and exported to a Google Earth KML file. The highest amplitude reflections from MP 135–203 are shown in the Google Earth display in Figure 81. The yellow and red colors in the figure are indicative of high-amplitude zones. It is clear from the figure

that the high-amplitude reflection zones are localized because most of the plotted amplitude data are blue.

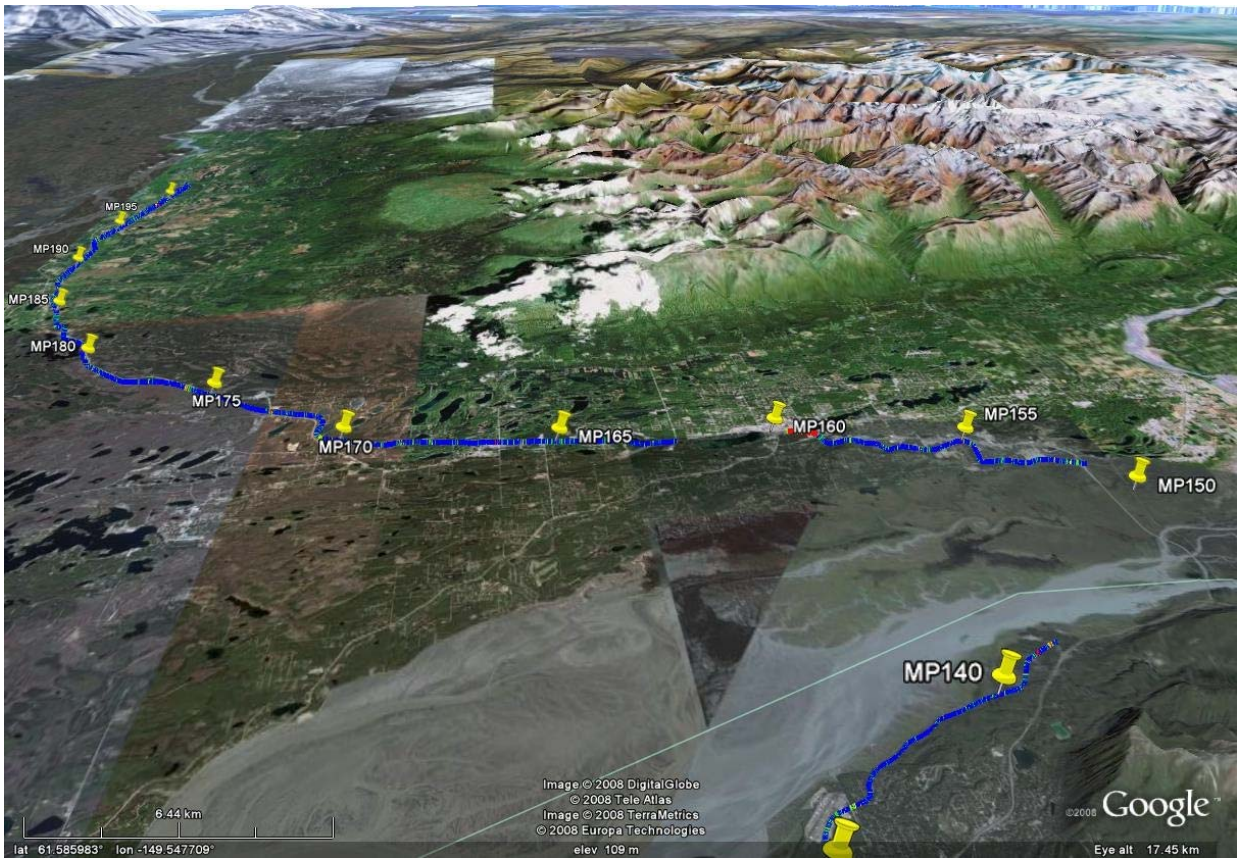

Figure 81. Automatically picked highest amplitude reflections between 30- and 75-inches deep. Color key: Blue < 67.5 dB, Green 64.5–70 dB, Yellow 70–72.5 dB, Red > 72.5 dB.

The locations of frost heaves and track surface geometry defects are plotted along with the GPR amplitudes in Figure 82. The Google Earth interface permits the user to easily compare the track condition data with the high-amplitude reflection zones. Comparisons of the defect locations with GPR data are shown in Figures 83 and 84. In general, there is no definitive correlation between the location of the surface track geometry defects and anomalous high amplitude zones identified in the 500 MHz data.

Two instances, where the frost heave locations correspond to local anomalous high-amplitude zones in the GPR data, are shown in Figures 85 and 86. The comparisons are favorable and suggestive that there may be a correlation between the anomalous reflection amplitudes and the frost heaves at these locations. However, there are many other high amplitude zones where no frost heaves exist. Likewise, there were frost heave locations without any significant high amplitudes in the 500 MHz data. At this time, the value of the 500 MHz horn antenna data for predicting frost heave locations cannot be determined. Much more data and ground truth would need to be obtained to make a more definitive conclusion.

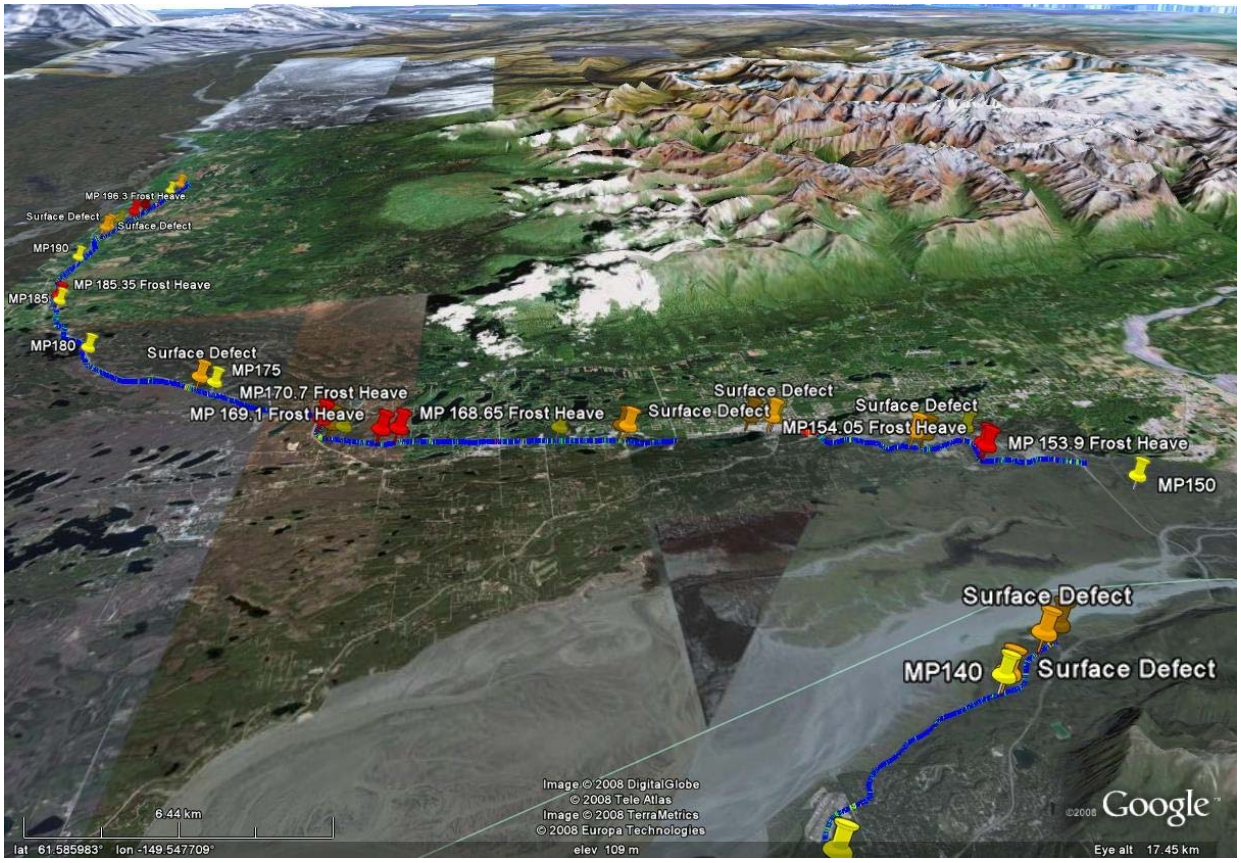

Figure 82. Locations of Surface track geometry defects (orange pushpins) and frost heaves (red pushpins) superimposed on top of the highest amplitude GPR reflections between 30- and 75-inches in depth. GPR Color key: Blue < 67.5 dB, Green 64.5-70 dB, Yellow 70-72.5 dB, Red > 72.5 dB.

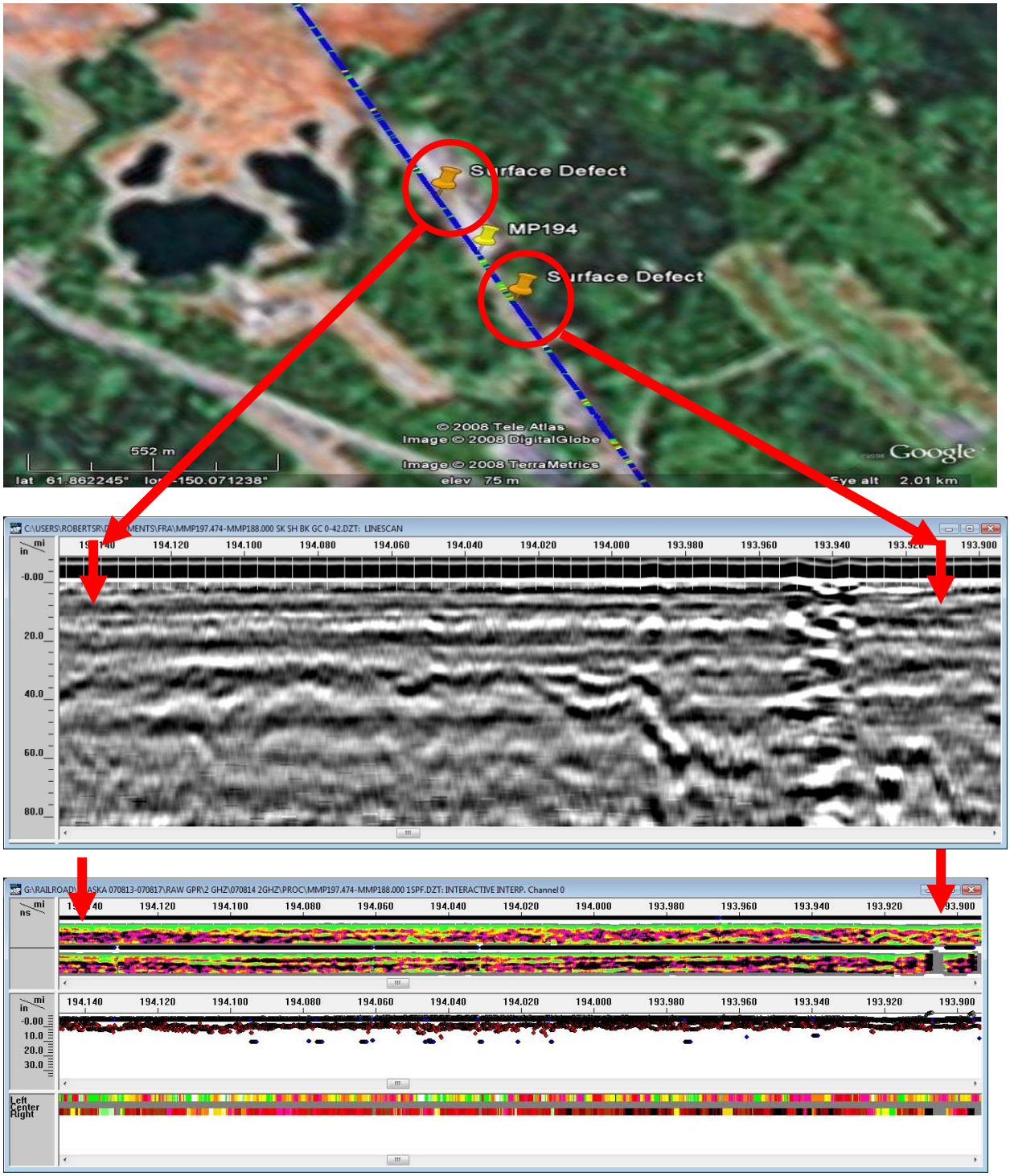

Figure 83. Locations of two surface track geometry defects (orange pushpins) near MP 194 superimposed on top of the highest amplitude GPR reflections between 30- and 75-inches deep (top), and corresponding 500 MHz GPR data (bottom middle) and processed 2 GHz data (bottom).

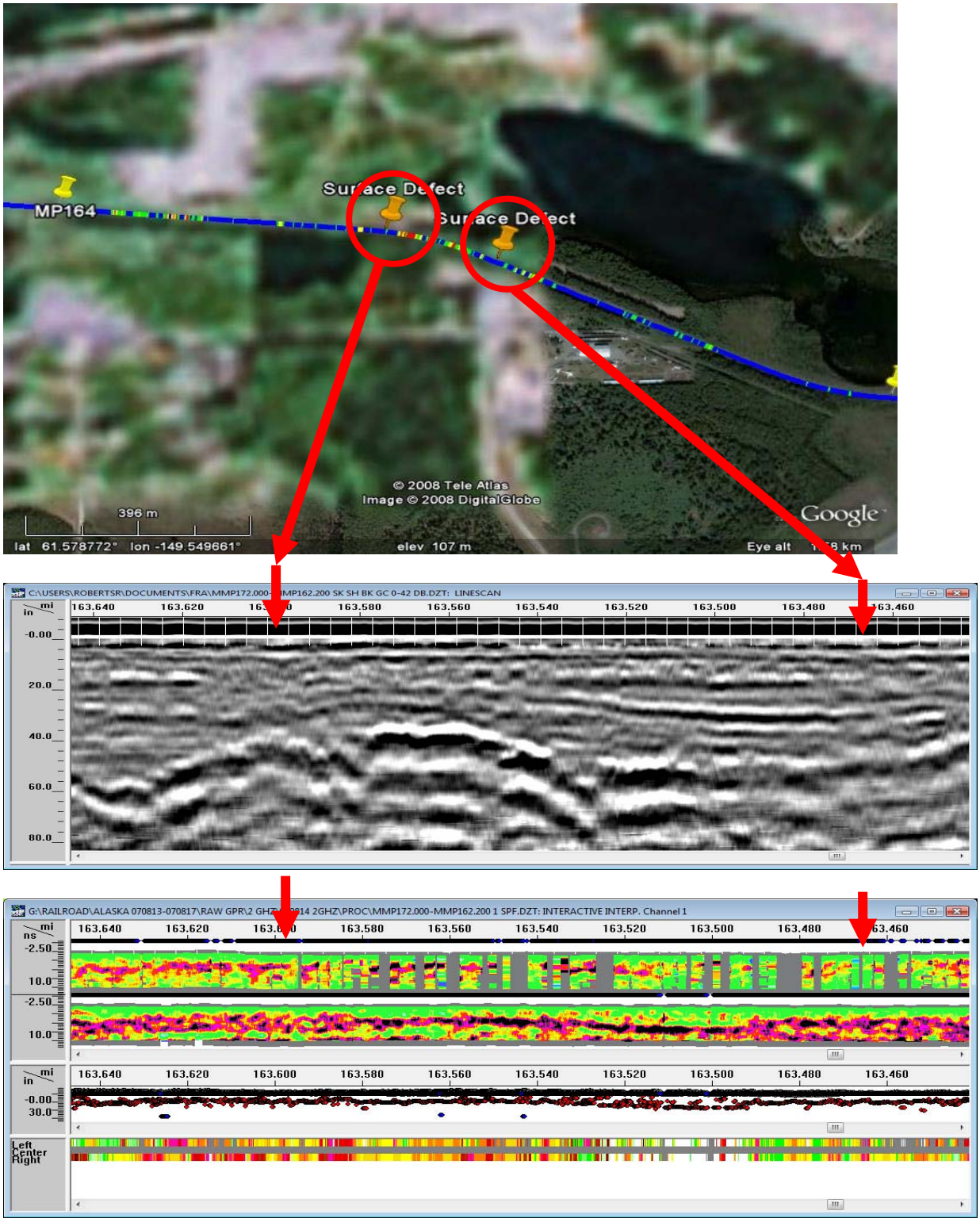

Figure 84. Locations of two track geometry-surface defects (orange pushpins) between MP 164 and 165 superimposed on top of the highest amplitude GPR reflections between 30- and 75- inches deep (top) and , corresponding 500 MHz GPR data (bottom middle), and processed 2 GHz data (bottom).

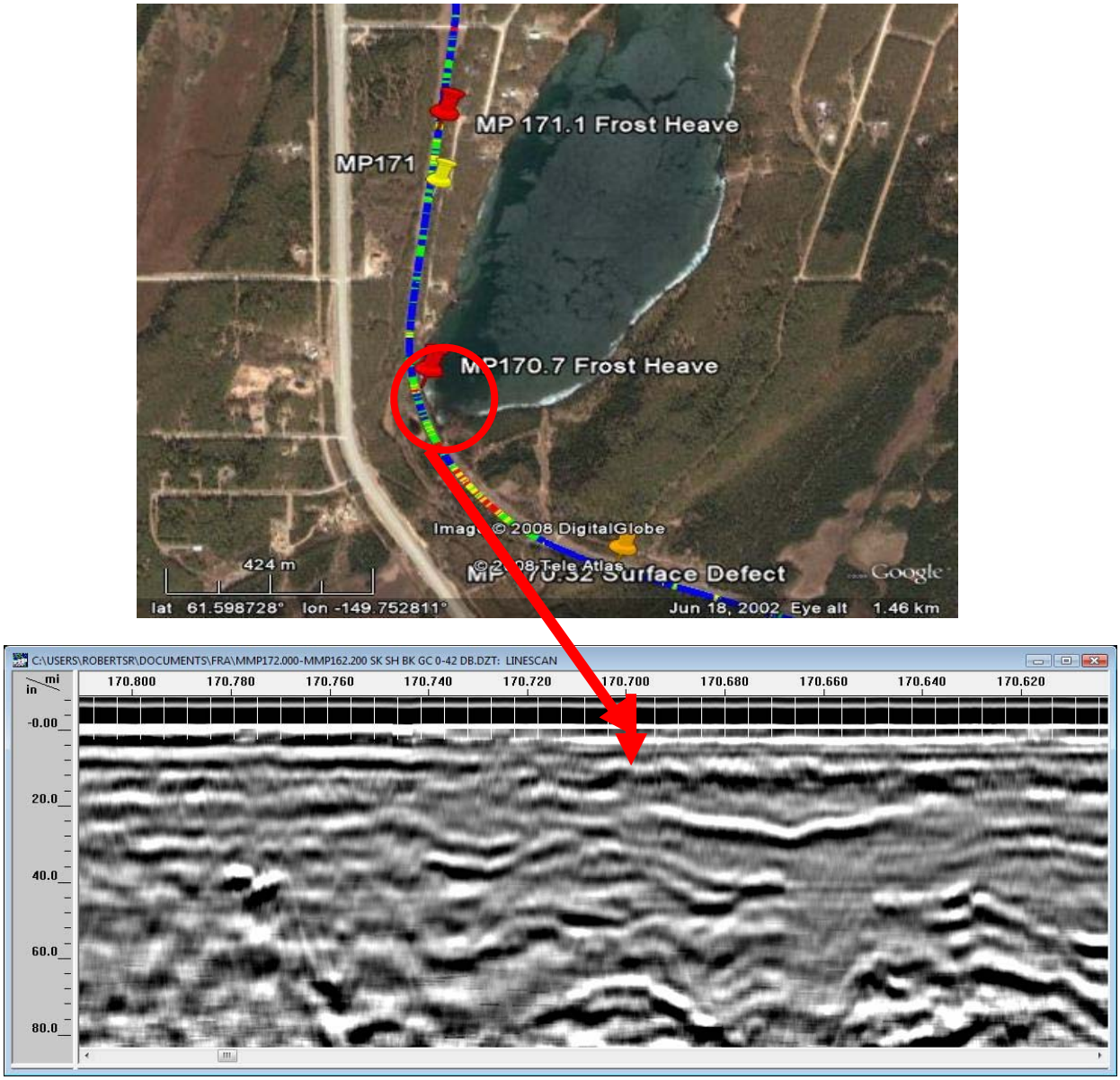

Figure 85. Location frost heave at MP 170.7 superimposed on top of the highest amplitude GPR reflections between 30- and 75-inches deep (top) and corresponding 500 MHz GPR data (bottom).

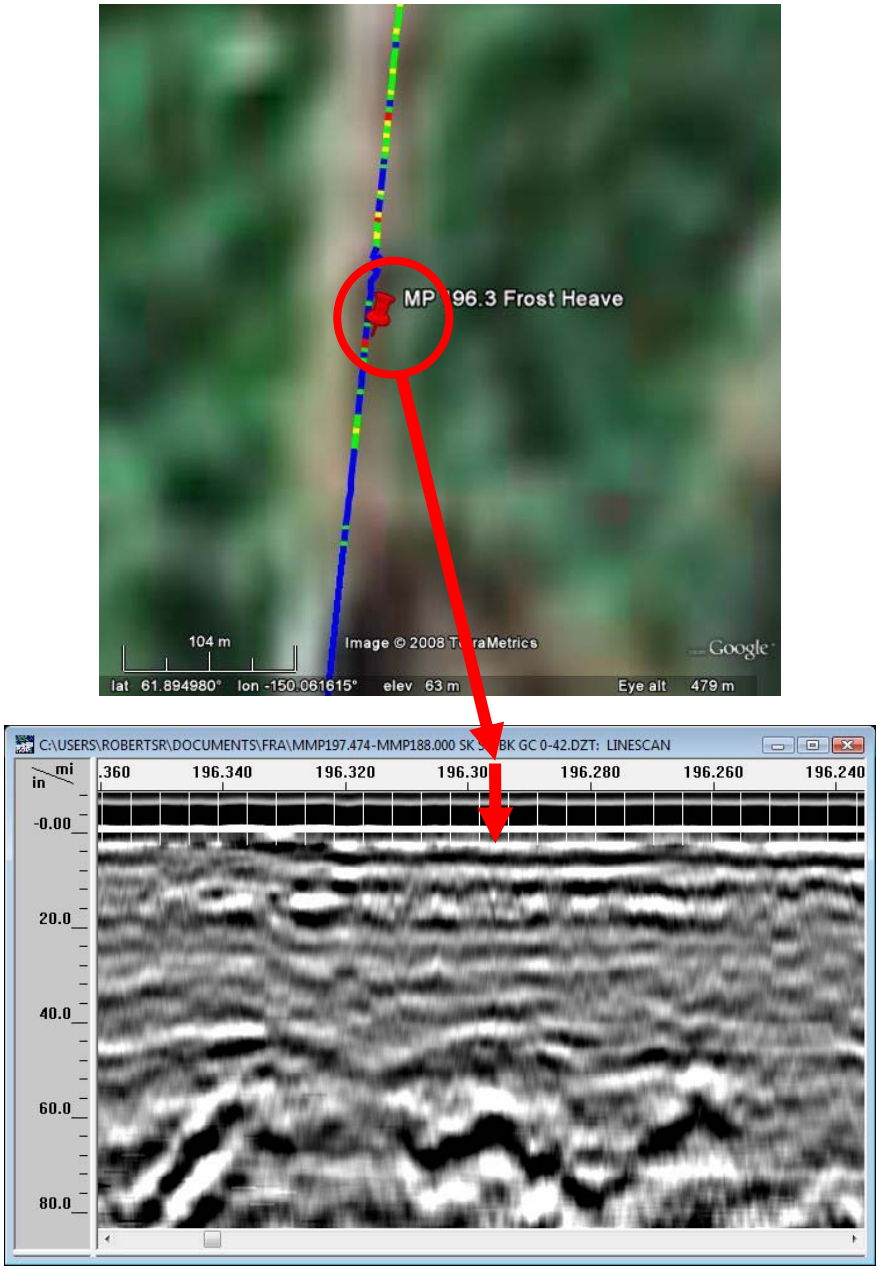

Figure 86. Location frost heave at MP 196.3 superimposed on top of the highest amplitude GPR reflections between 30- and 75-inches deep (top) and corresponding 500 MHz GPR data (bottom).

6. CURRENT HARDWARE AND SOFTWARE STATUS

6.1. Equipment

A fully functional GPR configuration has been established during this phase of the project. This configuration consists of off-the-shelf components. The GPR control unit and antennas are standard GSSI equipment. Mounting hardware has also been developed during the course of the project. The two 2 GHz horn antennas are mounted approximately 6 in beyond the end of the ties on this fixed setup. This setup does not conform to Plate C specifications, which require a clearance height of approximately 24 in above the top of the ties. In the future it may be desirable to design a setup that accommodates obstacles that impede the antenna. It was found that the clearance requirement was generally not a problem for a hi-rail vehicle traveling about 25 mph on the Orin Subdivision and Alaska Railroad tracks. However, the passenger platforms along the Amtrak railroad were frequently located so that one of the outer antennas had to be moved to prevent it from being damaged while the hi-rail vehicle traversed the length of the platforms.

6.2. Data Collection Rate

Data collected during the project was obtained at scan densities no less than 4 scans/ft. at speeds up to 25mph, which was possible by setting the transmit rate of the control unit to 300 KHz. Current FCC regulations require that the transmit rates of equipment manufactured for sale in the United States to be limited to 100 KHz. This means that maximum scan density of purchased equipment traveling at 25 mph is 1.3 scans/ft. This data density is sufficient for network level surveys. All of the large-scale processed data presented in this report was first decimated to 0.5 scans/ft prior to processing. For detailed high-resolution surveys with a data collection density of 4 scans/ft, the maximum speed will be approximately 8 mph. Table 9 summarizes these parameters.

Figure 87. Current ballast evaluation survey types and maximum data collection speeds.

Survey Type	Data Density (scans/ft)	Maximum Speed (MPH)
High resolution	4	8
Network level	1.3	25
Network level	0.5	65

6.3. Sensitivity to External Noise

Current FCC regulations limit the transmit power of the 2 GHz horn antennas. The data from 2 GHz antennas meeting this power limit were significantly impacted by external radio frequency (RF**)** interference at the Amtrak data collection site. Recently, GSSI has developed a RF filter that removes frequency modulation (known as FM) interference from the data. This filter is currently being evaluated.

6.4. Data Collection Software

Standard data collection software is used to obtain the GPR data. No antenna calibration is required. Data collection settings are stored on the control unit. Thus, the data collection is simple to initiate and needs no user input during data collection.

6.5. Data Post-Processing Software

Data post-processing can be performed on the same unit as data collection. The data processing is integrated in GSSI's data post-processing software, RADAN. All of the 2 GHz horn antenna data processing steps have been combined into a single macro which can be run by pressing a single button. The outputs from the data processing are the color-coded data shown in this report and an ASCII comma separated variable (CSV) file. There are no user options or adjustable parameters. Every dataset is processed in precisely the same way. The data post-processing software is commercially sold as the BallastVue Module.

RADAN can also be used to process the 500 MHz antenna data. Some processing steps, such as mapping the anomalous high reflection amplitude areas, can be performed automatically. Detailed layer mapping can be performed in an interactive manner.

7. Summary and Findings

An investigation of railroad ballast using recently developed 2 GHz horn antennas has yielded data that contain scattering from the void space between individual ballast aggregate. A simple GPR data processing approach was introduced to yield scattering amplitude envelopes. Comparison of the processed GPR data to ground truth samples collected from cross trenches, locations of surface splashing, and undercutting records revealed good agreement between the characteristics of the scattering amplitude envelope and ballast distress.

The color-coded processed data provides a very intuitive data display for minimally trained users. Ballast characterization can be achieved on both large and small scales. The extent of recently undercut ballast is clearly observed from the processed network-level data. Likewise, very localized ballast fouling, extending over several ties, can be observed from high-resolution data obtained at slow speeds.

Two key indications of distressed ballast are easily identified from this type of display focusing on the area near the bottom of the ties: (1) very low amplitude areas indicated by red and black colors, and (2) high-amplitude reflections indicated by blue areas. The former corresponds to severely fouled ballast, and the latter corresponds to a significant reflecting boundary between clean ballast and ponding water or fouled ballast.

GPR and ground truth data from 382 mi of track are presented in this report. Table 10 summarizes the data locations and ground truth. The data were obtained on five tracks with different substructure conditions. In Colorado, GPR data were obtained in a dry environment with stable, sandy subgrade. Data from the northeastern United States were obtained in an area with a shallow water table and unstable subgrade. Data from Wyoming were obtained on relatively stable sandy soil and much of the data from Nebraska were obtained on track placed over expansive clays. The track in Alaska was susceptible to frost heaves. The 2 GHz data processing approach developed from analysis of the Colorado data was applied to the other datasets and yielded very good correlation with available ground truth.

This developed methodology for ballast fouling assessment presents a feasible approach for routine inspection of working railroads and is especially suited to assess the ballast fouling condition near the bottom of railroad ties.

Table 9. Summary of data collection areas and ground truth.

Location	Miles Data	Subgrade Type	Samples and Cross Trenches	# Mudspots	Records of Undercutting And Shoulder cleaning (miles)
TTC	15	Sand	15	0	-
Providence, RI – Sharon, MA	29.5	Sand/Clay	0	5	29.5
West Bill, WY-Shawnee Junction, WY	75	Sand	5	260	21.9
Crawford, NE-Ardmore, SD	34.9	Expansive Clay	0	54	0.55
Gillette Area, Wyoming	131	Sand	20	-	-
Alaska Railroad	97	Sand/Clay	20	-	-

The 500 MHz horn antenna data were useful for mapping reflections that were associated with subballast and subgrade layering. Anomalous high amplitude zones between 2.5 and 6.25 ft in depth were automatically mapped and could be exported to Google Earth for quick, efficient analysis. The geometry car-detected surface defects track geometry defect locations and frost heave locations were compared to the anomalous high amplitude zones in the Alaska Data. No definitive correlation was observed between the high amplitude zones in the 500 MHz GPR data and the surface defects. Examination of the ballast fouling condition on the shoulders calculated from the 2 GHz antenna data at numerous defect locations indicates considerable shallow fouling. The ballast fouling condition likely may contribute to some of the observed track geometry defects.

Some correlation was observed between several frost heave locations and high amplitude reflections. At other locations there were high amplitude reflections but no frost heaves. Consequently, at this time, it can only be inferred that in some subset of the frost heaves, there is a relationship with high amplitude reflections in the 2.5–6.25 ft depth interval in the 500 MHz data.

8. Recommendations for Future Research and Development

The evolution of the 2 GHz horn antenna data processing methodology for ballast fouling assessment has led to a commercial product. The accuracy of the method has been validated on more than 382 mi of track. Industry response to the use of GPR data for ballast condition assessment has indicated the current method provides useful information for classifying ballast fouling. The technique is efficient and should provide the industry with considerable cost savings by enabling railroad companies to locate and prioritize sections of track for scheduled undercutting and shoulder cleaning. The fact that automatic data processing is performed on the data is a very marketable feature. The data can be obtained and processed by minimally trained users. From a GPR manufacturer perspective, the product has achieved a very sellable level. Enhancing the visibility of the method in the industry should be a priority.

The 500 MHz antenna clearly is useful for mapping strong layer reflections. This was demonstrated in Wyoming, where the subballast and subgrade interfaces were mapped. On the Alaska Railroad, several of the anomalous high amplitude areas correlated to frost heave locations. The data provided by the 500 MHz antenna may, therefore, be useful in certain situations. Anomalous reflection amplitudes can be mapped automatically. The mapping of layer reflections in general, however, requires a highly trained user. This drives up the expense of the method and discourages end users from purchasing the product. The usefulness of the 500 MHz antenna will likely be evident over time as the information provided by the antenna will help in planning and prioritizing track maintenance.

It is recommended that future research and development be focused on the attainment of a large quantity of high quality 2 GHz and 500 MHz GPR data concurrent with data from other instrumentation typically used to assess track structural quality. The resultant combined dataset will achieve numerous objectives including, but not limited to:

- Providing the necessary information to make an unbiased assessment of the relationship between subsurface features characterized with the 500 MHz GPR and track structural quality;

- Enabling a better understanding of the cost-benefit analysis of using GPR; and

- Quantifying, to a greater extent, the relation between ballast fouling and track structural problems.

Acknowledgments

The authors gratefully acknowledge the very helpful assistance of the staff at TTC during data collection and cross-trenching. The generous assistance of numerous individuals at Amtrak is appreciated, especially Michael Trosino, who coordinated the GPR data collection and gathered the ground truth. Hank Lees and Mark Meyer of BNSF provided invaluable help during data collection and ground truth verification. Special thanks to Steve Pfeiffer and Lloyd Tesch of the Alaska Railroad who coordinated the data collection and ground truth effort in Alaska. The ground truth samples were analyzed for moisture content and aggregate size distribution by Zach Dombrow and Hai Huang from the University of Illinois. The authors are also grateful to Dr. Ted Sussmann of the Volpe National Transportation System Center for his guidance during the course of the project and Mr. Mahmood Fateh of FRA, who served as the Contracting Officer's Technical Representative for this project.

References

Al-Qadi, I.L. and Lahouar S. 2004. Use of GPR for Thickness Measurement and Quality Control of Flexible Pavements. *The Journal of AAPT* 73;501–528.

Al-Nuaimy, W., Eriksen, A., Gasgoyne, J. Train-mounted GPR for High-speed Rail Trackbed Inspection. Tenth International Conference on Ground Penetrating Radar, June 21–24, 2004, Delft, The Netherlands.

Annan, A.P. Ground penetrating radar principles, procedures & applications. Mississauga, Canada: John Wiley & Sons, 2003.

Balanis, C.A., Advanced Engineering Electromagnetics, New York: John Wiley & Sons, 1989.

Barber, P. and Yeh, C. 1975. Scattering of electromagnetic waves by arbitrarily shaped dielectric bodies. *Applied Optics* 14 (12) 2864–2872.

Clark, M.R., Gillespie, R., Kemp, T., McCann, D.M., Forde, M.C. 2001. Electromagnetic properties of railway ballast. *NDT & E International Journal*, 34 (5) 305 – 311.

Daniels, D.J., Surface penetrating radar. London: The Institution of Electrical Engineers, London, 1996.

Eriksen A., Zetica J.G., and Al-Nuaimy, W. *Improved Productivity & Reliability of Ballast Inspection Using Road-Rail Multi-Channel GPR.* London: Railway Engineering, Commonwealth Institute, July 2004.

Eriksen, A., Benables, B., Gascoyne, J., Bandyopadhyay, S., Benefits of high speed of GPR to manage trackbed assets and renewal strategies, PWI conference, June 19, 2006, Brisbane, Australia.

Hyslip, J.P., Olhoeft, G.R., Smith, S.S., and Selig, E.T., 2005, Ground Penetrating Radar for Track Substructure Evaluation. Washington, DC: Federal Railroad Administration.

Kathage, A., Niessen, J., White, G., Bell, N. Fast inspection of railway ballast by means of impulse GPR equipped with horn antennas, Railway Engineering, 2005.

Keogh, T. and Keegan, T.R. An integrated system for accurate tie and ballast condition assessment, AREMA conference, Louisville, KY, 2006.

Kind, T., Maierhofer, C. “Railway ballast fouling inspection by monitoring the GPR propagation velocity with a multi-offset antenna array.” 11th International Conference on Ground Penetrating Radar, June 19–22, 2006, Columbus OH.

Li, D.Q., and Selig, E.T. 1998. Method for Railroad Track Foundation Design. I: Development. *Journal of Geotechnical and Geoenvironmental Engineering* 124, (4) 316–322.

Maser, K.R. 1996. Condition Assessment of Transportation Infrastructure Using Ground Penetrating Radar. *Journal of Infrastructure Systems*, 2 (2): 94–101.

Olhoeft, G.R., Smith, S., Hyslip, J.P., and Selig, E.T. GPR in railroad investigation. Tenth International Conference on Ground Penetrating Radar, Delft, The Netherlands, June 21–24, 2004.

Olhoeft, G.R. and Selig, E.T. 2002. Ground Penetrating Radar Evaluation of Railway Track Substructure Conditions, Ninth International GPR Conference, Proceedings of SPIE, Vol. 4758, pp. 48–53.

Olhoeft, G.R. Working in a difficult environment: GPR sensing on the railroads, IEEE, 2005.

Rao, C., Tutumluer, E., and Stefanski, J.A. “Coarse Aggregate Shape and Size Properties Using a New Image Analyzer,” ASTM Journal of Testing and Evaluation, JTEVA, Vol. 29, No. 5, Sept. 2001, pp. 79–89.

Roberts, R., Al-Qadi, I., Tutumluer, E., Boyle, J., and Sussmann, T. Advances in Railroad Ballast Evaluation Using 2 GHz Horn Antenna. International Conference on Ground Penetrating Radar, Columbus, OH, June 19–22, 2006.

Selig, E.T. and Waters, J. *Track Geotechnology and Substructure Management*. London: Thomas Telford, 1994.

Silvast, M., Levomaki, M, Nurmikolu, A., Noukka, J., NDT techniques in railway structure analysis, 7th World Congress on Railway Research, June 2006, Montreal, Canada.

Sussmann, T.R., Selig, E.T., and Hyslip, J.P. 2003. Railway track condition indicators from ground penetrating radar. *NDT & E International Journal*, 36 (3): 157–167.

Sussmann, T.R. and Selig E.T. 1999. Characterization of track substructure performance, Recent Advances in the Characterization of Pavement Geomaterials. Geotechnical Special Publication, American Society of Civil Engineers, pp. 37–48.

Sussmann, T.R., O’Hara, K., and Selig, E.T. 2002. “Development of Material Properties for Railway Application of Ground Penetrating Radar.” *Ninth International Conference on Ground Penetrating Radar*. Koppenjan S.K. and Lees, H. (Ed). Proceedings of SPIE Vol. 4758, pp. 42–47.

Sussmann, T.R. and Selig E.T. 1999. Characterization of Track Substructure Performance, Recent Advances in the Characterization of Pavement Geomaterials. Geotechnical Special Publication, American Society of Civil Engineers, pp. 37–48.

Tutumluer, E., Dombrow, W., and Huang, H. Laboratory Characterization of Fouled Ballast Behavior, Proceedings 2008 AREMA Annual Conference, Salt Lake City, UT, September 21–24, 2008.

Wenty, R. *Rehabilitation of Ballast and Subgrade*, Proceedings. 2007 AREMA Annual Conference, Chicago, IL, September 9–12, 2007.

Xu, P., Dai, M., and Chan, A.K. A Comparison on Texture Classification Algorithms for Remote Sensing Data. Elizabeth City, NC: IEEE, 2004.

Acronyms

BNSF	Burlington Northern Santa Fe
CBR	California bearing ratio
DCP	dynamic cone penetrometer
DMI	distance measuring instrument
FM	frequency modulation
EM	electromagnetic
FCC	Federal Communication Commission
FRA	Federal Railroad Administration
GPR	ground penetrating radar
GPS	global positioning system
GSSI	Geophysical Survey Systems Incorporated
HTL	high-tonnage loop (at TTC)
LED	light-emitting diode
MP	Milepost
RFI	radio frequency interference
STFT	Short-Time Fourier Transform
TTC	Transportation Technology Center